MODIFICATION OF POLYMERIC SUBSTRATES USING SURFACE-GRAFTED NANOSCAFFOLDS

A Dissertation
Presented to
The Academic Faculty

By

Kimberlee Fay Thompson

In Partial Fulfillment
Of the Requirements for the Degree
Doctor of Philosophy in the
School of Polymer, Textile & Fiber Engineering

Georgia Institute of Technology

August 2005

MODIFICATION OF POLYMERIC SUBSTRATES USING
SURFACE-GRAFTED NANOSCAFFOLDS

Approved by:

Dr. Stephen Michielsen, Advisor
College of Textiles
North Carolina State University

Dr. Fred Cook
School of Polymer, Textile & Fiber Engineering
Georgia Institute of Technology

Dr. Haskell Beckham
School of Polymer, Textile & Fiber Engineering
Georgia Institute of Technology

Dr. Anselm Griffin
School of Polymer, Textile & Fiber Engineering
Georgia Institute of Technology

Dr. W. Brent Carter
School of Materials Science & Engineering
Georgia Institute of Technology

Dr. Lawrence Bottomley
School of Chemistry & Biochemistry
Georgia Institute of Technology

Date Approved: May 6, 2005

ACKNOWLEDGEMENTS

- To my thesis advisor, Dr. Stephen Michielsen, for his direction and expertise regarding polymer science, for his motivation which was invaluable, and for his consistent encouragement and support even across the large distance between Georgia and North Carolina
- To my committee comprised of Drs. Cook, Beckham, Griffin, Carter and Bottomley, for their guidance and input into my research, which helped me become a more effective chemist and produce a professional document detailing my research
- To my research group, for their friendship and understanding, for their debate in group meetings and their assistance in preparation for my thesis defense, and especially to Chris Hubbell, for assistance with carpet/fabric evaluation
- To the Center for Competitiveness of the Apparel, Textile and Carpet Industry (CCACTI, State of Georgia) for partial funding of this work
- To my parents, Sidney and Darlene Thompson, and my sister, Jacinda Thompson, for their love, support, and patience during this process

TABLE OF CONTENTS

LIST OF TABLES

LIST OF FIGURES

LIST OF ABBREVIATIONS

AATCC	American Association of Textile Chemists and Colorists
AFM	atomic force microscopy
AG	adsorption-grafted
AG/D	adsorption-grafted/desorbed
AmM	acrylamide-modified
A-RSA	adaptive RSA
ARXPS	angle-resolved xps
BA	butyl amine
Bam	butyl acrylamide
BAmM	butyl acrylamide-modified
CDMT	2-chloro-4,6-dimethoxy-1,3,5-triazine
CF_3CO_2D	deuterated trifluoroacetic acid
DCC	1,3-dicyclohexyl carbodiimide
D_2O	deuterium oxide
DMF	dimethyl formamide
DMF-d_7	heptadeuterated dimethyl formamide
DMTMM	4-(4,6-dimethoxy-1,3,5-triazin-2-yl)-4-methyl morpholinium chloride
DMSO	dimethylsulfoxide
DMSO-d_6	hexadeuterated dimethylsulfoxide
EDC	1-ethyl-3-(3-dimethylaminopropyl) carbodiimide
FHMA	1,1-dihydroperfluoroheptyl methacrylate
FTIR	Fourier transform infrared spectroscopy
HDMT	2-hydroxy-4,6-dimethoxy-1,3,5-triazine
HEA	hydroxyethyl amine
HEAm	hydroxyethyl acrylamide
HEAmM	hydroxyethyl acrylamide modified
HFBA	1H, 1H-heptafluorobutyl amine
HFBAm	1H, 1H-heptafluorobutyl acrylamide
HFBAmM	1H, 1H-heptafluorobutyl acrylamide modified
^{1}H NMR	proton nuclear magnetic resonance spectrometry
H_2O	water
KBr	potassium bromide
LEIS	low-energy ion scattering
MeOH	methanol
MeOH-d_4	tetradeuterated methanol
MHz	megahertz
MMA	methyl methacrylate
NaCl	sodium chloride
NaOH	sodium hydroxide
NaPAA	sodium poly(acrylate)
NaSCN	sodium thiocyanate
NHS	N-hydroxysuccinimide

NMM	N-methyl morpholine
NMM·HCl	N-methyl mopholine hydrochloride
NMP	N-methyl pyrrolidone
PAA	poly(acrylic acid)
PCC-RSA	post-adsorption conformational change RSA
PD-EHS-RSA	effective hard sphere PD-RSA
PD-RSA	polydisperse RSA
PDFOA	1H, 1H-pentadecafluorooctyl amine
PDFOAm	1H, 1H-pentadecafluorooctyl acrylamide
PDFOAmM	1H, 1H-pentadecafluoroctyl acrylamide modified
PFPA	1H, 1H-pentafluoropropyl amine
PFPAm	1H, 1H-pentafluoropropyl acrylamide
PFPAmM	1H, 1H-pentafluoropropyl acrylamide modified
PMAA	poly(methacrylic acid)
ppm	parts per million
QSPR	quantitative structure-property relationship
RAMEB	randomly methylated β-cyclodextrin
RMS	root mean square
RS	random site
RSA	random sequential adsorption () model
SG	solution-grafted
SG/D	solution-grafted/desorbed
SGN	surface-grafted nanoscaffold
SSIMS	static secondary ion mass spectroscopy
TAm	taurine acrylamide
TAmM	taurine acrylamide modified
TFAA	trifluoroacetic acid
T_g	glass transition temperature
XPS	x-ray photoelectron spectroscopy

SUMMARY

The main goal of this research was the development of a permanent method of imparting stain and soil resistance to nylon carpet fibers, as an alternative to current fluorochemical treatments, which use excess material to compensate for a lack of durability. A technique was developed for nylon carpet fibers using surface modification.

Poly(acrylic acid) (PAA), a highly functional polymer, was grafted onto nylon substrates, creating a surface-grafted nanoscaffold (SGN) to act as a platform for the permanent attachment of fluorochemical groups. PAA anions (CO_2^-) were expected to restrict diffusion of similarly charged dyes into the fiber, providing stainblocking properties. An efficient and water-soluble amidation reagent, 4-(4,6-dimethoxy-1,3,5-triazin-2-yl)-4-methylmorpholinium chloride (DMTMM) was selected to graft PAA to nylon amine groups and to modify residual PAA groups with a fluorochemical amine.

To optimize DMTMM-activated reactions, several model acrylamide derivatives of PAA were prepared by reaction of PAA with sulfonic acid, hydroxyl, butyl and perfluorooctyl functional amines using DMTMM. By altering reaction conditions, derivatives of differing side chain structures and lengths, hydrophobic character, and acrylamide content were prepared. The reactions achieved very high conversions in either water or alcohol (measured by NMR and FTIR). Reactions of PAA with taurine, hydroxyethyl amine, and butyl amine achieved ~100% modification in H_2O even though butyl amine reaction products with ≥77% acrylamide content precipitated from solution. Reactions of PAA with perfluorinated alkyl amines in MeOH proceeded to high, but incomplete, levels of modification. By decreasing PAA concentration to 0.5 g/L PAA,

~80% modification with 1H, 1H-pentadecafluorooctyl amine (PDFOA) was achieved and PDFOA reaction products with ≥52% acrylamide content precipitated from MeOH.

A highly successful PAA surface grafting method was developed. PAA layers were first deposited on nylon by adsorption, followed by grafting with DMTMM. The surfaces were analyzed by contact angle, which measures the top 0.1-1 nm, and by XPS, which measures 3-10 nm. Under optimized reaction conditions, the PAA grafting process achieved ~78% PAA surface coverage and transformed nylon substrate from a hydrophobic to a very hydrophilic surface.

Acrylamide-modified surfaces were prepared by reacting PAA-g-nylon with (a) butyl amine in H_2O or (b) 1H, 1H-pentadecafluorooctyl amine (PDFOA) in MeOH or H_2O. Randomly methylated β-cyclodextrin (RAMEB) was used to solubilize PDFOA in H_2O. The surfaces were analyzed by contact angle and XPS. For butyl amine and PDFOA reactions, contact angle indicated that ~ 100% of the surface was covered with hydrophobic groups, while XPS indicated that the surface reaction was limited to the acrylamide content observed for solution reactions at precipitation (~77% for butyl amine and ~50% for PDFOA). Greater reaction was achieved with PDFOA in H_2O at pH=12 (89% from XPS). Such conditions promoted (a) greater DMTMM efficiency, (b) greater access and (c) greater solubility during the reaction.

Angle-resolved XPS (ARXPS) analysis was performed for these surfaces and models were used to prepare compositional depth profiles from the experimental data. The PAA surface fractions of PAA-treated nylon 6,6 substrates measured by XPS and contact angle were confirmed by ARXPS. The PAA grafting mechanism was determined:

(1) PAA adsorbs in thick layers onto nylon and (2) DMTMM activates and grafts the PAA chains onto nylon, allowing PAA to spread across the surface in thinner layers.

ARXPS analysis of PAA-g-nylon modified with PDFOA in MeOH indicated that fluorinated groups covered >60% of the surface. The fluorinated layer was ~2 nm thick at the surface and an unreacted PAA layer was observed below. For the RAMEB/H_2O reaction with NaOH (pH=12), fluorinated groups covered >100% of the surface. The fluorinated layer extended much further below the surface and a distinct PAA layer was not detected. These results confirmed the previous contact angle and XPS results.

Nylon 6,6 fabrics and carpets were (a0 Adsorption-Grafted and (b) modified with PDFOA in RAMEB/H_2O at pH=12. After PAA-g-nylon was treated with NaOH, the stain resistance was slightly improved. Fluorochemically modified PAA-g-nylon was even more stain resistant (with or without NaOH treatment). More improvements will be necessary to prevent staining at the tips of the carpet tufts. Such improvements may involve applying traditional stain resisting polymers with PAA prior to grafting and fluorochemical modification. However, the fluorochemical treatment was shown to be stable to alkaline conditions and significant water and oil repellency was observed after fluorochemical modification, such that both wetting and wicking were prevented.

CHAPTER 1

INTRODUCTION

1.1 MOTIVATION AND OBJECTIVES

When a polymer interacts with another material or with its environment, the chemical and physical structure of the polymer surface determines the nature of the interaction. Therefore, the key to influencing such interactions is to control the polymer surface. Polymer surfaces are often modified for specific performance properties. Such alterations fall into two general categories, the first involves depositing an extraneous layer over the existing surface, the second with chemically altering the surface layer.

The simplicity of the first technique makes it the most common method for modifying polymer surfaces. However, the thickness of such coatings, generally 1 μm or greater, can significantly change the fundamental mechanical properties of the material. Also, the purely physical attachment between the coating and the substrate make the surface treatment susceptible to removal.

Chemical surface modification techniques include plasma treatment, radical polymerization and chemical grafting of small molecules to the surface. A drawback of these techniques is the need for large numbers of surface reactive groups. An alternate method involves chemically grafting preformed polymers onto the surface. This approach has the potential benefit of covering the entire surface using fewer reactive sites and less added material. Such grafted polymer layers are estimated to be 5-10 nm thick, which is the typical range observed for adsorbed or grafted polymer systems from atomic force microscopy (AFM) interaction force experiments.[1] Thus the bulk properties of the substrate are not expected to change.

In this research, a surface modification technique was developed in which a highly functional, preformed polymer was grafted onto a less reactive polymer surface, creating a surface-grafted nanoscaffold (SGN). The SGN was used as a platform for the further attachment of functional groups. By chemically binding functional groups to the SGN, an extremely durable, functional surface was achieved with much less material.

The goal of this research was attachment of an SGN to nylon, a hydrophilic polymer, as a platform for surface protecting groups with combined oil and water repellency to enhance the stain and soil resistance for carpet fibers (Figure 1.1).

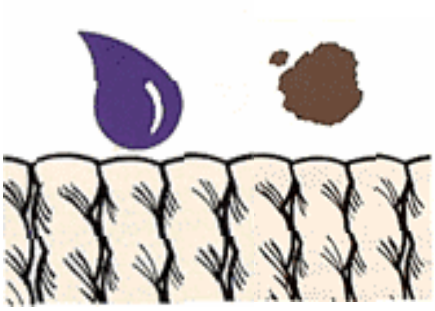

Figure 1.1 – Water and Oil Repellant Carpet Surface: Resists Stains and Soil

A fluorinated SGN is a desirable alternative to current fluorochemical treatments applied to nylon carpet fibers, where excess fluorochemical is applied to impart stain and soil resistance. Not only is this expensive, but the treatments are readily removed from the carpet by steam cleaning (~ pH=10) and end up in the environment. For this reason 3M has removed perfluorooctanesulfonate from its Scotchguard™ products (5/16/02 press release). A fluorinated SGN carpet treatment should be more durable to steam cleaning as well as being a more environmentally conscious and economical process.

Additionally, various functional groups (and thus surface properties) can be combined within the SGN structure. Fluorochemical treatments are typically applied with stainblockers (condensates of formaldehyde and phenolsulfonic acid, for example). The anionic charge of the stainblocker is thought to restrict diffusion of similarly charged dyes into the fiber. Permanent stainblocking could be achieved by incorporating anionic groups together with fluorochemical groups within an SGN structure.

A significant goal of the research was to obtain high SGN surface coverage on the substrate. The ideal surface should be covered with a homogeneous layer of polymer chains so that surface properties are completely controlled by the SGN. The polymer adsorption process will be important, since grafting can be thought of as irreversible adsorption. The relationship between the conformation and surface coverage of adsorbed polymers will be investigated.

1.2 MATERIALS AND METHODS

Polyacrylic acid (PAA) was selected as the SGN polymer. The carboxylic acid groups of PAA were grafted to nylon surface amine (NH_2) groups and were further modified with fluorochemical amines using an amidation agent. The residual carboxylic acid groups of PAA were ionized (CO_2^-) to restrict diffusion of similarly charged dyes (SO_3^-) into the fiber (Figure 1.2). The fluorinated SGN was evaluated in terms of water and oil repellency, stain resistance and stability to steam cleaning (alkaline) conditions.

A highly efficient and H_2O stable amidation agent, 4-(4,6-dimethoxy-1,3,5-triazin-2-yl)-4-methylmorpholinium chloride (DMTMM), was selected. DMTMM has not previously been studied for either surface grafting or modification of polymers, so

this research has focused on optimizing each process. Changes in the wetting behavior of the surfaces were evaluated from contact angle measurements. The chemical compositions of modified PAA were determined from ^{1}H NMR and FTIR. The chemical composition and surface structure of modified nylon surfaces were determined by x-ray photoelectron spectroscopy (XPS) and contact angle measurement.

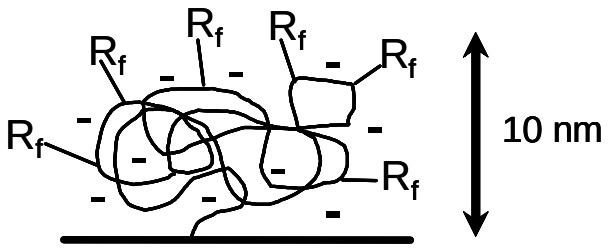

Figure 1.2 – Schematic of a Fluorinated-PAA Surface-Grafted Nanoscaffold

1.3 SCOPE OF THE DISSERTATION

The first goal was to optimize the reaction conditions in solution to identify any limitations for future work with surface-grafted systems. PAA CO_2H groups were modified in solution with various amine-functional molecules using DMTMM amidation reagent. Reactions with sulfonic acid, hydroxyl and butyl functional amines were performed in H_2O while reactions with fluorochemical amines of various fluorochemical segment lengths were performed in MeOH. Side chain conversions for modified PAA were determined from ^{1}H NMR and FTIR.

The second goal was to optimize the grafting conditions in terms of PAA surface coverage and reaction efficiency. PAA SGNs were synthesized by grafting PAA chains onto nylon 6,6 substrates. In one method, nylon was immersed in PAA solution and DMTMM was added. In a second method PAA was first adsorbed onto nylon and then

PAA-Adsorbed nylon was immersed in DMTMM solution. The PAA surface coverage achieved by each method was evaluated by contact angle goniometry and XPS.

The third goal was to optimize the acrylamide modification of surface-grafted PAA in terms of acrylamide group surface coverage. The CO_2H groups of PAA SGNs were modified with amines using DMTMM. Reaction with butyl amine was performed in H_2O, while fluorochemical reactions were performed in MeOH as well as in H_2O using methylated β-cyclodextrin (RAMEB) to solubilize the fluorochemical. For aqueous fluorochemical modification, the effect of NaOH was observed. The modified PAA surface coverage was evaluated by contact angle goniometry and XPS.

The fourth goal was to study the previously described films with angle-resolved XPS analysis using various models to describe the surface. The Fractional Overlayer model was used to evaluate the surface fraction f and thickness t of PAA layers on nylon substrates. The Cumpson and Trapezoid concentration gradient models were used to study gradual changes in concentration expected for acrylamide modified PAA-g-nylon surfaces.

The fifth goal was to apply the results of the previous work to nylon 6,6 fabrics and carpets and to evaluate the performance of these textile substrates in the areas of water and oil repellency, stain resistance and durability to alkaline conditions.

CHAPTER 2

POLYMER SURFACE CHARACTERIZATION

2.1 INTRODUCTION

A large number of techniques are available for the analysis of polymer surfaces, each with its own advantages and disadvantages. The suitability of a particular technique depends upon the specific problem under examination. It is highly desirable to examine the same specimen by different techniques. Using different techniques offers cross data and assists in interpretation. Selected techniques may have different surface sensitivities or provide qualitative vs. quantitative information. Various types of information may be observed such as chemical, electrostatic, or topographical properties. In the present study, chemical composition as a function of depth was obtained from x-ray photoelectron spectroscopy while surface chemical composition and surface energetics were evaluated from contact angle goniometry.

2.2 CONTACT ANGLE MEASUREMENT

Contact angle measurement is the most commonly used method of solid surface tension measurement. Contact angle is determined by the outermost atomic layers of a surface (0.1-1 nm). When a drop of liquid is placed on a solid surface, the drop shape will change under the pressure of the different surface and interfacial tensions around the perimeter of the drop, until equilibrium is reached. In 1805, Thomas Young expressed the three-phase equilibrium in terms of the vectorial sum shown in Figure 2.1, resulting in the following equation of interfacial equilibrium:[2]

$$\gamma_{SV} - \gamma_{SL} = \gamma_{LV} \cos\theta_Y \qquad (2.\ 1)$$

The Young contact angle θ_Y is defined as the angle (measured in the liquid) that is formed at the junction of three phases, typically the solid-liquid-gas junction.

The Young equation assumes that surfaces are homogeneous. However, real surfaces can be composed of domains of different composition and thus different wetting properties. Cassie[3] proposed an equation for heterogeneous surfaces composed of well-separated and chemically distinct patches, which for two components becomes:

$$\cos\theta_Y = \sum f_i \cos\theta_i = f_1 \cos\theta_1 + f_2 \cos\theta_2 = f_1 \cos\theta_1 + (1 - f_1)\cos\theta_2 \qquad (2.\ 2)$$

which gives the Young contact angle θ_Y of a liquid on a heterogeneous surface composed of a fraction f_1 of chemical group 1 having a Young contact angle θ_1 and a fraction f_2 of chemical group 2 having a Young contact angle θ_2. Surface fractions f_1 and f_2 (= 1 – f_1) are determined using the heterogeneous surface θ_Y and individual θ_1 and θ_2 values for reference surfaces composed of chemical group 1 and chemical group 2, respectively.

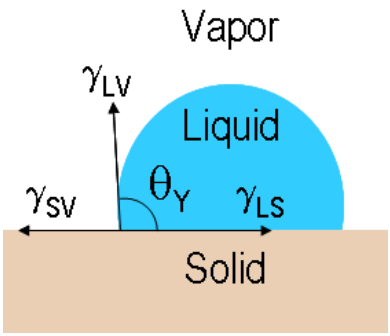

Figure 2.1 – Components of Interfacial Tension Used to Derive Young's Equation

The Young equation also ignores surface roughness. In 1936, Wenzel reasoned that within a measured unit area of a rough surface there is more surface than in the same measured unit area of a smooth surface.[4] While specific surface quantities are the same on the two surfaces, the relative magnitudes of the vectors composing the Young equation are modified, as shown in Figure 2.2. Wenzel proposed the following equation:

$$r(\gamma_{SV} - \gamma_{SL}) = \gamma_{LV} \cos\theta_W \qquad (2.3)$$

where r is the so-called roughness factor (= actual surface/geometric surface) and θ_W is the Wenzel contact angle, which is related to the Young contact angle θ_Y as follows:

$$\cos\theta_W = r\cos\theta_Y \qquad (2.4)$$

Since the roughness factor is always greater than unity, Equation 2.4 shows that surface roughness magnifies surface wetting. The Wenzel angle will increase with roughness for Young angles greater than 90° and will decrease if it is less than 90°. Therefore, an alternate characterization technique which does not rely on surface wetting properties should also be used. In the next section, such a technique is presented.

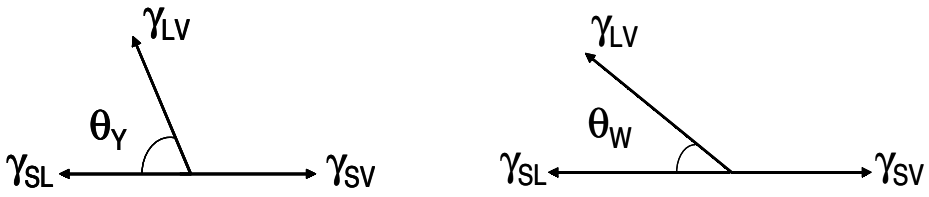

Figure 2.2 – Wenzel's Relationship to Young's Equation

2.3 X-RAY PHOTOELECTRON SPECTROSCOPY (XPS)

The surface composition of the SGN can be measured by X-ray photoelectron spectroscopy (XPS)[5]. XPS is a highly surface-specific analytical technique (3-10 nm) used to obtain the chemical structure and atomic composition of a material. The atomic sensitivity of XPS is 10^{-2}–10^{-3}, so 1.0–0.1 atomic % can be detected (except H and He).[5] A surface is irradiated with photons from a soft x-ray source, exciting the electrons in the surface region. Electrons escape the surface with a kinetic energy proportional to the difference between the incident photon energy and the binding energy of the electron to the nucleus. The average distance that electrons travel in the solid before undergoing an inelastic collision is the inelastic mean free path (λ). The λ value depends upon the material and the kinetic energy of the electron. Typical λ values are a few nanometers. Thus, only electrons generated in the outermost atomic layers of the solid have enough energy to escape the surface without energy loss. This is the source of the surface sensitivity of XPS. An emitted electron having traveled a distance λ in the material at an angle θ between the axis normal to the surface (z) and the analyzer axis will have originated from an escape depth $d = \lambda\cos\theta$ along the *z*-axis (Figure 2.3).

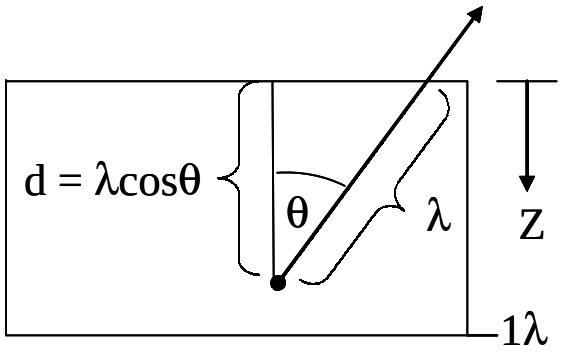

Figure 2.3 – Escape Depth d, Inelastic Mean Free Path λ, and Take-Off Angle θ.

The probability (p) that an electron will escape the material from a depth z without undergoing an inelastic collision is shown in Equation 2.5.

$$p = e^{-z/\lambda \cos\theta} \tag{2. 5}$$

At z=0, p=1 and p declines as z increases (Figure 2.4). The majority of the signal intensity (I=63%) comes from an escape depth d (also known as the information depth). An additional 23% comes from the next layer of thickness d (I=86%), and an additional 9% comes from the next layer of thickness d (I=95%). The maximum d is obtained at a take-off angle θ=0°. For polymers, d typically ranges from 3-10 nm. Since d is limited by the attenuation of emerging photoelectrons, it is also known as attenuation length.

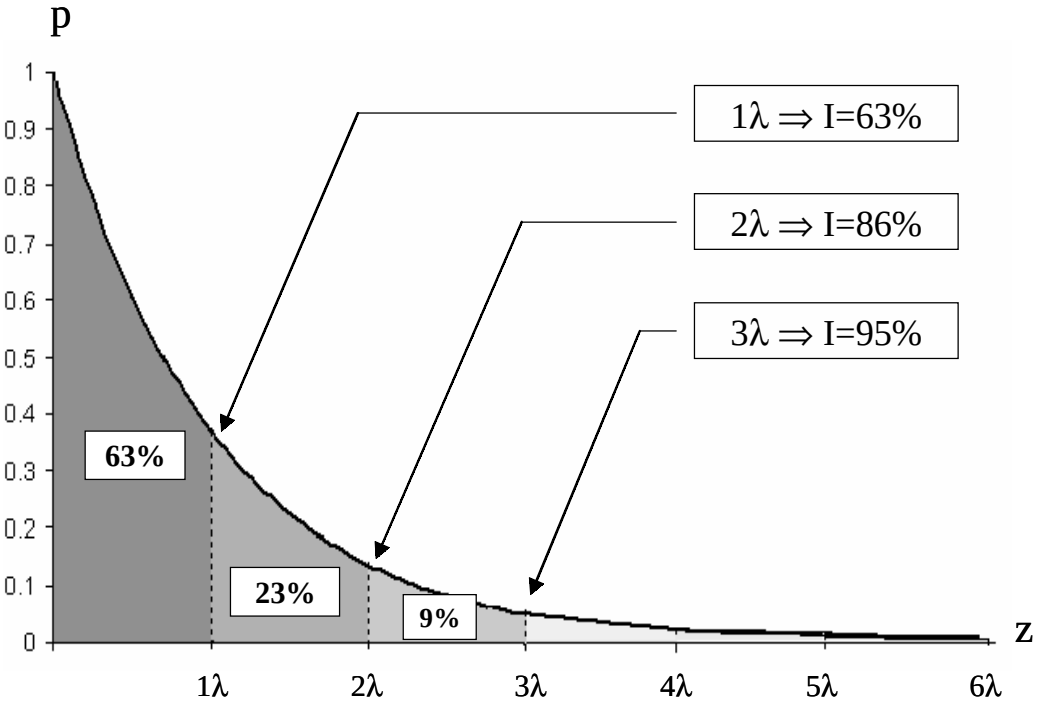

Figure 2.4 – Probability p as a Function of Depth z at θ = 0.

The energetic peak position in the emitted electron spectrum is characteristic of the individual element and core level of the electron. From peak intensity, the semiquantitative elemental composition of the surface can be determined. The photoelectron intensity $I_i(\theta)$ for element i at the surface varies with x-ray flux ϕ, transmission function T_i, analysis area A, photoemission cross-section σ_i, composition $C_i(z)$, λ_i and z (Equation 2.6). If a homogeneous surface is assumed, $C_i(z)$ becomes a constant C_i and the integral can be solved. In the calculation of atomic % of element i, instrumental factors (ϕ, A and θ) are eliminated and elemental factors (T_i, σ_i and λ_i) are combined into an atomic sensitivity factor S_i (Equation 2.7). XPS software typically assumes λ_i variations to be small and generates relative S_i values by correcting Scofield's[6] σ_i values for the transmission function T_i of the spectrometer.

$$I_i(\theta) = \phi A T_i \sigma_i \int_0^{\infty} C_i(z) e^{\frac{-z}{\lambda_i \cos\theta}} dz = \phi A T_i \sigma_i C_i \lambda_i \cos\theta \approx S_i C_i \qquad (2.6)$$

$$\text{atomic}\,\%\, i = \frac{C_i}{\sum_i C_i} = \frac{I_i / S_i}{\sum_i I_i / S_i} \qquad (2.7)$$

2.4 ANGLE-RESOLVED XPS (ARXPS)

If a sample composition is not homogeneous to 10 nm, XPS analysis will sample a range of compositions and return a weighted average. However, the concentration depth profile within the analyzed volume can be obtained by the angle-resolved XPS (ARXPS) method, which varies the vertical sampling depth via the photoelectron take-off angle.

Construction of a depth-profile requires obtaining spectra at various take-off angles (typically 5-6 data sets).

As shown in Equation 2.4, the measured peak intensity is proportional to the integral of the composition as a function of depth multiplied by the exponential decay constant. Thus, the measured peak intensity is proportional to the Laplace transform of the composition as a function of depth. The composition as a function of depth is, in turn, generated by the inverse Laplace transform of the variation of the measured peak intensity as a function of $(\lambda\cos\theta)^{-1}$. Unfortunately, many possible reciprocal concentration functions have Laplace transforms that fit the data equally well, so the inversion function does not have a unique solution.

Given the problems inherent to the inversion of the Laplace transform, many authors have adopted a different approach to the interpretation of ARXPS results. First, a model is proposed for the sample surface. Then, the equations are solved to calculate the angular dependence of the XPS peak intensities from the model. Finally, the parameters appearing in the model are optimized for the best fit between the calculated and experimental data. Cumpson has laid out the limitations of the ARXPS technique.[7] First, in the depth profile, certainty in the composition must be traded for depth resolution, or vice-versa. Even for an uncertainty in composition of ±50%, the fractional depth resolution $\Delta z/z$ is limited to 0.8. Second, for realistic signal-to-noise ratios, the number of degrees of freedom is three, so that the model used to fit a depth profile to the experimental data can have no more than three independent parameters. Limiting the number of independent parameters obviously limits the complexity and sophistication of the depth profile shapes. To this point, several profile models are typically used.

2.4.1 Fractional Overlayer Model

Paynter developed a simplified partial layer/substrate model which can be used to interpret angle-resolved XPS results.[8] This model is appropriate in the case of polymer chains adsorbed or grafted on a substrate. In this model, the homogeneous substrate is partially or completely covered by a homogeneous overlayer of uniform thickness (Figure 2.5). The aspect ratio of overlayer islands is assumed to be so low that shadowing effects can be ignored. Typical adjustable parameters are the layer thickness t and the surface fraction f covered by the layer. This leaves one compositional parameter C. If the substrate composition is fixed, one of the components of the overlayer can be varied with the other components as dependent variables. However, if the layer is known to cover 100% of the surface, then f can be fixed at unity and t and two composition parameters can be varied.

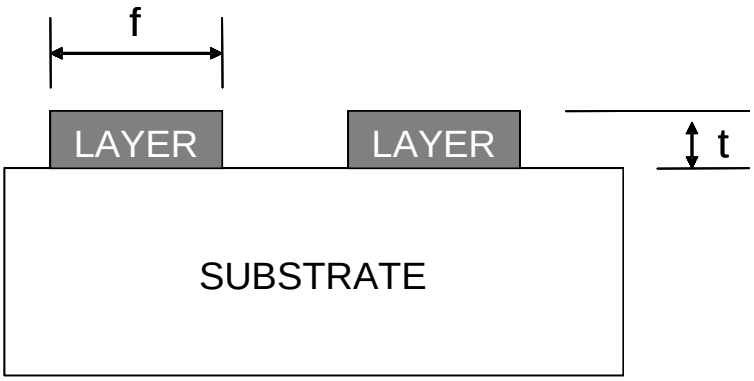

Figure 2.5 – ARXPS Fractional Overlayer Model

For a layered structure of homogeneous material, the photoelectron intensity $I(\theta)$ can be written as the sum of three cases: the layer, the substrate not covered by the layer material, and the substrate covered by the layer material:

$$\frac{I(\theta)}{\phi T A \sigma} = f\left[\int_0^t C_L e^{\frac{-z}{\lambda_L \cos\theta}} dz + \int_0^\infty C_S e^{\frac{-t}{\lambda_L \cos\theta}} e^{\frac{-z}{\lambda_S \cos\theta}} dz\right] + (1-f)\int_0^\infty C_S e^{\frac{-z}{\lambda_S \cos\theta}} dz \quad (2.8)$$

where C_L and C_S are the elemental compositions in the layer and substrate, respectively, and where λ_L and λ_S are the photoelectron inelastic mean free paths through the layer and the substrate, respectively. After evaluating the integrals, the following equation can be used to determine f, C, and t using λ_L and λ_S values from literature:

$$\frac{I(\theta)}{\phi T A \sigma \cos\theta} = c_L \lambda_L f\left[1 - e^{\frac{-t}{\lambda_L \cos\theta}}\right] + c_S \lambda_S \left[(1-f) + f e^{\frac{-t}{\lambda_L \cos\theta}}\right] \quad (2.9)$$

2.4.2 *Concentration Gradient Models*

There are several concentration gradient models which abandon the concept of layers for linear concentration gradients described by a series of j inflection points:

$$I(\theta) = C_1 \lambda \cos\theta + \sum_{i=1}^{i=j-1} \lambda^2 \cos^2\theta \frac{C_{i+1} - C_i}{z_{i+1} - z_i}\left[e^{\frac{-z_i}{\lambda \cos\theta}} - e^{\frac{-z_{i+1}}{\lambda \cos\theta}}\right] \quad (2.10)$$

where C_i is the concentration at the i^{th} inflection point at depth z_i. With the assumption that the total atom density (except H and He) is constant with depth, I(θ) and atomic % values can be determined for a postulated depth profile. The depth profile is optimized by comparing these values with experimental data.

Cumpson developed a model which varied atomic composition at three inflection points at fixed depths, which are specific multiples of the λ value for each photoelectron; $z_1 = 0$, $z_2 = \lambda/3$, $z_3 = 4\lambda/5$, $z_4 = 2\lambda$. In this profile, $C_1 = C_2$, so C_2, C_3, and C_4 are used to optimize the depth profile (Figure 2.6). Paynter developed a trapezoid profile, which assumes that the concentration of the first element falls to zero at some point (Figure 2.7). The three parameters are C_2 (= C_1), z_2 and z_3 (for which $C_3 = 0$). The C_3 value can be changed from zero to a bulk concentration of the element being profiled. The Cumpson model uses no special knowledge about the profile shape. It also assumes $C = C_4$ beyond $z = 2\lambda$ into the bulk when $z = 2\lambda$ is only ~5 nm for polymers. The trapezoid profile can profile the entire layer, however it is more sensitive to destabilization by noise in the data than the Cumpson profile.

Paynter has developed Microsoft Excel 97 spreadsheets for calculating composition depth profiles from ARXPS experiments. The ARXPS.xls[8] program sets up the fractional overlayer model to work with three element substrates and two element overlayers. The ARXPS version 4.xls[9] program sets up the Cumpson model for three elements samples and the "trapezoid" model for two element samples. Each spreadsheet uses "solver" non-linear optimization code to find a "least squares" match by minimizing the sum of the squared differences between the observed and calculated values for the apparent composition as a function of the take-off angle. Paynter recommends acquiring data at 0, 15, 30, 45, 60 and 75 degrees.

.

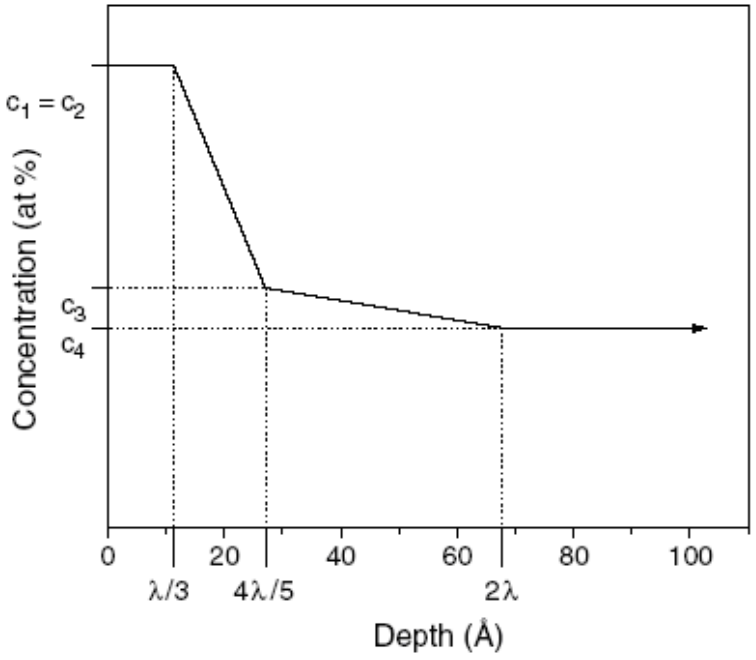

Figure 2.6 – ARXPS Cumpson Model

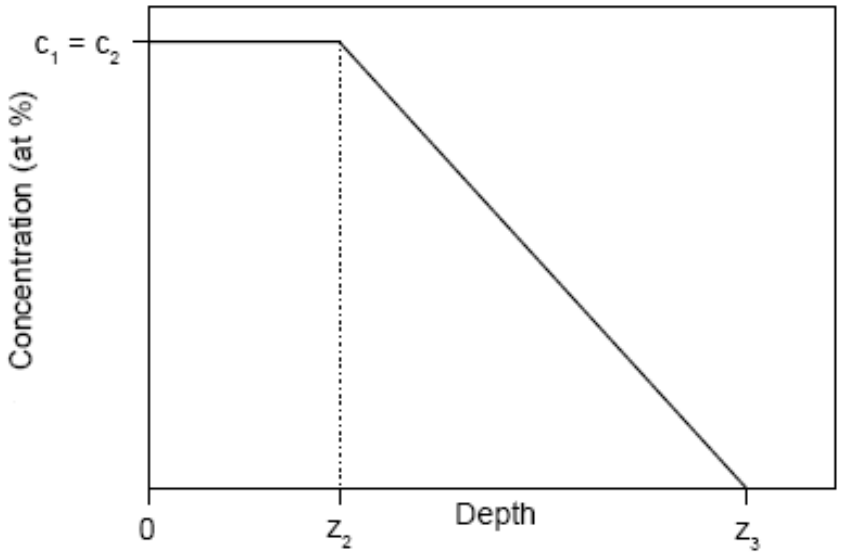

Figure 2.7 – ARXPS Trapezoid Model

2.4.3 Inelastic Mean Free Path (λ) Values for Polymers

XPS analysis performed at a single-take off angle assumes a homogenous surface and small λ_i differences for simplification. However, the kinetic energy of the electron and the material in which it travels should be taken into account for ARXPS analysis. Specific λ values for each element and for each substrate are required as input into ARXPS.xls[8] and ARXPS version 4.xls[9] depth profile calculations.

Cumpson developed a quantitative structure-property relationship (QSPR) for estimation of the λ values for organic materials, such as polymers.[10] The QSPR was developed by fitting an expression in terms of molecular indices to tabulated λ values given by Tanuma, Powell, and Penn[11] at an electron energy of 1 keV. The accuracy of this estimate was found to be better than existing methods, such as the TPP-2M equation for organic materials developed by Tanuma *et al*. The QSPR only requires a structural formula, whereas the TPP-2M requires other reference data that are difficult to find or measure, such as bandgap or number of valence electrons. Equations 2.11 and 2.12 show the relations used to obtain the inelastic mean free path of polymers at 1 keV ($\lambda_i^{1\ keV}$) and to convert $\lambda_i^{1\ keV}$ values to other kinetic energies:

$$\lambda_i^{1keV} = \frac{31.17\left({}^0\chi^v\right) + 4.207\left(N_{rings}\right)}{N_{non-H}} + 11.04\ \text{Å} \qquad (2.11)$$

$$\lambda_i = \lambda_i^{1\ keV}(K.E.)^{0.79} \qquad (2.12)$$

where ${}^{0}\chi^{v}$ is the zeroth-order valence connectivity index of Kier and Hall[12] (evaluated by Bicerano's[13] method for polymers), N_{rings} and $N_{non\text{-}H}$ are the number of aromatic six-member rings and the number of non-hydrogen atoms in the polymer repeat unit considered, respectively, and K.E. is the electron kinetic energy in keV.

2.5 SURFACE CHARACTERIZATION OF FLUOROPOLYMERS

2.5.1 Combined Contact Angle, XPS and LEIS

Low-energy ion scattering (LEIS)[14] measures the energy loss of noble gas ions reflected from a sample. The energy of a back-scattered ion is characteristic for the mass of the target atom. Thus the energy spectrum can be interpreted as a mass spectrum of the surface atoms. The low energy inert gas ions have a high neutralization probability. This results in a negligible scattered ion yield from target atoms below the first atomic layer. Therefore the information depth of LEIS is limited to one atomic layer.

The extreme surface specificity of low-energy inert-gas ion scattering comes at a price: uncertainties in the neutralization rate of ions scattered from different surface atoms requires the use of empirical calibration using standards. Other problems are surface damage caused by the ion beam probe and poor mass resolution. Tradeoffs among sample damage, signal intensity, and mass resolution have prevented LEIS from becoming a widely used. However, in certain cases, LEIS proves very useful.

Partially fluorinated copolymers such as poly(perfluoroalkyl methacrylates) are known to have low surface energies, due to the orientation of the perfluoroalkyl side chains to the air interface. The driving force for such orientation is believed to originate from the surface energy differences between the components of the copolymer. Surface

energies are determined by the composition and structure of the top layer. Recently, a combined contact angle, XPS, and LEIS analysis was performed for random copolymers of 1,1-dihydroperfluoroheptyl methacrylate (FHMA) and methyl methacrylate (MMA) to determine the effective thickness of the surface layer which determines macroscopic surface energy.[15]

Introduction of FHMA groups in the copolymer resulted in a large decrease in the surface energy determined from contact angle measurements. XPS measurements obtained at emission angles of 0° (3d=9 nm) and 60° (3d=4.5 nm) showed an increased average fluorine concentration in the surface layers of a few nanometers compared to the fluorine concentration in the bulk determined from elemental analysis. Static low-energy ion scattering (LEIS) experiments, which selectively probed the outermost atomic layer, showed an even higher surface enrichment of fluorine atoms.

For the LEIS measurements of FHMA-MMA copolymers, an almost linear correlation was found by plotting the fluorine atomic concentration of the first atomic layer as a function of the surface energy of the polymer film. Such a relationship was not found for the XPS results. Therefore, the surface energy of the FHMA-MMA copolymers was conclusively shown to be determined by the outermost atomic layer.

2.5.2 Combined Contact Angle, XPS and ARXPS

While LEIS is a useful technique for measuring the composition of the outermost atomic layer of fluorinated surfaces, similar information can be obtained from ARXPS analysis. Further, ARXPS models obtain information regarding the extreme surface, near surface and bulk region from a single experiment. For fluorochemically-modified SGN

surfaces, contact angle, XPS and ARXPS analysis can be performed to investigate the relationship between the extreme surface composition and surface wetting. Further, ARXPS analysis of fluorochemically-modified SGN surfaces allows the distribution of fluorinated groups within the surface layer to be determined.

Based on the results for poly(perfluoroalkyl methacrylates), contact angle analysis of fluorochemically-modified SGN surfaces is expected to display high correlations with the top 1-2 of ARXPS composition depth profiles determined for these surfaces. Contact analysis is expected to display lower correlations with compositions determined by ARXPS or XPS analysis of the fluorochemically-modified SGN surface from 3-10 nm.

CHAPTER 3

SOLUTION MODIFICATION OF PAA

3.1 INTRODUCTION

The successful preparation of a fluorinated SGN surface depends upon the chemistry used to graft and modify the SGN. PAA was selected as the SGN polymer in order to use the numerous CO_2H groups as sites for grafting and modification. The first goal was to optimize the reaction conditions in solution to identify any limitations for future work with surface-grafted systems. PAA derivatives are readily prepared by amidation or esterification of the CO_2H groups with selected amines or alcohols. These modifications can be performed in solution under homogeneous conditions, which should produce a random distribution of functional groups along the polymer backbone. Also, functional group content or structure can be investigated, while keeping the molecular weight and distribution of the backbone polymer constant.

3.1.1 Condensation Chemistry

Carbodiimides are frequently used in condensation reactions, e.g., to form amide bonds between carboxylic acids and amines by activating carboxylate anions to form an *O*-acylurea intermediate.[16-18] The intermediate can be attacked directly by the amine to form the amide or by a second carboxylate anion to give the anhydride, which can then be attacked by the amine to give the amide and a carboxylate. Hydrophobically modified acrylamide derivatives of PAA have been made using 1,3-dicyclohexylcarbodiimide (DCC). Amine-terminated alkyl or perfluoroalkyl groups have been introduced using aprotic polar solvents such as N-methyl pyrrolidone (NMP), dimethylformamide (DMF)

or dimethylsulfoxide (DMSO).[19-24] Reaction efficiencies for alkyl amines are ~100%, but only ~70% for perfluorinated alkyl amines under similar reaction conditions. [19,20,23,24]

Water-soluble carbodiimides have used in such condensation reactions, the most common is 1-ethyl-3-(3-dimethylaminopropyl) carbodiimide (EDC).[25,26] However, EDC has several disadvantages. First, EDC is over 10 times as expensive as DCC. Also, the *O*-acylurea intermediate is formed optimally at pH 4-5 while the amine is protonated and unreactive in this pH range. Moreover, the *O*-acylurea intermediate is very short-lived and undergoes rapid hydrolysis, resulting in extremely low and variable coupling yields. Nevertheless, EDC is preferred over DCC for aqueous modification of PAA due to its high water solubility and the ease of removing excess reagent and byproducts by washing the PAA derivative with water and dilute acid. Adding N-hydroxysuccinimide (NHS) to such reactions greatly enhanced the yields. NHS reacts with activated carboxylate anions to give stable aminoacyl esters, which hydrolyze more slowly in water.

3.1.2 Acrylamide-Modification of PAA Using EDC

EDC has been used to couple poly(γ-glutamic acid) with taurine (2-aminoethane sulfonic acid) to create a biodegradable material with heparin-like anticoagulant activity.[27] While taurine and EDC ratios were varied, the amount of EDC was the most important variable for controlling the sulfonate content. Using equimolar amounts of CO_2H and NH_2, the efficiency of modification was ~ 50% for all EDC/CO_2H ratios and a maximum sulfonate content of 81% was achieved using a 2/1 EDC/CO_2H ratio. Using equimolar amounts of CO_2H and EDC, the sulfonate content increased with the NH_2/CO_2H ratio up to a maximum of ~ 50%, even with excess amine.

3.1.3 Acrylamide-Modification of PAA Using DMTMM

While EDC has been used successfully in acrylamide synthesis, a more efficient, less costly condensing reagent is preferred. A triazine-based condensing reagent has recently been developed, 4-(4,6-dimethoxy-1,3,5-triazin-2-yl)-4-methyl-morpholinium chloride (DMTMM), from the reaction of 2-chloro-4,6-dimethoxy-1,3,5-triazine (CDMT) with N-methylmorpholine (NMM) in THF. Treatment of a carboxylate anion with DMTMM forms a 2-acyloxy-4,6-dimethoxy-1,3,5-triazine intermediate ("active ester") which reacts with an amine to form the amide product with NMM·HCl and 2-hydroxy-4,6-dimethoxy-1,3,5-triazine (HDMT) byproducts. The mechanism for DMTMM activated amidation of carboxylic acids is presented in Figure 3.1.

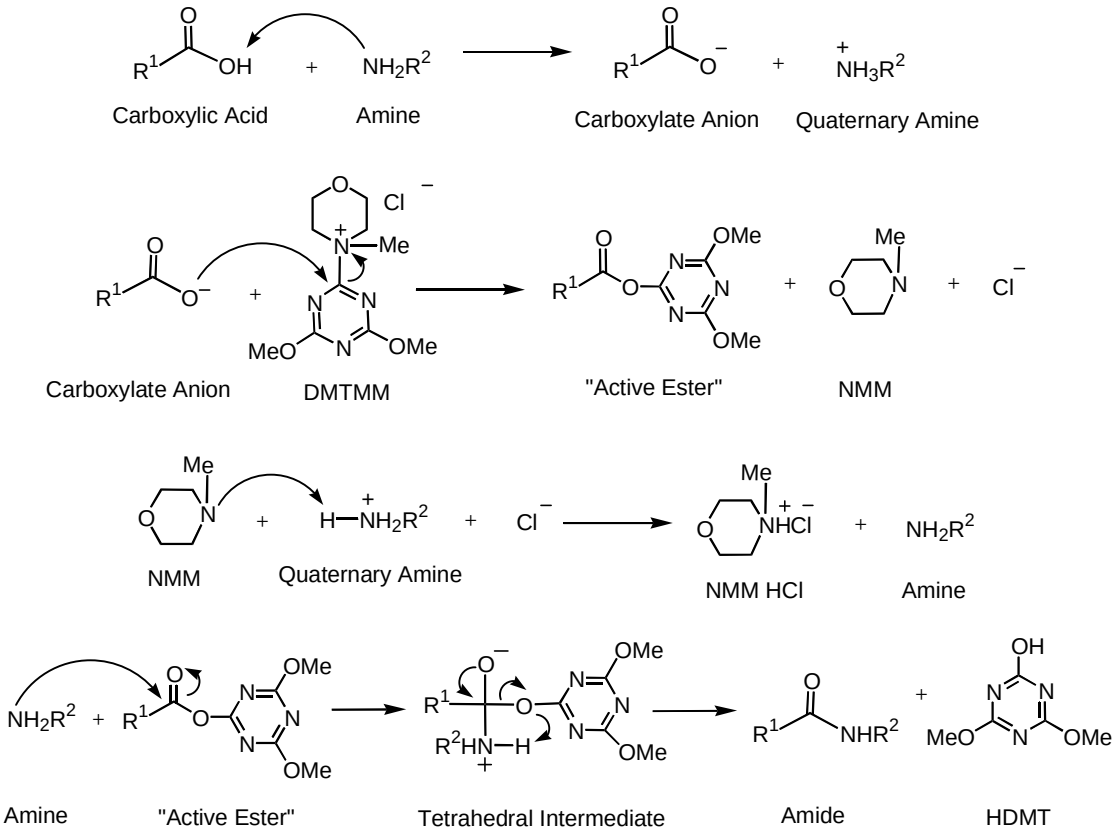

Figure 3.1 – Mechanism for DMTMM Activated Amidation of Carboxylic Acids

DMTMM displays high solubility in water and alcohols without any detectable decomposition. Kunishima and coworkers[28-30] successfully used DMTMM in a one-step condensation of acids and amines in water and alcohols in much higher yields than observed for EDC or DCC. While the effect of pH was not evaluated, neutral conditions should promote the most effective reaction since primary amines are less reactive at low pH, while ester hydrolysis is catalyzed by strong acid and promoted by strong base.

To evaluate DMTMM for polymer modification, acrylamide derivatives were prepared by reacting PAA CO_2H groups with various amines (Table 3.1) using DMTMM in H_2O or MeOH. The overall scheme is shown in Figure 3.2.

Table 3.1 – Amines Used to Prepare Acrylamide-Modified PAA (AmM-PAA)

Amines Investigated (R-NH_2)	**R group**	**AmM-PAA**
Taurine	-$CH_2CH_2SO_3H$	TAmM-PAA
Hydroxyethylamine	-CH_2CH_2OH	HEAmM-PAA
Butyl Amine	-$CH_2(CH_2)_2CH_3$	BAmM-PAA
1H,1H-Pentafluoropropyl Amine	-$CH_2C_2F_5$	PFPAmM-PAA
1H,1H-Heptafluorobutyl Amine	-$CH_2C_3F_7$	HFBAmM-PAA
1H,1H-Pentadecafluorooctyl Amine	-$CH_2C_7F_{15}$	PDFOAmM-PAA

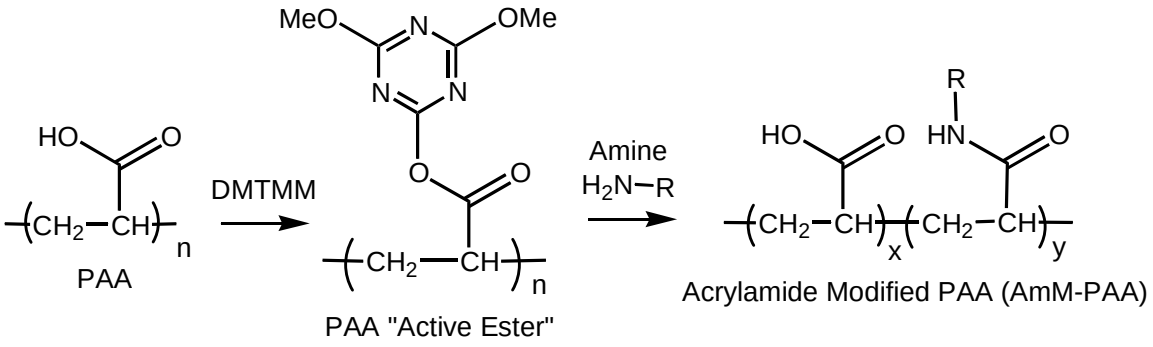

Figure 3.2 – DMTMM Synthesis of Acrylamide-Modified PAA (AmM-PAA)

3.2 EXPERIMENTAL SECTION

3.2.1 Materials

Poly(acrylic acid) (PAA, M_w=450 kg/mole, d=1.41 g/cm^3, Aldrich) powder was dried under vacuum at 60°C before use. Reagent grade methanol (MeOH, Aldrich), sodium chloride (NaCl, Fisher), sodium hydroxide (NaOH, Fisher), *n*-butyl amine (Aldrich), hydroxyethyl amine (2-aminoethanol, Aldrich), taurine (2-aminoethane sulfonic acid, Aldrich), and 4-(4,6-dimethoxy-1,3,5-triazin-2-yl)-4-methylmorpholinium chloride (DMTMM, Acros Organics) were used as received.

1*H*,1*H*-pentafluoropropylamine (PFPA, $C_2F_5CH_2NH_2$, 97%), 1*H*,1*H*-heptafluorobutylamine (HFBA, $C_3F_7CH_2NH_2$, 98%), 1*H*,1*H*-pentadecafluorooctylamine (PDFOA, $C_7F_{15}CH_2NH_2$ 97%), 1,1,2-Trichloro-1,2,2-trifluoroethane (Freon113), and trifluoroacetic acid (TFAA, 99.5 %,) were obtained from SynQuest Labs, Inc. (Alachua, FL) and used as received. Cellu·Sep® H1 regenerated cellulose dialysis membranes with a molecular weight cutoff of 2,000 were obtained from Membrane Filtration Products.

3.2.2 Instrumentation

Proton nuclear magnetic resonance spectra (^{1}H NMR) were recorded on Bruker 300 MHz instruments using deuterated solvents using the solvent peak as a reference. Polymer samples were dissolved in D_2O (99.9% D, Aldrich), MeOH-d_4 (99.5% D, Aldrich), DMSO-d_6 (99.9% D, Aldrich), DMF-d_7 (99.5% D, Aldrich) or CF_3CO_2D (99.5% D, Aldrich) at 1% (w/v). Infrared spectra were recorded on a Bruker Vector 22 instrument. Samples were cast from MeOH or MeOH/Freon 113 onto KBr plates. Spectra were measured at 4 cm^{-1} resolution using 32 scans.

3.2.3 Nomenclature

As listed in Table 1, the sample codes designate the amine incorporated by an amide bond onto the PAA backbone and the acrylamide content of the modified PAA molecule. For example, in the sample code for $TAmM_{96}$-PAA_4, 'TAmM' stands for Taurine Acrylamide Modified, the subscript '96' is the mol % of acrylamide repeat units, 'PAA' stands for poly(acrylic acid), and the subscript '4' is the mol % of acrylic acid repeat units. The sample code '$TAmM_{100}$-PAA_0' stands for poly(taurine acrylamide).

3.2.4 Characterization of Starting Materials

Figure 3.3 shows the ^{1}H NMR spectrum of PAA: (300 MHz, MeOH-d_4) δ 1.7-1.9 (br, 2H, CH_2–CH), 2.5 ppm (s, 1H, CH_2–C*H*). The carboxylic acid proton exchanged completely with hydroxyl protons of the solvent. Thus the carboxylic acid peak was not observed. The ^{1}H NMR spectrum of hydroxyethyl amine is shown in Figure 3.4: (300 MHz, D_2O) δ 2.6 (m, 2H, N–CH_2), 3.4 ppm (m, 2H, O–CH_2). The ^{1}H NMR spectra for taurine: (300 MHz, D_2O) δ 3.2 (m, 2H, N–CH_2), 3.4 ppm (m, 2H, S–CH_2); and butyl amine: (300 MHz, MeOH-d_4) δ 0.93 (s, 3H, CH_3), 1.4 (m, 4H, CH_2–CH_x), 2.6 ppm (m, 2H, N–CH_2). Figure 3.5 shows the ^{1}H NMR spectrum for 1H, 1H-pentadecafluorooctyl amine: (300 MHz, DMF-d_7) δ 2.0 (br, 2H, NH_2) and 3.4 ppm (t, 2H, N–CH_2). Peaks for the protons of amine, hydroxyl and sulfonic acid groups were not observed for ^{1}H NMR spectrum measured in D_2O or MeOH-d_4, due to rapid proton exchange with solvent. All chemical shifts agree well with the literature values.[31,32]

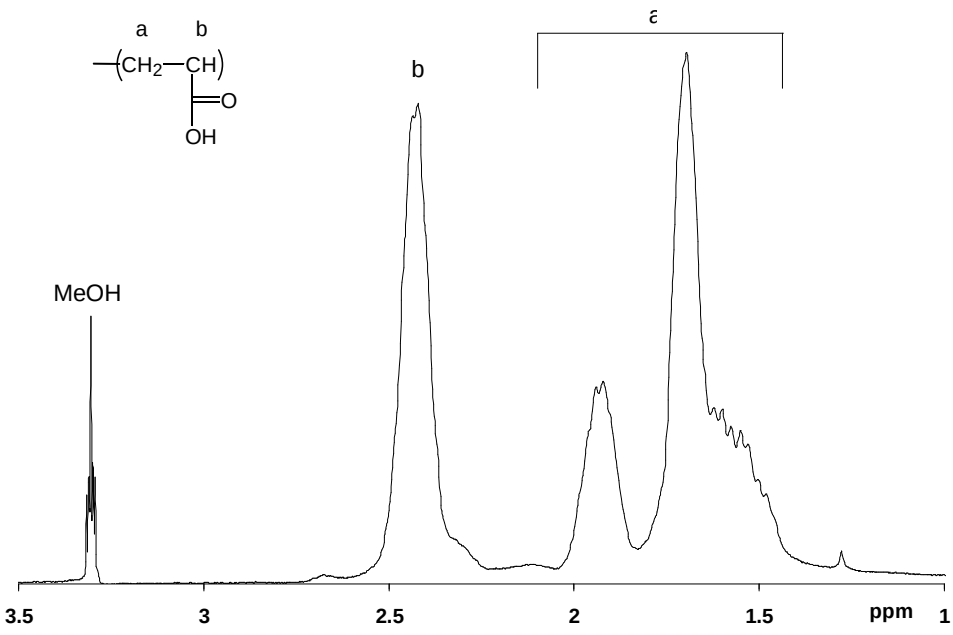

Figure 3.3 – ^{1}H NMR (300 MHz, MeOH-d_4): PAA

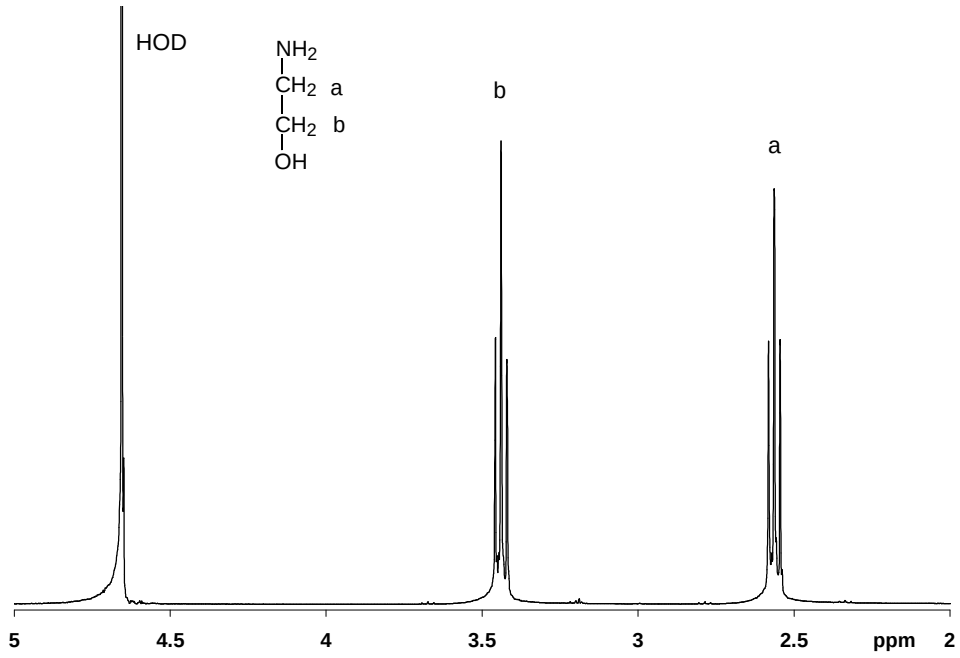

Figure 3.4 – ^{1}H NMR (300 MHz, D_2O): Hydroxyethyl Amine

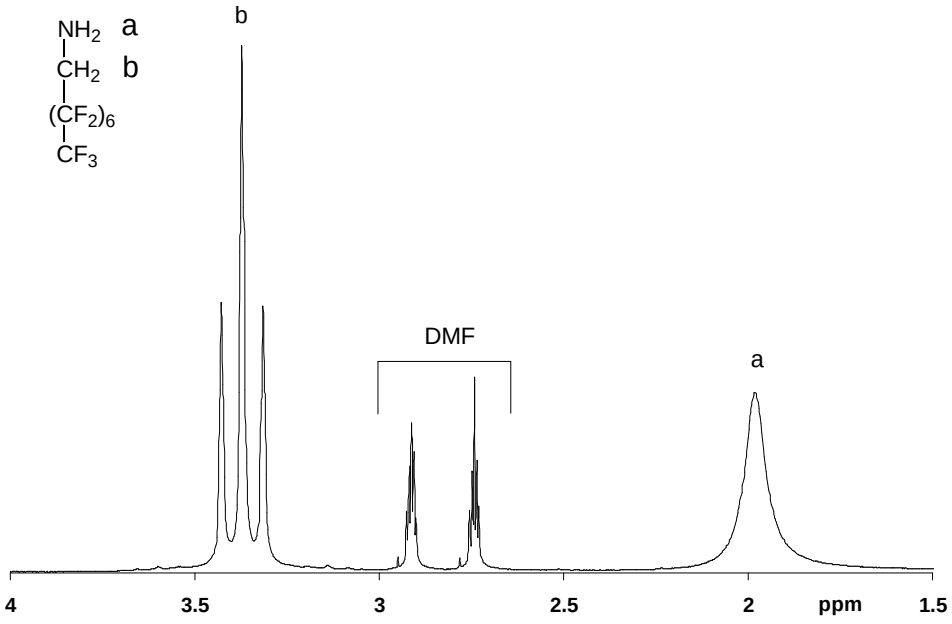

Figure 3.5 – ^{1}H NMR (300 MHz, DMF-d_7): 1H,1H-Pentadecafluorooctyl Amine

Figure 3.6a shows the FTIR spectrum for PAA: 3600-2400 (O–H), 2953 (C–H), 1709 (C=O), 1448 (C–O–H), 1320-1130 (C–O), 795 cm^{-1} (C–H). Figure 3.6b shows the FTIR spectrum of butyl amine: 3616-3060 (N–H stretch), 3034-2675 (C–H stretch), 1595 (N–H bend), 1462 (CH_2 scissoring), 1080 (C–N stretch), 985-721 cm^{-1} (N–H wag). The FTIR spectra of taurine: 3649-3279 (O–H stretch), 3194 (N–H stretch), 3044 (C–H stretch), 1614 (N–H bend), 1510 (CH_2 scissoring), 1261-1126 (asymmetric S=O), 1040 cm^{-1} (symmetric S=O); hydroxyethyl amine: 3346-3173 (overlapping O–H/N–H stretch), 2953-2735 C–H stretch), 1593 (N–H bend), 1454 (CH_2 scissoring), 1074-866 cm^{-1} (C–O stretch); and 1H, 1H-pentadecafluorooctyl amine: 3472-3150 (N–H stretch), 3007-2835 (C–H stretch), 1628 (N–H bend), 1440 (CH_2 scissoring), 1377-1065 cm^{-1} (C–F).

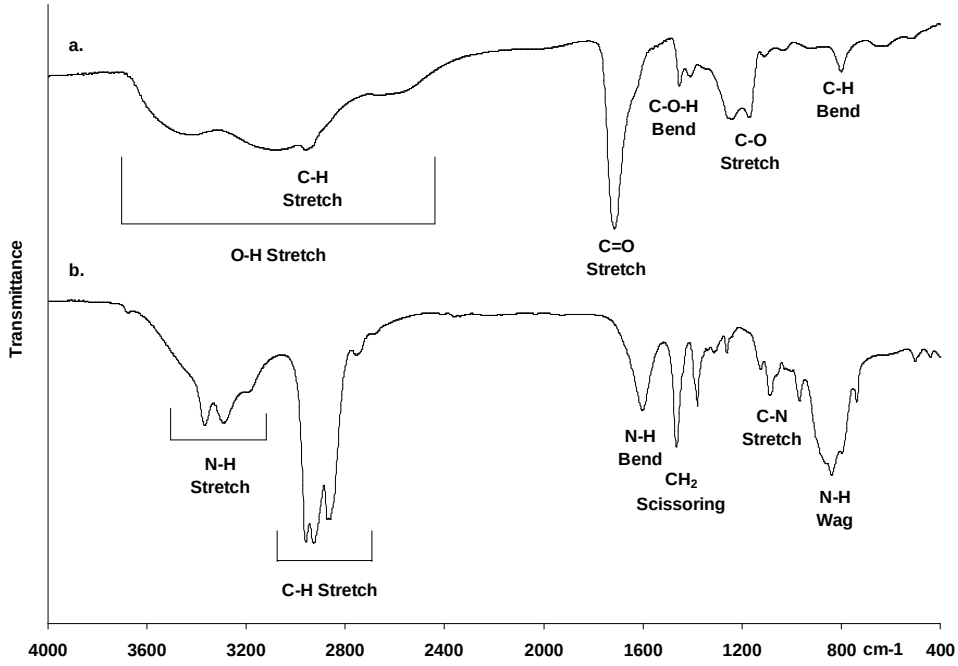

Figure 3.6 – FTIR: (a) PAA and (b) Butyl Amine

3.2.5 Typical Preparation of Acrylamide-Modified PAA

Taurine Acrylamide-Modified PAA (TAmM-PAA)

PAA (0.135 g, 1.88 mmol) was dissolved in distilled H_2O (35 ml). Taurine (0.469 g, 3.75 mmol) was added to the solution with NaOH (0.150 g, 3.75 mmol) to neutralize the taurine SO_3H groups. Then DMTMM (1.037 g, 3.75 mmol) was dissolved in distilled H_2O (10 ml) and added to the solution. The reaction proceeded with mixing for 24 hours. The clear reaction mixture was dialyzed against distilled H_2O for 7 days. A white solid product was isolated by drying under vacuum at 60°C for 24 hours (0.302 g, 92%). Figure 3.7 shows the $TAmM_{96}$-PAA_4 ^1H NMR spectrum: (300 MHz, D_2O) δ 1.27 (br, 2H, C*H*$_2$–CH), 1.82 (br, 1H, CH_2–C*H*), 3.0 (s, 2H, N-C*H*$_2$), 3.4 ppm (s, 2H, S-C*H*$_2$). The acrylamide content (96%) was determined from the ratio of the average peak intensity of the main chain methylene and methyne protons (0.5% standard deviation between peaks

a and b) vs. the average peak intensity of the side chain methylene protons adjacent to the nitrogen and sulfur atoms (2% standard deviation between peaks c and d).

Figure 3.8 shows the FTIR spectrum for $TAmM_{96}$-PAA_4 cast from MeOH: 3300-2500 (O–H), 3300-3000 (N–H), 2930 (C–H), 1707 (C=O, acid), 1651 (C=O, amide I), 1544 (N–H, amide II), 1443 (CH_2), 1195 (S=O), 1045 cm^{-1} (S=O). The acrylamide content was confirmed by the decrease of the carboxylic acid peak at 1707 cm^{-1} and the appearance of the amide I and II bands at 1651 and 1544 cm^{-1} from the FTIR spectrum.

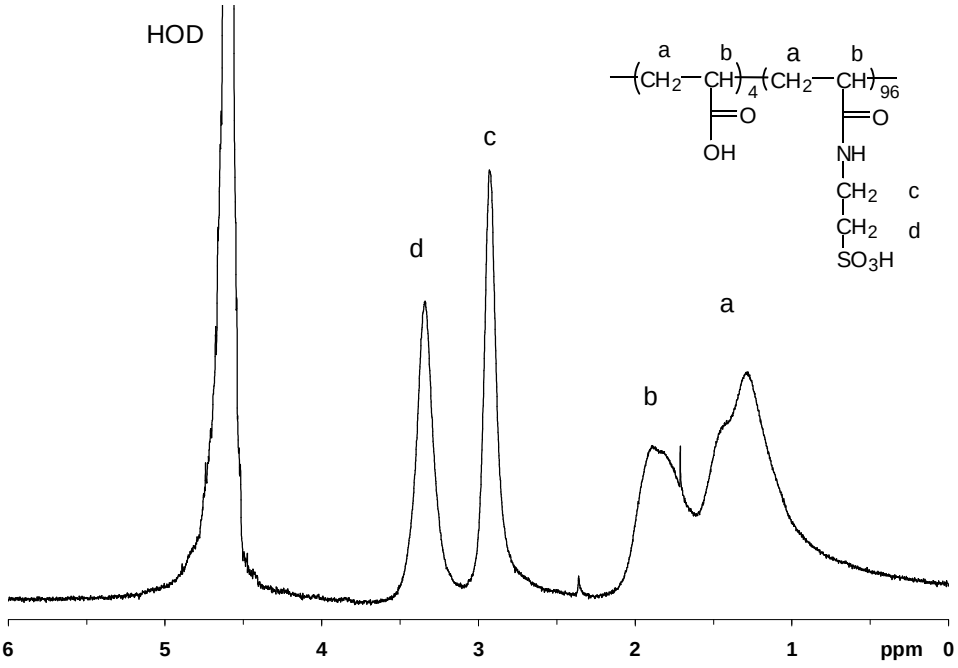

Figure 3.7 – ^1H NMR (300 MHz, D_2O): $TAmM_{96}$-PAA_4

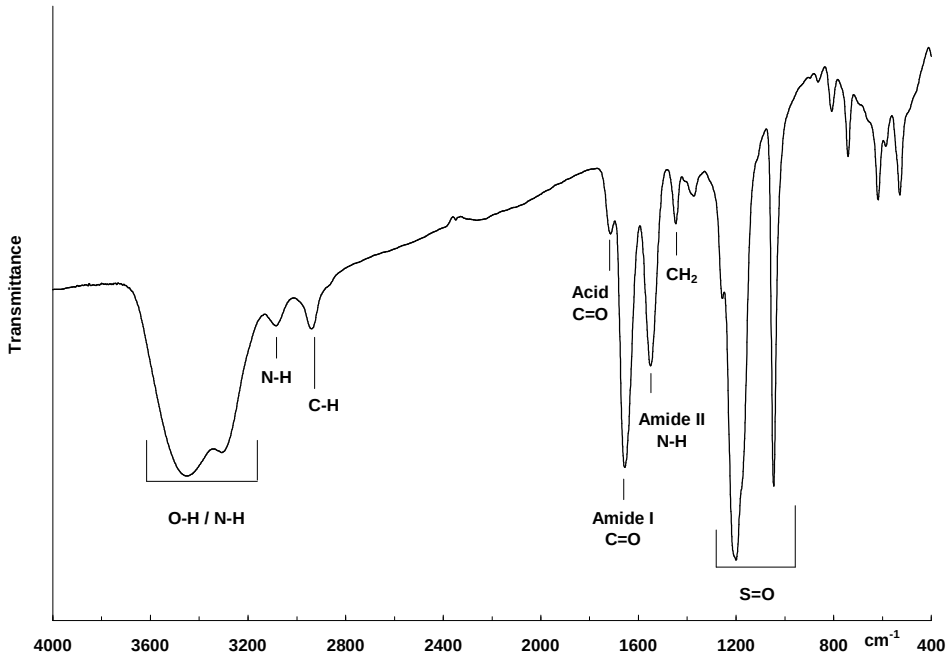

Figure 3.8 – FTIR: $TAmM_{96}$-PAA_4

Hydroxyethyl Acrylamide-Modified PAA (HEAmM-PAA)

PAA (0.135 g, 1.88 mmol CO_2H) was dissolved in distilled H_2O (35 ml) and hydroxyethyl amine (0.230 g, 3.75 mmol) was added to the solution. Then DMTMM (1.037 g, 3.75 mmol) was dissolved in distilled H_2O (10 ml) and added to the solution. The reaction proceeded with mixing for 24 hours. The clear reaction mixture was dialyzed against distilled H_2O for 3 days for complete purification. A white solid product was isolated by drying under vacuum at 60°C for 24 hours (0.208 g, 96%). Figure 3.9 shows the $HEAmM_{100}$-PAA_0 ^1H NMR spectrum: (300 MHz, D_2O) δ 1.27 (br, 2H, C*H*$_2$–CH), 1.82 (br, 1H, CH_2–C*H*), 3.0 (s, 2H, N-C*H*$_2$), 3.4 ppm (s, 2H, S-C*H*$_2$). The acrylamide content (100%) was determined from the ratio of the average peak intensity of the main chain methylene and methyne protons (0.5% standard deviation between

peaks a and b) vs. the average peak intensity of the side chain methylene protons adjacent to the nitrogen and oxygen atoms (1% standard deviation between peaks c and d).

Figure 3.10 shows the FTIR spectrum for $HEAmM_{100}$-PAA_0 cast from MeOH: 3300-2500 (O–H), 3300-3000 (N–H), 2930 (C–H), 1647 (C=O, amide I), 1553 (N–H, amide II), 1443 (CH_2), 1061 cm^{-1} (O–H). The acrylamide content was confirmed by the complete disappearance of the carboxylic acid peak at 1709 cm^{-1} and the appearance of the amide I and II bands at 1647 and 1553 cm^{-1} from the FTIR spectrum.

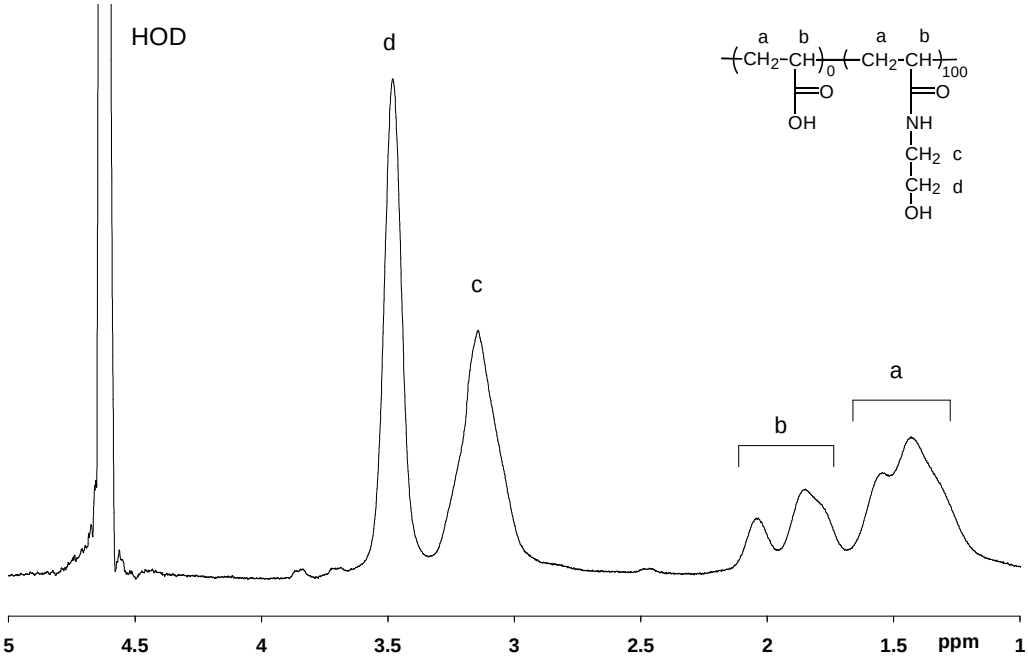

Figure 3.9 – ^1H NMR (300 MHz, D_2O): $HEAmM_{100}$-PAA_0

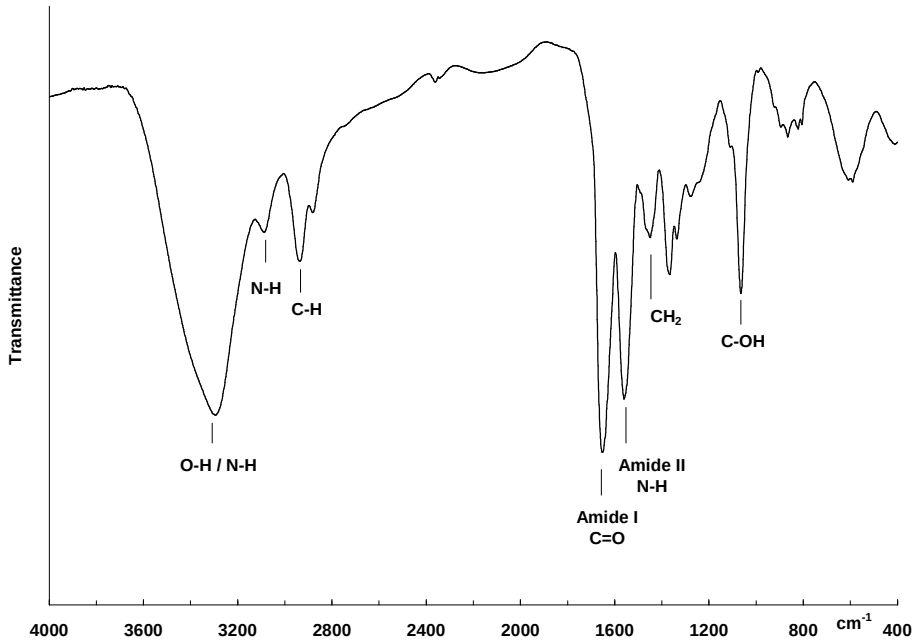

Figure 3.10 – FTIR: $HEAmM_{100}$-PAA_0

Butyl Acrylamide-Modified PAA (BAmM-PAA)

PAA (0.135 g, 1.88 mmol CO_2H) was dissolved in distilled H_2O (35 ml) and butyl amine (0.344 g, 4.70 mmol) was added to the solution. Then DMTMM (1.301 g, 4.70 mmol) was dissolved in distilled H_2O (10 ml) and added to the solution. A white solid began to precipitate from solution within several hours of DMTMM addition. Mixing was continued for 24 hours. The product was purified by two precipitations from MeOH into H_2O and dried under vacuum at 80°C for 3 days (0.142 g, 60%). Figure 3.11 shows the $BAmM_{98}$-PAA_2 ^{1}H NMR spectrum: (300 MHz, DMSO-d_6) δ 0.9 (s, 3H, CH_3), 1.2-1.8 (br, 6H, CH_2), 1.8 (br, 1H, C*H*), 3.0 (s, 2H, N-CH_2), 3.35 (s, 2H, H_2O), 4.5 ppm (br, 1H, N*H*). A large amount of H_2O was observed in spite of extensive drying. However enough DMSO-d_7 was present for the amide peak to be observed in the spectrum. The acrylamide content (98%) was determined from the ratio of the peak intensity of the main

chain methyne protons (peak b) vs. the average peak intensity of the side chain methyl, methyne, and amine protons (6% standard deviation between peaks e, c and f). Typically, CH_3 peaks > N-CH_2 peaks > NH peaks.

Figure 3.12 shows the FTIR spectrum for BAmM_{98}-PAA_2 cast from MeOH: 3300-2500 (OH), 3300-3000 (N–H), 3000-2800 (C–H), 1703 (C=O, acid) 1651 (C=O, amide I), 1545 (N–H, amide II), 1441 cm^{-1} (CH_2). The acrylamide content was confirmed by the decrease of the carboxylic acid peak at 1703 cm^{-1} and the appearance of the amide I and II bands at 1651 and 1545 cm^{-1} from the FTIR spectrum.

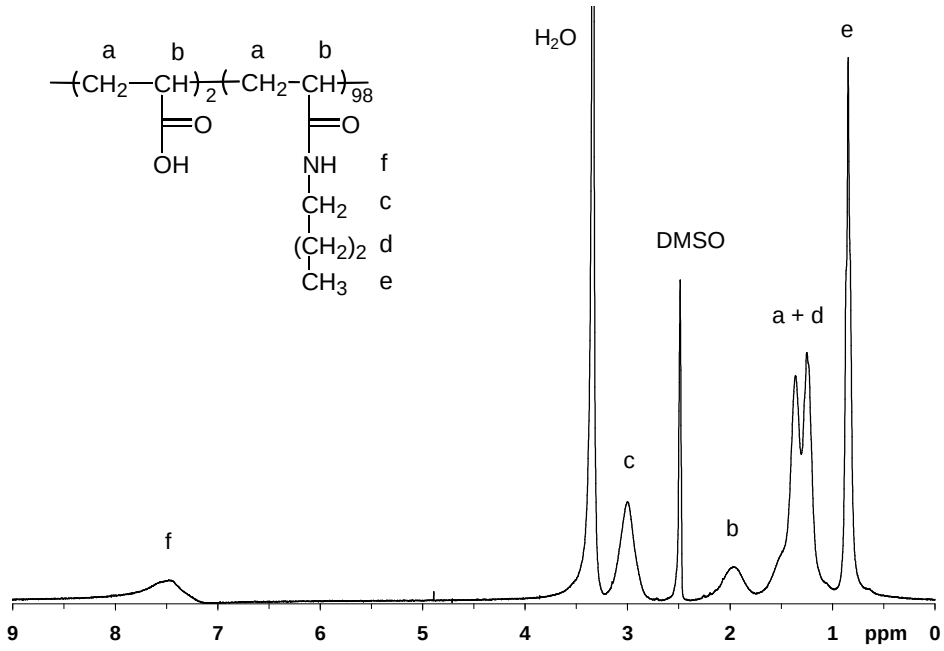

Figure 3.11 – ^{1}H NMR (300 MHz, DMSO-d_6): BAmM_{98}-PAA_2

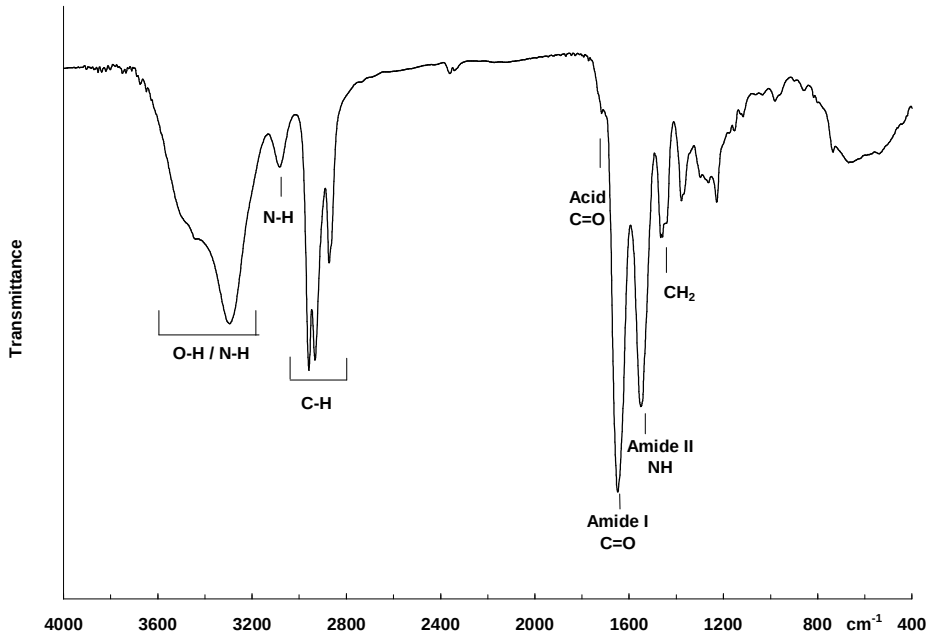

Figure 3.12 – FTIR: $BAmM_{98}$-PAA_2

1H, 1H-Pentadecafluorooctyl Acrylamide Modified PAA (PDFOAmM-PAA)

PAA (0.090 g, 1.25 mmol CO_2H) was dissolved in MeOH (35 ml) and PDFOA (0.187 g, 0.469 mmol) was added to the solution. Then DMTMM (0.130 g, 0.470 mmol) was dissolved in MeOH (10 ml) and added to the solution. The reaction proceeded with mixing for 24 hours. The reaction product was precipitated into H_2O, purified by two precipitations from 0.1M CF_3CO_2H (in MeOH) into H_2O, and dried under vacuum at 50°C for 24 hr (0.131 g, 51%). Figure 3.13 shows the $PDFOAmM_{35}$-PAA_{65} ^{1}H NMR spectrum: (300 MHz, MeOH-d_4 /CF_3CO_2D) 1.7-1.9 (br, 2H, CH_2–CH), 2.4 (br, 1H, CH_2–CH), 3.7 (N–CH_2), 4.0 ppm (NH^+). The acrylamide content (35%) was determined from the ratio of the average peak intensity of the main chain methyne and methylene protons (peaks a and b) vs. the side chain methyne protons adjacent to the nitrogen (peak c). As the NH_2/CO_2H and/or $DMTMM/CO_2H$ ratios were increased, the acrylamide

contents of the reaction products increased. While reaction products having acrylamide contents > 50% precipitated from solution within one hour of DMTMM addition, all reaction mixtures were mixed for 24 hours.

The FTIR spectrum for PDFOAmM_{52}-PAA_{48} cast from MeOH/Freon 113 is shown in Figure 3.14: 3300-2500 (O–H), 3076 (N–H), 2928 (C–H), 1720 (C=O, acid), 1657 (C=O, amide I), 1541 (N–H, amide II), 1448 (CH_2), 1234-1144 cm^{-1} (C–F). In this case, the C=O acid band at 1720 cm^{-1} is quite strong, as expected for approximately equal acid and acrylamide contents.

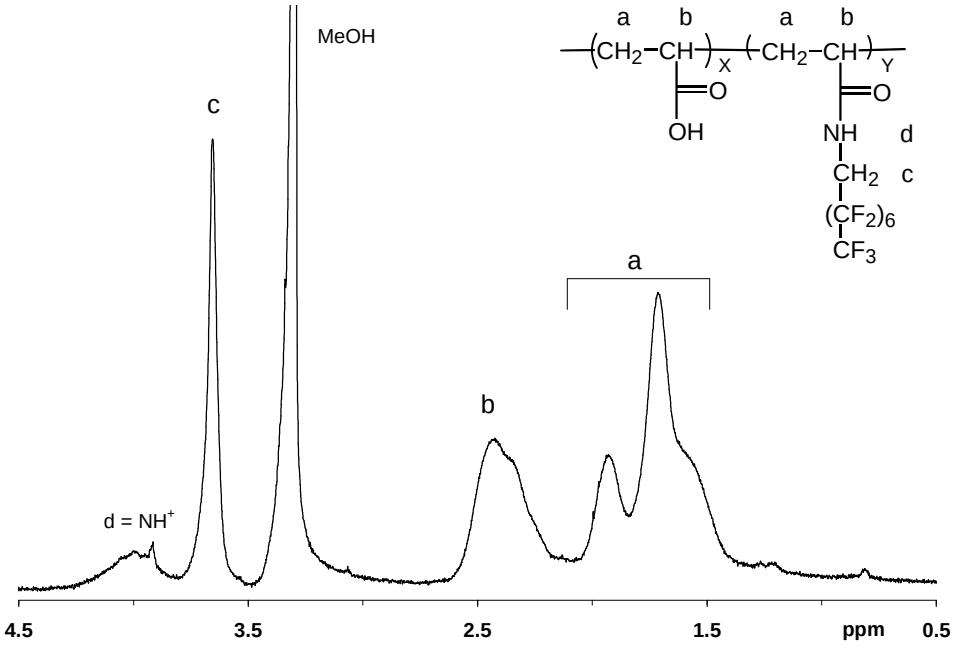

Figure 3.13 – ^{1}H NMR (300 MHz, MeOH-d_4/CF_3CO_2D): PDFOAmM_{35}-PAA_{65}

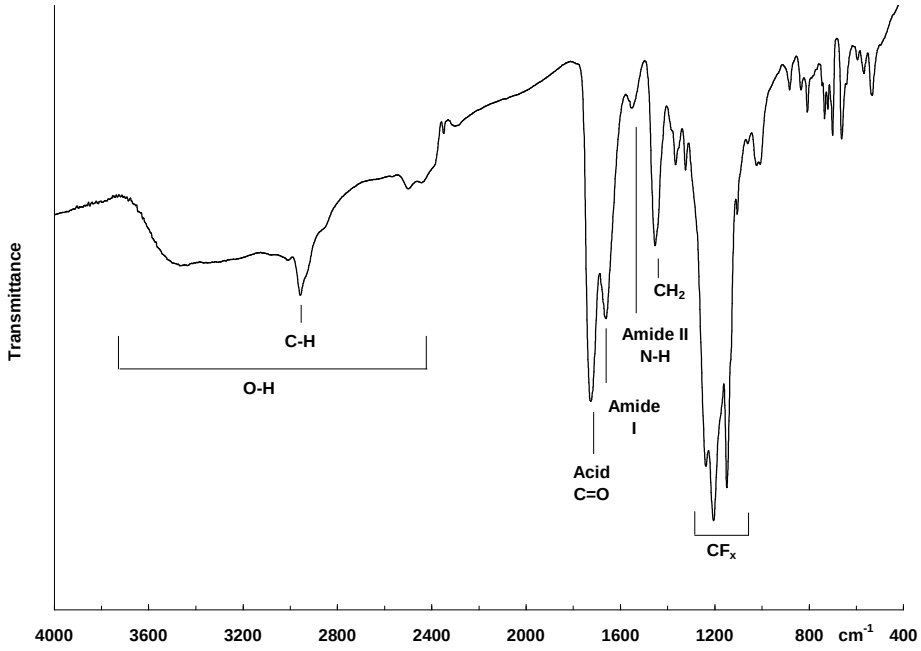

Figure 3.14 – FTIR: PDFOAmM$_{52}$-PAA$_{48}$

3.3 RESULTS AND DISCUSSION

By altering the synthetic conditions, it was possible to control the acrylamide content of the PAA derivatives. Tables 3.2–3.4 show the reaction conditions and acrylamide contents for TEAmM-PAA, HEAmM-PAA, and BAmM-PAA, respectively. Product yields for TEAmM-PAA and HEAmM-PAA were very high. However, strong ionic interactions between TEAmM-PAA and residual taurine increased the dialysis times for these reaction mixtures. Product yields for BAmM-PAA, PFPAmM-PAA, HFBAmM-PAA, and PDFOAmM-PAA were lower due to losses during reprecipitation.

For TEAmM-PAA and HEAmM-PAA, nearly 100% acrylamide contents were achieved with a 2/2/1 DMTMM/NH_2/CO_2H ratio. The grafting efficiency (~50%) was independent of conversion and concentration. All TEAmM-PAA and HEAmM-PAA products were H_2O soluble. For BAmM-PAA, nearly 100% acrylamide content was

achieved using a 2.5/2.5/1 DMTMM/NH_2/CO_2H ratio. The grafting efficiency (~40%) decreased with increasing acrylamide content for equal amine and DMTMM levels, but increased with increasing amine levels for constant levels of DMTMM. BAmM-PAA products with ≥77% acrylamide content precipitated from H_2O. These results indicate that DMTMM reacts with amine, but complete amidation of PAA can be achieved with an excess of both reagents even if the final reaction product precipitates from H_2O.

Table 3.2 – PAA Modification with Taurine

Run #	PAA in H_2O (g/L)	DMTMM/NH_2/CO_2H Molar ratio	% Amide	% DMTMM Efficiency	H_2O
1	3	1.00 / 1.00 / 1	46	46	Soluble
2	3	2.00 / 2.00 / 1	96	48	Soluble
3	11	2.00 / 2.00 / 1	96	48	Soluble

Table 3.3 – PAA Modification with Hydroxyethyl Amine

Run #	PAA in H_2O (g/L)	DMTMM/NH_2/CO_2H Molar ratio	% Amide	% DMTMM Efficiency	H_2O
1	1	2 / 2 / 1	99	49	Soluble
2	10	2 / 2 / 1	100	50	Soluble

Table 3.4 – PAA Modification with Butyl Amine

Run #	Solvent for PAA 3g/L	DMTMM/NH_2/CO_2H Molar ratio	% Amide	% DMTMM Efficiency	H_2O
1	H_2O	0.50 / 1.00 / 1	34	68	Soluble
2	H_2O	0.75 / 1.00 / 1	35	47	Soluble
3	H_2O	1.00 / 1.00 / 1	41	41	Soluble
4	H_2O	1.25 / 1.00 / 1	44	35	Soluble
5	H_2O	1.00 / 2.00 / 1	53	53	Gelation
6	H_2O	2.00 / 1.00 / 1	77	38	Insoluble
7	H_2O or MeOH	2.00 / 2.00 / 1	88	44	Insoluble
8	H_2O or 50 mM NaCl	2.50 / 2.50 / 1	98	39	Insoluble

Tables 3.5-3.7 show the reaction conditions and acrylamide contents for PFPAmM-PAA, HFBAmM-PAA, and PDFOAmM-PAA. The solubility of the reaction products in MeOH decreased with increasing acrylamide content and fluorocarbon segment length. For all acrylamide contents, PFPAmM-PAA products were MeOH soluble in while HFBAmM-PAA products were semi-soluble. PDFOAmM-PAA products with ≥52% acrylamide content precipitated from MeOH.

Table 3.5 – PAA Modification with 1H, 1H-Pentafluoropropyl Amine (PFPA)

Run #	PAA in MeOH (g/L)	DMTMM/NH_2/CO_2H Molar ratio	% Amide	% DMTMM Efficiency	MeOH
1	2	2.00 / 2.00 / 1	59	30	Soluble
2	1	2.00 / 2.00 / 1	65	33	Soluble
3	0.5	2.00 / 2.00 / 1	82	41	Soluble

Table 3.6 – PAA Modification with 1H, 1H-Heptafluorobutyl Amine (HFBA)

Run #	PAA in MeOH (g/L)	DMTMM/NH_2/CO_2H Molar ratio	% Amide	% DMTMM Efficiency	MeOH
1	2	2.00 / 2.00 / 1	51	26	Semisoluble
2	1	2.00 / 2.00 / 1	59	30	Semisoluble
3	0.5	2.00 / 2.00 / 1	68	34	Semisoluble

Table 3.7 – PAA Modification with 1H, 1H-Pentadecafluorooctyl Amine (PFPA)

Run #	PAA in MeOH (g/L)	DMTMM/NH_2/CO_2H Molar ratio	% Amide	% DMTMM Efficiency	MeOH
1	2	0.20 / 0.20 / 1	20	100	Soluble
2	2	0.40 / 0.40 / 1	35	88	Soluble
3	2	0.60 /0.60 / 1	37	62	Soluble
4	2	0.40 / 1.00 / 1	30	75	Soluble
5	2	0.60 / 1.00 / 1	46	77	Soluble
6	2	0.80 / 1.00 / 1	55	69	Insoluble
7	2	1.50 / 1.50 / 1	52	33	Insoluble
8	2	2.00 / 2.00 / 1	60	30	Insoluble
9	1	2.00 / 2.00 / 1	70	35	Insoluble
10	0.5	2.00 / 2.00 / 1	79	40	Insoluble

The reaction efficiency decreased with increasing acrylamide content, but increased with higher levels of amine for constant DMTMM. Further, the efficiency of PAA reaction with perfluoroamines increased with dilution (0.5 g/L PAA, ~40%), which is comparable to butyl amine (3 g/L PAA, ~38%) but less than taurine or hydroxyethyl amine (• 3 g/L PAA, ~50%). MeOH reactions with perfluorinated alkyl amines did not achieve complete PAA conversion over the evaluated concentration range. This may be due to the ability of PAA carboxylic acid groups ionize in H_2O, enhancing PAA solubility during reaction with butyl amine. The longer perfluorinated acrylamide reaction products typically precipitated within one hour of DMTMM addition while the butyl acrylamide reaction products precipitated after several hours. This indicates that the inherent solubility of longer perfluorinated reaction products in MeOH is lower compared to butyl acrylamide reaction products in H_2O. Aqueous PAA ionization also extends the PAA backbone in solution. An open structure allows greater access to PAA reaction sites and may allow the butyl amine reaction to proceed further. In contrast, PAA carboxylic acid groups remain unionized in MeOH and are coiled in solution.

Another factor is the association of the side chains of hydrophobically modified PAA. The perfluorinated side chains of acrylamide-modified sodium polyacrylate associate more strongly than their hydrocarbon analogues in aqueous solution and the associations increase at higher extent of modification and polymer concentration.[24] PFPAmM-PAA and PDFOAmM-PAA had similar acrylamide contents and reaction efficiencies, despite differences in solubility, and the acrylamide contents and reaction efficiencies increase similarly as polymer concentration is lowered. These results suggest that high molecular weight, interconnected aggregates restricted access of DMTMM and perfluorinated alkyl amines to PAA groups during the modification process.

3.4 CONCLUSIONS

Several model acrylamide derivatives of poly(acrylic acid) (PAA) were prepared by reaction of PAA with amine-functional molecules in homogeneous solution using DMTMM condensing reagent. By altering reaction conditions, derivatives of differing side chain structures and lengths, hydrophobic character, and acrylamide content were prepared. Reactions proceeded very smoothly in very high conversions using DMTMM in either water or alcohol. Reactions of PAA with taurine, ethanolamine, and butyl amine in H_2O advanced to ~100% modification with 40-50% DMTMM/NH_2 efficiencies in the PAA concentration range of 0.5–11g/L. For the reaction of PAA with taurine, the DMTMM reaction efficiency was equivalent to the reaction efficiencies reported for the EDC-activated taurine modification of poly(γ-glutamic acid).[27] Reaction products of taurine and hydroxyethyl amine were H_2O soluble, while reaction products of butyl amine were insoluble in H_2O after exceeding 77% acrylamide content.

By decreasing PAA concentration higher levels of modification were achieved. At 0.5 g/L PAA, ~80% modification with 1H, 1H-pentadecafluorooctyl amine (PDFOA) was observed at 40% DMTMM/NH_2 efficiency. Reaction products of PDFOA were insoluble in MeOH after exceeding 52% acrylamide content. The relationship between solubility and extent of modification will be an important factor in the modification of PAA surface-grafted nanoscaffolds, and will be discussed further in Chapter 5.

CHAPTER 4

SYNTHESIS OF SURFACE-GRAFTED NANOSCAFFOLDS

4.1 INTRODUCTION

The successful preparation of a fluorinated SGN surface relies on high SGN surface coverage. SGN surface coverage likewise relies on how the scaffold polymer bonds to the surface. Surface-grafting can be regarded as a case of irreversible adsorption. Simple models of irreversible adsorption for particles will be used to develop reasonable predictions for SGN adsorption, reorganization and grafting processes.

4.1.1 Models of Particle Adsorption

Random Sequential Adsorption (RSA) Model

The essentials of polymer adsorption can be described by the random sequential adsorption (RSA) model of Feder[33] (Figure 4.1). Polymer molecules (denoted by impenetrable spheres) adsorb sequentially in randomly selected locations on a uniform surface. If overlap with a preadsorbed particle occurs, the trial is abandoned. Otherwise, the particle remains fixed. Surface coverage at time τ (θ_τ) is given by:

$$\theta_\tau = \pi R^2 \rho_p \qquad (4.1)$$

where R is the radius of the adsorbing particle and ρ_p is the particle surface concentration. The surface fills rapidly at first, but adsorption slows with time as

additional molecules crowd the surface. When no further spheres can be added, the "jamming limit" surface coverage ($\theta_\infty = 0.547$) is reached.

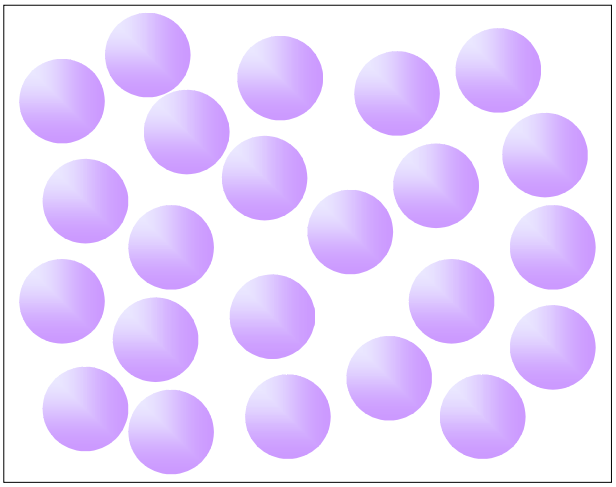

Figure 4.1 – RSA Model

Polydisperse RSA (PD-RSA) Model

Adamczyk and coworkers[34] developed the polydisperse RSA (PD-RSA) model, Figure 4.2, to consider the influence of particle size polydispersity. Particle radius (a) was chosen randomly from a distribution of average radius ($\bar{a}$), standard deviation (σ), and relative standard deviation ($\bar{\sigma}$) for $\bar{\sigma} < 0.20$. One definition of surface coverage was:

$$\theta_p = \sum S_i \rho_i = \sum \pi a_i^2 \rho_i \qquad (4.2)$$

where S_i is the projected area of the i^{th} particle. This equation is correct, but the measurement of all adsorbed particle sizes is experimentally impractical. Therefore, a second definition of surface coverage was used:

$$\theta_e = \bar{S}\rho_p = \pi \bar{a}^{-2} \rho_p \qquad (4.3)$$

where $\bar{s}$ is the average projected area which can be measured experimentally from the average particle size ($\bar{a}$) in the bulk. As polydispersity increased, surface coverage exceeded the RSA jamming limit (0.547) with smaller particles adsorbing preferentially. The value of $\theta_{p,\infty}$ increased linearly with $\bar{\sigma}$, reaching full coverage at $\bar{\sigma}$ = 0.85, while the value of $\theta_{e,\infty}$ increased parabolically with $\bar{\sigma}$, reaching full coverage at $\bar{\sigma}$ = 0.24:

$$\theta_{p,\infty} = 0.547 + 0.53\bar{\sigma} \qquad (4.4)$$

$$\theta_{e,\infty} = 0.547 + 0.458\bar{\sigma} + 6.055\bar{\sigma}^{2} \qquad (4.5)$$

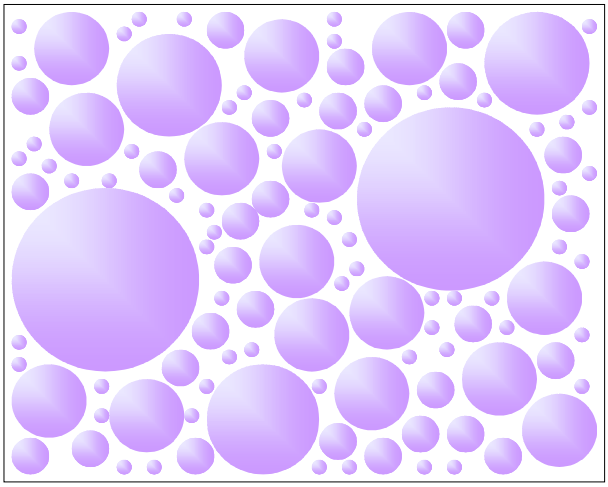

Figure 4.2 – PD-RSA Model

Effective Hard Sphere PD-RSA (EHS-PD-RSA) Model

Adamczyk and coworkers[34-37] included inter-particle repulsions into an effective hard sphere PD-RSA (PD-EHS-RSA) model. Hard spheres interacted through a repulsive electrostatic potential described by the Debye parameter (κ) that is proportional to the square root of the salt concentration. This force increased the effective particle radius (a_{eff}) by h ($\sim\kappa^{-1}$) and decreased surface coverage (Equations 4.6 and 4.7).

$$a_{eff} = a + h \tag{4. 6}$$

$$\theta_{\infty} = 0.547\left(a/a_{eff}\right)^2 \tag{4. 7}$$

At low κa values, the repulsion between particles was strong, the distance between adsorbed particles was greater and θ_{∞} was lower than for the RSA model (Figure 4.3).

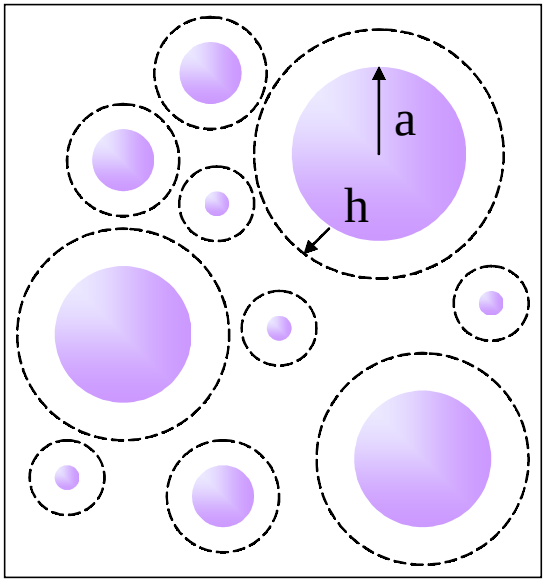

Figure 4.3 – EHS-PD-RSA Low κa

At high values of κa, electrostatic repulsions are screened which allowed closer packing and higher surface coverage (Figure 4.4). As κa increased, θ_∞ asymptotically approached the RSA jamming limit.

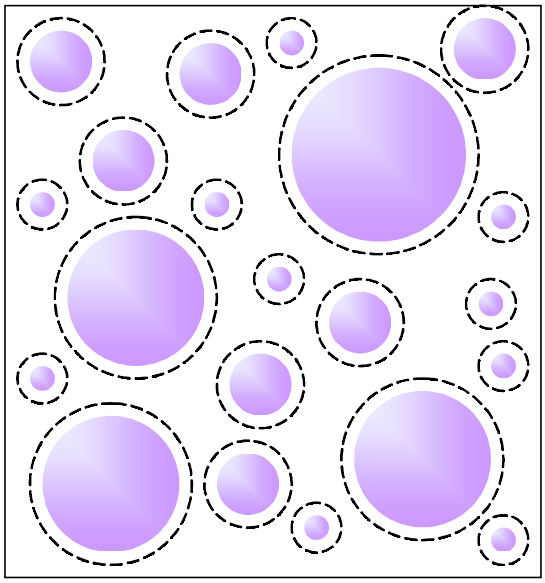

Figure 4.4 – EHS-PD-RSA High κa

Random Site (RS) Model

RSA models assume that binding sites are uniformly (or continuously) distributed on the surface. For many real surfaces, however, the binding sites vary in number, distribution and selectivity. In the Random Site (RS) model, developed by Jin and coworkers[38], the binding sites are randomly distributed point sites on a surface of area L^2 with a site density ρ_s. The adsorbing particles are impenetrable hard spheres. If a particle of diameter σ can be centered on a binding site without overlapping with a previously adsorbed particle, then it irreversibly adsorbs. Elapsed time is proportional to

the number of attempts (N_A) made to adsorb particles. The dimensionless time (τ) and dimensionless site density (α) are defined as:

$$\tau = \pi\sigma^2 N_A / 4L^2 \quad (4.8)$$

$$\alpha = \pi\sigma^2 \rho_s / 4 \quad (4.9)$$

Surface coverage $\theta(\tau, \alpha)$ depended upon τ and α. At small α values, the distance between binding sites was generally greater than σ. For high α values, the surface was fairly uniform and approached the RSA jamming limit. An exact mapping relationship was found between the RS and RSA model such that θ_∞ for the RS model was equal to θ_∞ of the RSA model at $\tau = \alpha$ and is given by the following equation:

$$\theta_\infty(\tau = \alpha) = 0.547\left(1 - \frac{1 + 0.3136\tau^2 + 0.45\tau^3}{1 + 1.8285\tau + 0.6553\tau^3 + \tau^{7/2}}\right) \quad (4.10)$$

Adaptive RSA (A-RSA) Model

RSA models also assume that particles are non-deformable, i.e. hard spheres. Real macromolecules, such as polymers or proteins, are flexible. Douglas and coworkers[39] created the adaptive RSA (A-RSA) model, Figure 4.5, for flexible chains adsorbing onto attractive surfaces. When a chain arrives at a surface, it adapts its conformation to the space available for adsorption. The first chains to arrive adsorb in relatively flat conformations, while those arriving later adsorb more loosely. The A-RSA

model assumes that particle deposition occurs as a random sequential adsorption of hemispherical objects with a disc-shaped base. The volume of the particle is fixed, but the shape and cross-section vary. The size of the disc base adjusts to fill the available uncovered space surrounding the disc center.

The surface coverage increased as the ratio (λ) of the smallest disc radius to the largest disc radius decreased. Complete coverage of the surface occurred when there was no lower cut-off limit. This is a significant departure from the classical RSA model. For real polymer deposition, a maximum disc base size is set by the maximum area onto which a given chain length can spread during adsorption. The minimum disc base size could be set by the number of bonds that are necessary for firm surface attachment. However, polymer chains in solution may be sterically hindered by previously adsorbed polymer chains from approaching neighboring regions on the surface. In this case, the diameter of the polymer chain in solution may be a more reasonable lower cut-off limit.

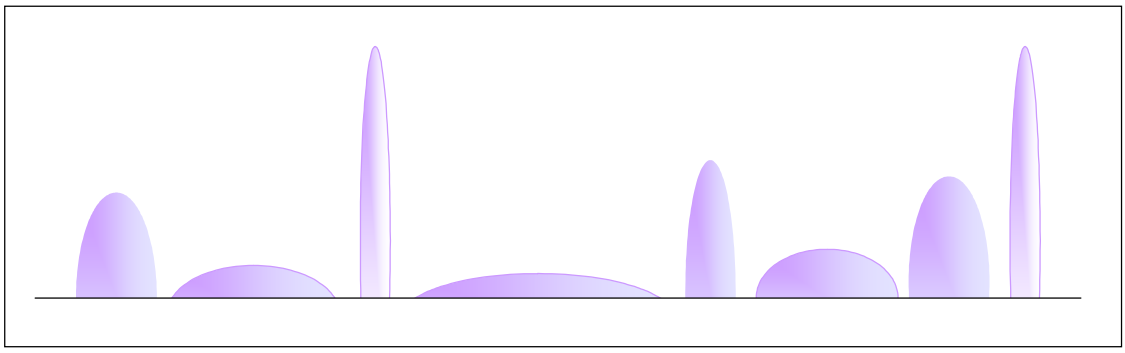

Figure 4.5 – A-RSA Model

Post-Adsorption Conformational Change RSA (PCC-RSA) Model

Although proteins adopt compact forms in solution, they have been observed to spread on contact with a surface. Such behavior can be described as an initial reversible adsorption of the macromolecule in a solution state (α) followed by a conformational transition to an altered state (β) of greater surface contact and irreversible binding, shown in Figure 4.6. Molecules arriving late in the process may be sterically hindered from converting to the second state, and will be more likely to desorb.

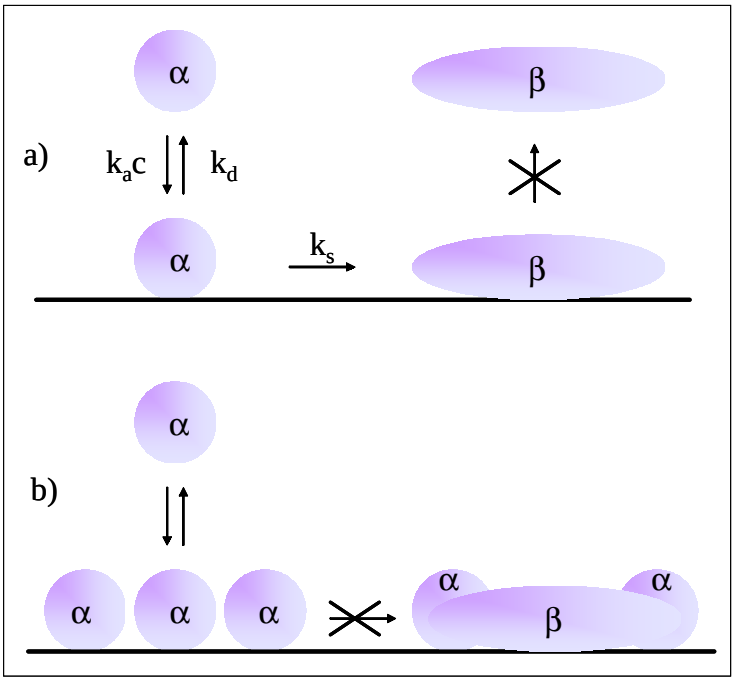

Figure 4.6 – (a) Reversible Adsorption Followed by Irreversible Post-Adsorption Transition where $k_a c$, k_d, and k_s are the Adsorption, Desorption, and Spreading Rates and *c* is the Absorbing Particle Concentration in Solution. (b) Neighboring Particles Preventing Post-Adsorption Transition.

Van Tassel and coworkers[40,41] developed the post-adsorption conformational change RSA (PCC-RSA) model (Figure 4.7) to describe macromolecules such as proteins. Macromolecules (denoted as discs of diameter σ_α) adsorb sequentially onto a

surface. Following adsorption, a particle (i) desorbs from the surface or (ii) attempts to spread discretely and symmetrically to a larger diameter σ_β. Both of these competing events occur at prescribed rates. Spreading that leads to overlap with another particle is rejected and the particle remains with diameter σ_α. Following successful spreading, the particle becomes irreversibly bound to the surface. Several values of spreading magnitude $\Sigma=\sigma_\beta/\sigma_\alpha$, relative spreading rate $K_s = k_s/\left(k_a c\left(\pi\sigma_\alpha^2/4\right)\right)$, and relative desorption rate $K_d = k_d/\left(k_a c\left(\pi\sigma_\alpha^2/4\right)\right)$ were evaluated. For proteins, Σ can be defined as the dimension ratio of the denatured state vs. the native state. For polymers, Σ can be defined as the dimension ratio of a fully extended chain vs. a chain in solution.

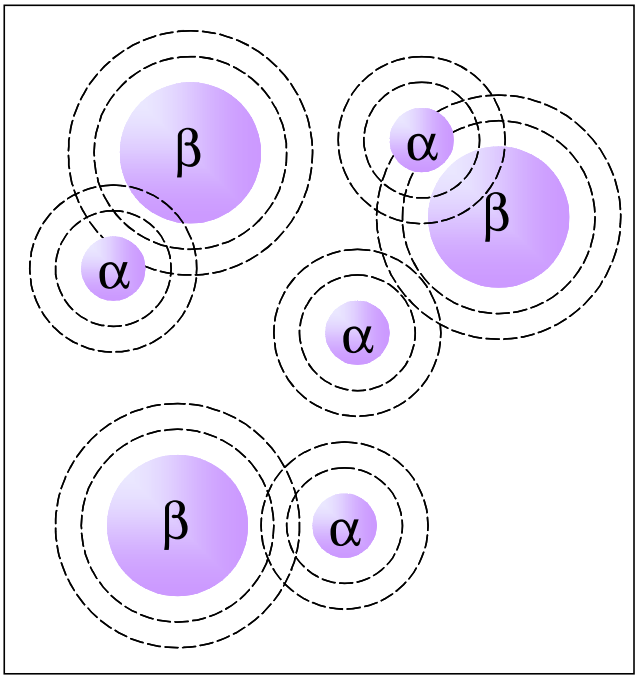

Figure 4.7 – PCC-RSA model. Exclusion Circles Surround Each Disk.

The first model was the case of purely irreversible adsorption, when $K_d = 0$. For instantaneous spreading ($K_s=\infty$), the α-particle density increased and the β-particle

density decreased as Σ increased, due to steric restrictions to spreading. The total surface coverage increased with Σ, due to greater particle polydispersity, and θ_∞ significantly exceeded the RSA jamming limit. For large K_s, both α-particle and β-particle coverage approached those for instantaneous spreading. For small K_s, the α particle coverage approached the RSA and the β-particle coverage approached zero. For moderate spreading (K_s=1), α-particle density was initially higher than β-particle density, and both increased linearly with time. However, β-particle saturation surface coverage approached zero for large Σ, since for finite K_s all particles became blocked from spreading by neighboring particles. Thus, the total surface coverage displayed a maximum for $\Sigma > 1$ where θ_∞ slightly exceeded the RSA jamming limit.

The second model was the case of reversible adsorption, when $K_d \neq 0$. Values of surface coverage exceeding the RSA jamming limit were obtained for large Σ, and smaller K_d and K_s. These values were higher than those obtained for the case of irreversible adsorption. This was attributed to a more fluid layer of α-particles that equilibrates to more efficient packing. Surface coverage exceeding $\theta_\infty = 0.68$ was observed for $\Sigma = 1.5$ at the lowest K_d and K_s values.

4.1.2 Molecular Dimensions of Polymers

In the Adaptive RSA (A-RSA) and Post-Adsorption Conformational Change RSA (PCC-RSA) models, polymer molecules are represented as hard discs of a certain diameter which have the ability to spread symmetrically to a larger diameter. In reality, a polymer molecule in solution is a constantly coiling and uncoiling chain whose

conformation in space is dynamic. In very dilute solution the individual molecules are considered to move independently. Each molecule can be pictured as a spherical cloud of chain segments having radial symmetry. The radius of the molecular cloud can be used as a parameter to characterize the average size of the polymer chain. For linear chains, this may be represented by the root-mean-square (RMS) end-to-end distance $\sqrt{\overline{r^2}}$, the RMS distance of all atoms in the molecule from its center of mass, known as the radius of gyration R_g, or the radius of a hard sphere that has the same hydrodynamic friction as the polymer molecule, known as the hydrodynamic radius R_h[42].

The number-average molecular weight M_n and RMS end-to-end distance $\sqrt{\overline{r^2}}$ are determined from dilute solution viscometry, while the weight-average molecular weight M_w and z-average radius of gyration $R_{g,z}$ are determined from static small-angle light (SLS), x-ray (SAXS) or neutron (SANS) scattering methods. The RMS end-to-end distance and the radius of gyration follow the relation[42]:

$$\overline{r^2} = 6R_g^2 \tag{4. 11}$$

In "good" solvents polymer coils are relatively extended, while in "poor" solvents they are relatively contracted when compared to their unperturbed state. One measure of the expansion of the polymer coil is the expansion factor α defined as:

$$\alpha = \frac{\sqrt{\overline{r^2}}}{\sqrt{\overline{r_0^2}}} = \frac{R_g}{R_{g,o}} \qquad (4.12)$$

where $\sqrt{\overline{r_0^2}}$ and $R_{g,o}$ are unperturbed dimensions of the polymer chain. A value of α=1 corresponds to an extremely poor solvent, known as a Flory (Θ) solvent, or a temperature near the critical solution temperature, known as the Flory (Θ) temperature[42]. The radius of gyration R_g varies with molecular weight as follows:

$$R_g \propto M^{1/\nu} \qquad (4.13)$$

where $1/\nu$ is the fractal dimension of the molecule. As shown by Flory[42], the fractal dimension $1/\nu$ is predicted to be 3/5 for fully solvated chains, 1/2 for unperturbed chains in a Flory (Θ) solvent, and 1/3 for collapsed chains. Polymer chains are fully solvated in good solvent in which polymer-solvent interactions are favored over polymer-polymer interactions. In a Flory (Θ) solvent, polymer-polymer interactions are equal to the polymer-solvent interactions and the polymer behaves as a Gaussian chain. Polymer chains are collapsed in poor solvent where polymer-polymer interactions are favored over polymer-solvent interactions. The fractal dimension $1/\nu$ provides a measure of polymer coil expansion. Smaller fractal dimensions imply more tightly coiled chains.

The hydrodynamic radius R_h is defined as the radius of a hard sphere having the same hydrodynamic friction as the polymer molecule in the given medium. The value of R_h is sensitive to the size and shape of the molecule, which are determined by its

conformation and hydrodynamic interactions with the solvent. The diffusion coefficient D is related to R_h by the Stokes-Einstein equation:

$$D = k_B T / 6\pi\eta_o R_h \qquad (4.\ 14)$$

where k_B is the Boltzmann constant, T is temperature, and η_0 is solvent viscosity.[43] Hydrodynamic radius R_h follows the same molecular weight scaling relation as R_g and has the same scaling exponent $1/\nu$. The relation between R_g and R_h is more complex:

$$R_g = \rho\, R_h \qquad (4.\ 15)$$

where ρ is a constant that depends upon the molecular geometry. For uncharged polymers in the globular state, $\rho \cong 0.77$, which corresponds to a sphere, while for strongly charged polyelectrolyte in the globular state ρ is close to 1.5. For uncharged polymers in the random coil state, $\rho \sim 1.5$ while for strongly charged polyelectrolytes in the random coil state, $\rho \sim 2.5$. This indicates that strongly charged polyelectrolytes form less dense structures compared to neutral polymers[44].

The diffusion coefficient D has previously been obtained from dynamic light scattering (DLS) measurements. Pulse field gradient (PFG) NMR has been used to measure the diffusion coefficients of molecules in solution. Böhme and Scheler[45] used PFG NMR to study the size R_h of polystyrene sulfonate in aqueous solution. The effect of ionic strength on R_h and the fractal dimension were determined. As ionic strength was

increased, the R_h of the polyelectrolyte decreased while the fractal dimension decreased, indicating that the polyelectrolyte chains contracted as the ionic strength increased.

Wilkins and coworkers[46] used PFG NMR to determine the effective R_h and scaling exponent $1/\nu$ for native and denatured proteins. The value $1/\nu = 0.29$ for native folded proteins resembled the 0.33 value predicted by Flory for a collapsed polymer, while the $1/\nu = 0.57$ for highly denatured proteins was similar to the 0.6 value predicted by Flory for polymer in a good solvent. A good correlation was observed between the effective R_h values obtained from PFG NMR and literature R_h values obtained for the same proteins from either PGF NMR or DLS, as well as with literature R_g values obtained from either SAXS or SANS. The R_h values were first converted to R_g values by setting ρ equal to the offset between the logarithmic plots of R_g and R_h vs. the number of residues in the polypeptide chain. A reference molecule (1,4-dioxane) with a known R_h value was used as a viscosity probe. The R_h values for each protein were obtained from:

$$R_h = \left(D^o / D\right) R_h^o \qquad (4.16)$$

where $D°$ and $R_h°$ are the diffusion coefficient and hydrodynamic radius of the reference 1,4-dioxane molecule. This approach eliminates the use of absolute solution viscosity and diffusion coefficient values, both of which are subject to error.

4.1.3 Control of PAA Dimensions

Polyacrylic acid (PAA) was selected as the SGN polymer because the carboxylic acid functional groups of PAA will be used to bond the SGN to the nylon 6,6 substrate as

well as to incorporate fluoroalkyl side chains within the SGN. However, PAA was also selected because it is a polyelectrolyte, which allows the molecular dimensions of the polymer chain to be readily controlled.

Polyelectrolytes are polymers containing ionizable or charged groups on the main chain or in side groups. These charges are the basis of the water solubility of polyelectrolytes. PAA molecules in aqueous solution are weak polyelectrolytes, since only a small fraction of the acid groups dissociate (the pK of acrylic acid in water at 25°C is 4.25).[47] The fundamental model of polyelectrolytes in aqueous solution consists of polymer chains of charged monomers, an equal number of oppositely charged counter-ions and optionally salt ions of both charge signs. The conformation of the polyelectrolyte is controlled by the electrostatic interaction between these charged species, polyelectrolyte concentration, chain length, and the ionic strength of the solution.

PAA molecules are uncharged random coils in polar organic solvents such as MeOH, DMF, 1,4-dioxane, NMP, and DMSO. Specifically, 1,4-dioxane at 30 °C is a theta solvent for PAA with an "inverted" phase diagram and a lower critical solution temperature of 30 °C, below which the PAA solubility increases. Therefore, PAA is unperturbed (α=1) in 1,4-dioxane at 30 °C and slightly perturbed at 25 °C (α= 1.26).[48]

However, in aqueous salt-free solution, PAA ionizes. Okubo[49] determined the degree of ionization *i* using electric conductance measurements. The degree of ionization *i* for dilute PAA solutions ($\leq$ 0.4 g/L) was 3–5 % at 25°C and decreased with increasing concentration, characteristic of polyelectrolyte behavior. The conformation of PAA molecules in aqueous solution was determined by Okubo[49,50], Hoffmann and coworkers[51] using solution viscosity, which is related to the RMS end-to-end distance of the PAA

molecule. PAA molecular conformation was also determined by Okubo[49,50] using the conductance stopped-flow method and Hoffman and coworkers[51] using transient electric birefringence measurements. These techniques induce anisotropic molecular orientation and follow the relaxation process as the molecules revert to random orientations. The relaxation is an exponential process having a rotational relaxation time constant τ_r, which is related to the size of the molecule. The effective length L of a PAA molecule was estimated from τ_r, using a spherical model for unionized PAA and a rod model for ionized PAA. Such lengths were determined as a function of polymer concentration, pH, and ionic strengths.

All of these experiments revealed a conformational transition with changing pH. At low pH, PAA molecules are uncharged and adopt a tightly coiled form. At pH ~ 6, the acid groups begin to dissociate and the coils begins to open. At pH ~ 8, chains are fully ionized and stretch to a more extended form due to electrostatic repulsion of the anionic groups. With further increase of pH, chains recoil due to increased ionic strength. The addition of salt or an increase in polymer concentration also causes the highly extended chains to shrink due to increased ionic strength.

PAA molecular dimensions in aqueous solution have been reported from intrinsic viscosity and scattering techniques, such as SLS[48,52,53], DLS[52,53] or SAXS[54,55]. Table 4.1 lists PAA molecular dimensions determined for various molecular weights, % ionization (NaOH), and ionic strength (NaCl). A molecular weight independent dimension was calculated, represented by $R_{g,z} / \sqrt{N}$ where N is the number of repeat units in the polymer. The expansion factor α was calculated from these dimensions measured in theta solvent and good solvents. Where R_g or R_h values were determined for various

molecular weights, the fractal dimension $1/\nu$ was calculated. When R_g and R_h values were determined, the ratio $R_h / \sqrt{N}$ and the constant $\rho = R_g/R_h$ have been calculated.

Values for α indicate that PAA expands as the solvent quality improves. Uncharged PAA chains in salt-free aqueous solution or sodium poly(acrylate) (NaPAA) chains at low ionic strength are more expanded than NaPAA chains in high ionic strength aqueous solution. The ratio $\rho \sim 1.5$ for NaPAA chains at high ionic strength indicates that all charges have been screened and the polymer is a random coil. The fractal dimension $1/\nu$ for PAA in dioxane at 30 C° and NaPAA in ≥ 1.0M NaCl at 25°C are both ~0.5, indicating Flory (Θ) conditions. Even so, the molecular dimensions of NaPAA are greater than those of PAA, as shown by an expansion factor $\alpha > 1$.

Table 4.1– Molecular Dimensions of Polyacrylic Acid from Literature

	Dioxane **30 °C**	**Dioxane** **25 °C**	**Water** **25 °C**	**0.1 M NaCl** **25 °C**	**1.0 M NaCl** **25 °C**	**1.5 M NaCl** **25 °C**
M_W (kg/mol)	134-1220	450	590	73-3300	18-296	171-3150
% Ionized	0	0	0	100	100	100
$R_{g\,z}/\sqrt{N}$ (Å)	2.65	3.33	6.60	7.42	4.41	4.59
$R_h/\sqrt{N}$ (Å)				4.05	2.90	2.99
ρ				1.84	1.47	1.53
α	1.00	1.26	2.49	2.41 - 3.02	1.66	1.73
$1/\nu$	0.48			0.60	0.52	0.52
Solvent	Theta	≅ Theta	Good	Very Good	Theta	Theta
Method	SLS[48]	SAXS[54]	SAXS[55]	SLS/ DLS[52]	SLS/ DLS[53]	SLS/ DLS[52]

4.1.4 Particle Adsorption Models and SGN Synthesis

Surface grafting of PAA, the SGN scaffold polymer, onto nylon 6,6 can be optimized using the Post-Adsorption Conformational Change RSA (PCC-RSA) model. The spreading magnitude Σ will be greater when $R_{gz}/\sqrt{N}$ is low, since the PAA chains will be more compact in solution. This will result in greater surface coverage of PAA chains. However, spreading magnitude Σ, relative spreading rate K_s, and relative desorption rate K_d will decrease as the number of surface attachments per chain increases. PAA chains with multiple surface attachments may form trains or small loops close to the surface and will have lower surface coverage, while PAA chains with fewer surface attachments will have more expanded structures and greater surface coverage.

The number of reactive sites on nylon 6,6 is also important. Nylon 6,6 is the polycondensation product of hexamethylene diamine and adipic acid (Figure 4.8), which results in amine and carboxyl end groups. Generally, the amine end group content in textile fibers ranges 20–80 μmol/g.[56] Since the number of amine groups on the surface of nylon 6,6 is relatively scarce, PAA surface coverage will depend even more on the spreading magnitude Σ of the PCC-RSA model.

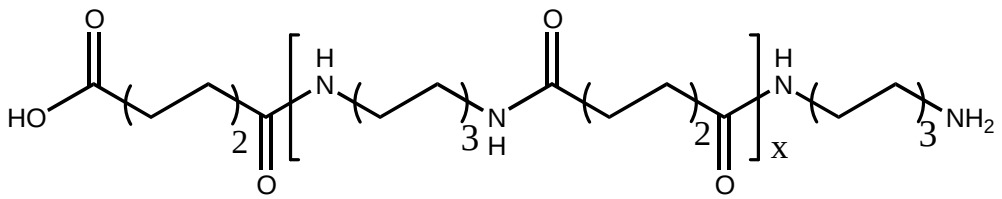

Figure 4.8– Chemical Structure of Nylon 6,6

4.1.5 Surface Grafting of Polymers onto Nylon 6,6

Michielsen[57] developed a surface modification technique which reduced the frictional properties of nylon fibers by grafting polymeric lubricants onto the nylon amine end groups. For nylon 6,6 (M_w = 34 kg/mol, ρ = 1.14 g/cm^3) assuming (a) 2 end groups are present per chain, (b) 1/3 of all chain ends are amine groups, and (c) only amine groups within 1 nm of the surface are accessible for reaction: the number of amine groups on the surface was 0.014 NH_2/nm^2, which corresponds to a surface area per graft site of A=90 nm^2. The surface fraction of the graft chain, represented by $\pi R_g^2/A$, where R_g is the radius of gyration of the lubricant, was determined. The friction coefficients of the modified fibers decreased as the surface fraction of the graft chain increased, with the minimum friction coefficient corresponding to a surface fraction of unity.

Tobiesen and Michielsen[58] and Sherrill and coworkers[59] developed a technique to increase the hydrophilicity of nylon 6,6 polymers surfaces by grafting polyacrylic acid (PAA) with nylon 6,6 amine end groups from aqueous solution. The PAA chain dimensions were determined to be much larger than the area between nylon 6,6 graft sites. Under optimized conditions, ~57% of the surface was covered with PAA, measured by XPS. This appears to conform with, rather than exceed, the RSA jamming limit. However, the influence of PAA adsorption on the structure and surface coverage of the PAA chains was overlooked.

4.1.6 Mechanism of PAA Adsorption onto Nylon 6,6

Nylon 6,6 is a strongly attractive surface for PAA. Cole and Howard[60,61] studied the PAA adsorption mechanism on nylon 6,6 powders. Nylon amine chain ends and

amide repeat units were the primary sites for interaction with PAA carboxylic acid groups. Protection of amine groups reduced PAA adsorption 50% while protection of the amide groups reduced adsorption 60%. At low pH, charge effects were not as important as coil size. Adding NaCl to uncharged PAA solutions led to similar equilibrium adsorption. Charge effects and coil size were factors when PAA was partially ionized with NaOH. When 485 kg/mol PAA was 10% ionized, viscosity increased 3-fold and adsorption dropped 33%. However, 12% ionization in the presence of 1% NaCl did not increase viscosity and adsorption was only reduced 13%.

Charge effects were dominant at higher degrees of ionization (pH>5.5): 120 kg/mol PAA did not adsorb at 50% ionization, while 3 kg/mol PAA did not adsorb at 38% ionization, despite smaller dimensions. Further, ionization with NaOH was shown to remove adsorbed PAA from the nylon surface. Alternately, adsorbed PAA has been removed by high levels of salt, which compete with polymer chains for surface sites.[62] Successive rinsing in high ionic strength solution was used to completely remove noncovalently bound PAA from amine functional surfaces.

4.1.7 PAA Surface-Grafted Nanoscaffolds on Nylon 6,6

In the present study, two approaches were considered to achieve the most successful PAA grafting and highest SGN surface coverage. The first approach was to follow the technique of Tobiesen and Michielsen[58] and Sherrill and coworkers[59] using DMTMM condensing reagent. In a second approach, the inherent attraction between PAA and nylon 6,6 was utilized. By adsorbing PAA onto nylon 6,6 first, the grafting

process was made more efficient, the number of graft points per molecule was optimized, and surface coverage exceeding the RSA "jamming limit" was observed.

First, a Solution-Grafting was performed using DMTMM condensing reagent (Figure 4.9) in which PAA concentration and DMTMM/CO_2H ratios were varied. Results were compared to the work of Tobiesen and Michielsen[58] and Sherrill and coworkers.[59] Next, Adsorption-Grafting was performed using DMTMM condensing reagent (Figure 4.10). In the first step of this process, PAA was adsorbed from solution onto the nylon 6,6 substrate using the strong ionic interactions between PAA anions and nylon amine and amide groups.[60,61] In the second step, adsorbed PAA was grafted in-situ by immersing the substrate in a solution of DMTMM condensing reagent. At each step in the reaction, the chemical composition of the film was measured with x-ray photoelectron spectroscopy (XPS) while the wetting ability of the film was measured by static water contact angle. Each technique was also used to calculate the PAA surface fraction on the film and the results from each technique were compared.

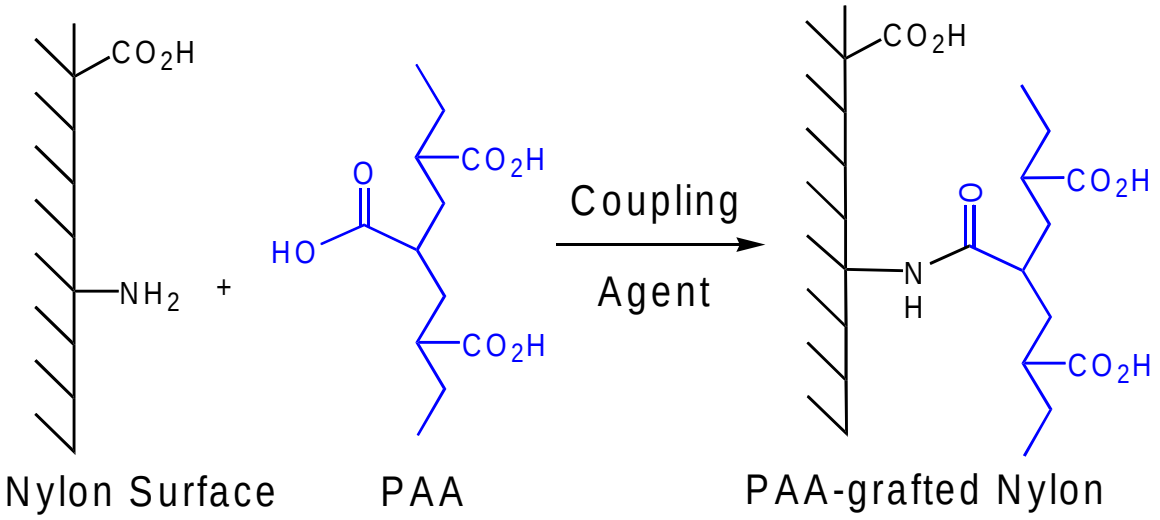

Figure 4.9– Solution-Grafting Process

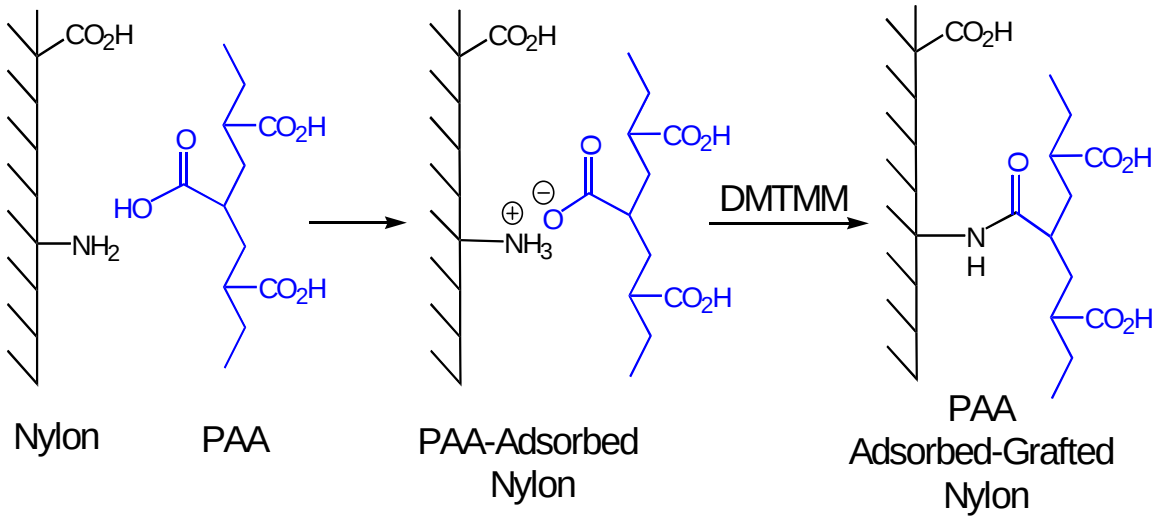

Figure 4.10– Adsorption-Grafting Process

4.2 EXPERIMENTAL SECTION

4.2.1 Materials

Nylon 6,6 film (M_n: 12 kg/mole, DuPont Canada), poly(acrylic acid) (PAA, M_w: 450kg/mol, Aldrich), sodium hydroxide (NaOH, Fisher), sodium thiocyanate (NaSCN, Fisher) and 4-(4,6-dimethoxy-1,3,5-triazin-2-yl)-4-methylmorpholinium chloride (DMTMM, Acros Organics) were used as received.

4.2.2 Typical Procedures

Nylon 6,6 Stability at Various pH

Control treatments were performed on nylon 6,6 films. A 2×2 cm^2 nylon 6,6 film was (1) immersed in 1M NaOH (pH=14) for 2 hr, (2) rinsed in distilled H_2O for 2 hr, (3) heated in distilled H_2O for 2 hours at 65°C, and (4) air dried. A second film was (1) immersed in 0.1M HCl (pH=3) for 15 minutes, (2) rinsed in distilled H_2O for 2 hr, (3) heated in distilled H_2O for 2 hours at 65°C, and (4) air dried.

Solution-Grafted (SG) Nylon

PAA (0.050 g, 0.69 mmol) was dissolved in distilled H_2O (35 ml) with vigorous mixing at 25°C. Then 2×2 cm^2 nylon 6,6 films were immersed in the PAA solution for 15 min. DMTMM (0.192 g, 0.69 mmol) was dissolved in distilled H_2O (10 ml) and added to solution to initiate grafting. The reaction proceeded for 24 hr. Selected films were wiped with a Kimwipe™ cloth wet with distilled H_2O, wiped with a Kimwipe™ cloth wet with acetone, and air dried prior to surface analysis. The rest of the Solution-Grafted films underwent the PAA desorption process.

Adsorption-Grafted (AG) Nylon

PAA (0.050 g, 0.69 mmol) was dissolved in distilled H_2O (45 ml) with vigorous mixing at 25°C. Then 2×2 cm^2 nylon 6,6 films were immersed in the PAA solution overnight to adsorb PAA onto the surface. Next, the films were immersed in distilled H_2O and rinsed with vigorous mixing for 24 hr. This step was repeated twice with fresh distilled H_2O. Selected films were wiped with a Kimwipe™ cloth wet with distilled H_2O, wiped with a Kimwipe™ cloth wet with acetone, and air dried prior to surface analysis. Others underwent the PAA desorption process. The rest of the PAA adsorbed films were immersed in solutions prepared by dissolving DMTMM (0.048 g, 0.17 mmol) in distilled H_2O (45 ml) with vigorous mixing at 25°C. The reaction proceeded for 24 hr. Selected films were wiped with a Kimwipe™ cloth wet with distilled H_2O, wiped with a Kimwipe™ cloth wet with acetone, and air dried prior to surface analysis. The rest of the Adsorption-Grafted films underwent the PAA desorption process.

Desorption of PAA from Nylon 6,6

PAA-treated nylon 6,6 surfaces were (1) rinsed overnight with vigorous shaking in 1M aqueous NaSCN solution (repeated twice with fresh solution), (2) rinsed overnight in distilled H_2O (repeated twice with fresh solution), (3) heated in distilled H_2O for 3 hours at 65°C, (4) wiped with a Kimwipe™ cloth wet with distilled H_2O, (5) wiped with a Kimwipe™ cloth wet with acetone, and (6) and air dried.

4.2.3 Surface Characterization

Contact Angle Analysis

Contact angles were measured from sessile water drops using a goniometer and camera (VCA 2500XE video contact angle system, AST Products, Inc.) at 23°C in air. All measurements were made using 3μl drops of distilled water. Measurements were made on both sides of 3 drops, each drop on a new spot, and averaged.

XPS Analysis

XPS experiments were done on a model SSX-100 spectrometer (Surface Science Instruments, Mountain View, Calif.). The electron gun bombards a monochromatic Al K_α x-ray source at 120W. The emitted x-rays ($h\nu$ = 1486.6 eV) were focused on a spot on the sample nominally 800 μm in diameter. Polymer films were mounted on an aluminum sample holder using a beryllium/copper clip. The analysis chamber pressure was maintained at ~10^{-8} Torr during analysis. Proper focus was attained by adjusting the stage height to maximize the C(1s) count rate before each measurement. A low voltage electron flood gun was used to neutralize surface charging, which occurs due to the insulating nature of polymer films. A reference binding energy of 285.0 eV (aliphatic

CH_x) was used to correct for binding energy shifts due to surface charging. Survey spectra were collected from 0 to 1100 eV with 150eV pass energy. Experimental photoelectron intensities (peak areas) were determined after subtracting a 'Shirley'-type background. Peak areas were normalized by the number of scans, the number of electron volts scanned per step, the analyzer resolution, the Scofield photoemission cross sections, and the spectrometer transmission function. XPS data were acquired at a take-off angle of 55°, defined as the angle between the surface normal and the axis of the analyzer lens. The inelastic mean free path of a C(1s) photoelectron traveling in polymers is ~3 nm[10], corresponding to a maximum sampling depth of 3d=5 nm (95% of XPS signal intensity).

4.2.4 Data Analysis

Contact Angle Analysis for PAA-treated Nylon

The Cassie[3] expression was used to obtain the PAA surface fraction from contact angle measurements of PAA-treated surfaces:

$$f_{PAA}(\theta_{Eff}) = (\cos\theta_{Eff} - \cos\theta_{Nylon}) / (\cos\theta_{PAA} - \cos\theta_{Nylon}) \quad (4.17)$$

where θ_{Eff} is the effective contact angle for a PAA-treated nylon film, θ_{PAA} and θ_{Nylon} are contact angles for PAA and nylon references, respectively, and $f_{PAA}(\theta_{Eff})$ is the fractional PAA surface coverage for a PAA-treated nylon film with θ_{Eff} contact angle. The PAA reference was assumed to have a θ_{PAA} value of 0°.

XPS Analysis for PAA-treated Nylon

For PAA-treated nylon films, surface fractions for PAA (C=60%, O=40%) and nylon (C=75%, O=12.5%, N=12.5%) were estimated from XPS N(1s) and O (1s) peaks. An assumption is made that N(1s) photoelectrons emerging from the nylon substrate are completely screened by PAA layers but remain unperturbed in the absence of PAA. The fractional PAA surface coverage $f_{PAA}^{N(1s)}$ is defined by the following expression:

$$f_{PAA}^{N(1s)} = 1 - \left(\%N_{\text{Treated Nylon}} / \%N_{\text{Nylon}}\right) \qquad (4.\ 18)$$

where $\%N_{Eff}$ and $\%N_{Nylon}$ are the atomic percentages of nitrogen determined from the N(1s) photoelectron signal (~400 eV) of PAA-treated nylon and untreated nylon, respectively. Since XPS analyzes ~ 5 nm, PAA layers <5 nm thick will not fully screen N(1s) photoelectrons and the fractional PAA surface coverage will be underestimated.

PAA contains more oxygen than the nylon substrate, therefore the O(1s) photoelectron yield from XPS was used to measure the surface concentration of PAA. The fractional PAA surface coverage $f_{PAA}^{O(1s)}$ is defined by the following expression:

$$f_{PAA}^{O(1s)} = \left(\%O_{\text{Treated Nylon}} - \%O_{\text{Nylon}}\right) / \left(\%O_{PAA} - \%O_{\text{Nylon}}\right) \qquad (4.\ 19)$$

where $\%O_{\text{Treated Nylon}}$, $\%O_{PAA}$, and $\%O_{\text{Nylon}}$ are the atomic percentages of oxygen observed from the O(1s) photoelectron signal (~532 eV) on PAA-treated nylon, a PAA reference and untreated nylon, respectively. For PAA, $\%O_{PAA}$ = 40 was determined from

the molecular formula (minus hydrogen). Thin PAA layers will result in underestimation of the fractional PAA surface coverage. An XPS average PAA surface fraction f_{PAA}^{XPS} can be combined with $f_{PAA}(\theta_{Eff})$ into an overall average f_{PAA}^{Avg} both defined below:

$$f_{PAA}^{XPS} = \left(f_{PAA}^{N(1s)} + f_{PAA}^{O(1s)}\right)/2 \quad (4.20)$$

$$f_{PAA}^{Avg} = \left(f_{PAA}(\theta_{Eff}) + f_{PAA}^{XPS}\right)/2 \quad (4.21)$$

The surface coverage from the Cassie and XPS equations may vary. First, contact angle observes the top 0.1-1 nm of a solid, while XPS analyzes 5 nm. For PAA layers greater than 5 nm, $f_{PAA}(\theta_{Eff})$ will equal f_{PAA}^{XPS}, otherwise $f_{PAA}(\theta_{Eff})$ will exceed f_{PAA}^{XPS}. Also, surface roughness may increase the contact angles of untreated and PAA-treated nylon, resulting in overestimated $f_{PAA}(\theta_{Eff})$ values.

4.3 RESULTS AND DISCUSSION

4.3.1 *Contact Angle Analysis*

Contact angles for various films are shown in Figure 4.11. Nylon 6,6 was hydrophobic (θ_{Nylon} = 80°). PAA-Adsorbed nylon (11 g/L) (θ_{Eff} = 63°), Solution-Grafted/Desorbed nylon (SG/D, 40mM DMTMM) (θ_{Eff}=57°), and Adsorption-Grafted/Desorbed nylon (AG/D, •100mM DMTMM) (θ_{Eff}=52–35°) were all hydrophilic. PAA surface fractions $f_{PAA}(\theta_{Eff})$ are listed in Table 4.2. Values ranged from 0.34 ± 0.04 for PAA-Adsorbed to 0.78 ± 0.07 for AG/D nylon (11g/L PAA, 5 mM DMTMM), respectively. All $f_{PAA}(\theta_{Eff})$ values were statistically different.

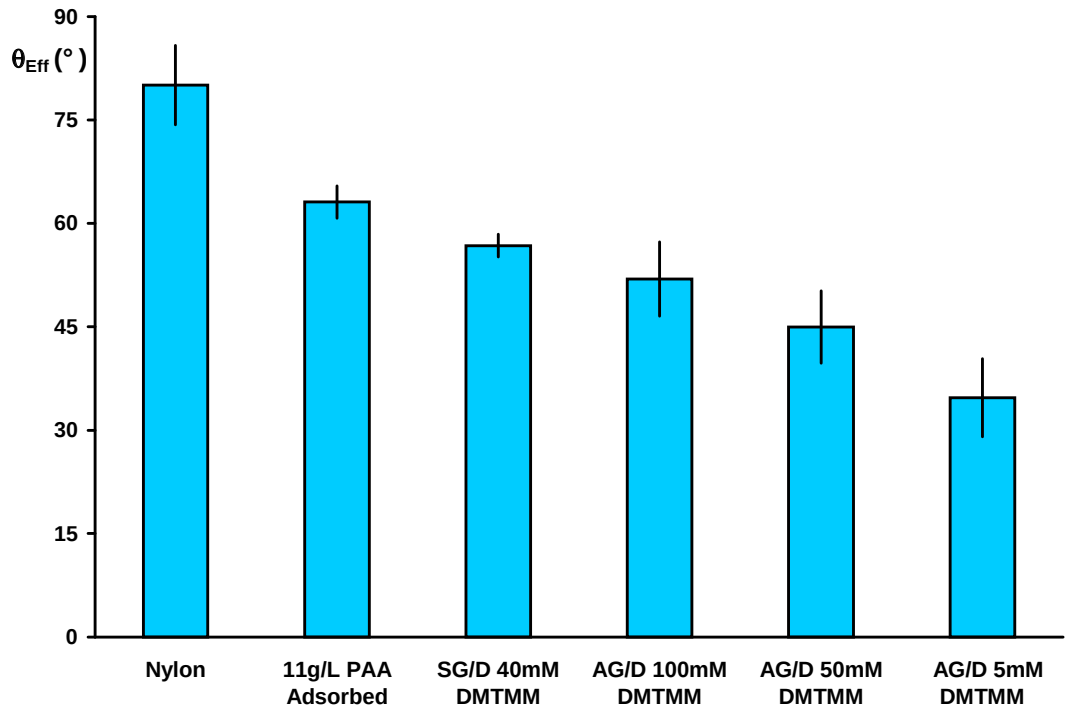

Figure 4.11– Contact Angles for Untreated and PAA-Treated Nylon

Contact Angle vs. XPS Analysis

While the next section provides XPS results in more detail, PAA surface fractions from contact angle and XPS are compared in Table 4.2. All $f_{PAA}(\theta_{Eff})$ and corresponding f_{PAA}^{XPS} values were statistically equal, so f_{PAA}^{AVG} values are shown. A straight line (y=x) with high correlation (R^2=0.974) is obtained by plotting f_{PAA}^{XPS} vs. $f_{PAA}(\theta_{Eff})$(Figure 4.12). Thus XPS results are valid despite high standard deviations, PAA layers are ≥ 5 nm, and surface roughness has a minimal effect. The highest f_{PAA}^{AVG} value (0.73) was achieved by 11 g/L PAA Adsorption-Grafting with 5 mM DMTMM. The next highest f_{PAA}^{AVG} values were observed for 11 g/L PAA Adsorbed-Grafted/Desorbed nylon at 50 and 100 mM DMTMM, and these values were statistically equal. As shown in Figure 4.12, only the Adsorption-Grafting process exceeds the RSA jamming limit.

Table 4.2– PAA Surface Fractions: XPS vs. Contact Angle

Nylon 6,6 Surfaces	**Surface Fraction**		
	$f_{PAA}(\theta_{Eff})$	f_{PAA}^{XPS}	f_{PAA}^{AVG}
Untreated	0	0	0
PAA-Adsorbed	0.34 ± 0.04	0.41 ± 0.11	0.38 ± 0.09
SG/D 40 mM DMTMM	0.45 ± 0.03	0.43 ± 0.04	0.44 ± 0.04
AG/D 100 mM DMTMM	0.53 ± 0.09	0.60 ± 0.12*	0.57 ± 0.11
AG/D 50 mM DMTMM	0.64 ± 0.08	0.60 ± 0.11*	0.62 ± 0.10
AG/D 5 mM DMTMM	0.78 ± 0.07	0.72 ± 0.18*	0.73 ± 0.16
PAA Reference	1	1	1
Statistics	$f_{PAA}^{XPS} = f_{PAA}(\theta_{Eff})$		

* Average of AG and AG/D values

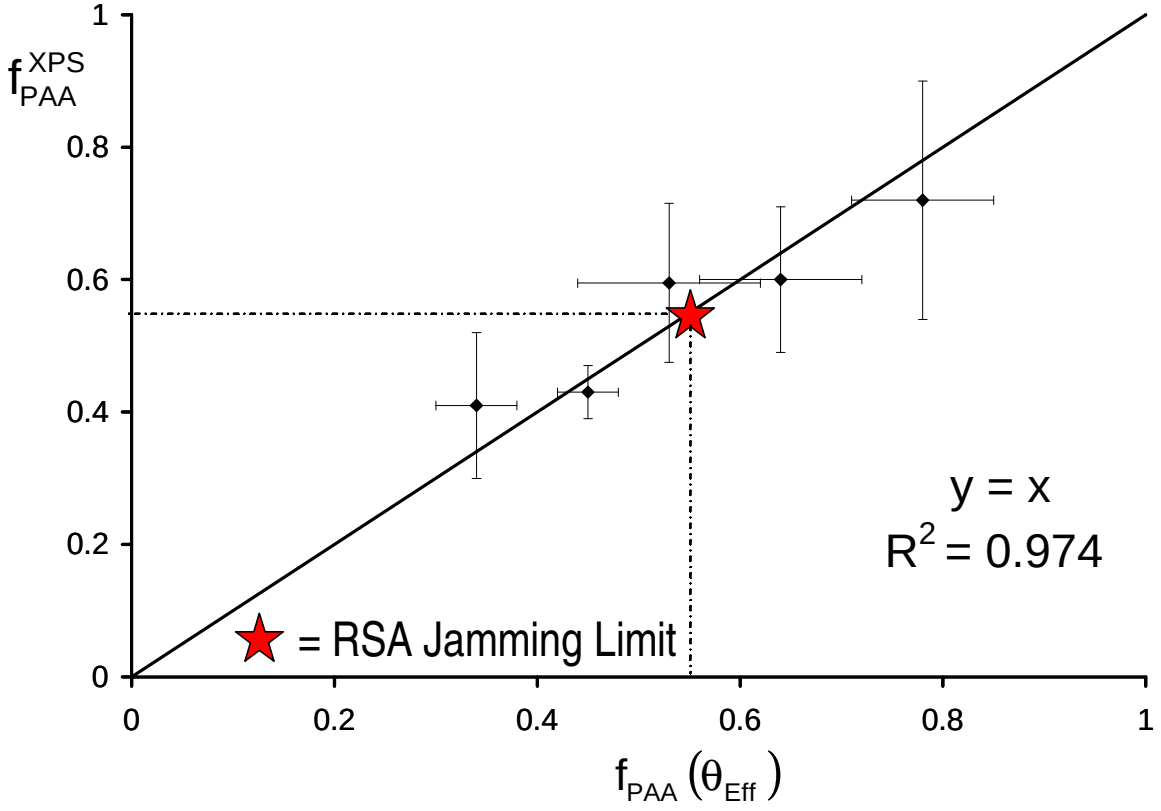

Figure 4.12– PAA Surface Fractions: XPS vs. Contact Angle

4.3.2 *XPS Analysis*

Nylon 6,6 and PAA treated Nylon 6,6

XPS analysis of untreated nylon 6,6 film (Figure 4.13) revealed slightly higher oxygen and slightly lower nitrogen levels (%O = 15 ± 2, %N = 11 ± 1) than expected for a theoretical nylon 6,6, surface(%O = %N = 12). Similar results were observed for nylon 6,6 after 2 hours at pH=14 (%O = 15 ± 1, %N = 10 ± 2) as well as after 15 minutes at pH=3 (%O = 18 ± 2, %N = 9 ± 2).

For the PAA-grafted surfaces, such as the Adsorption-Grafted/Desorbed (AG/D) nylon film shown in Figure 4.14, grafting is clearly illustrated by the simultaneous increase in the oxygen content and decrease in the nitrogen content relative to nylon 6,6.

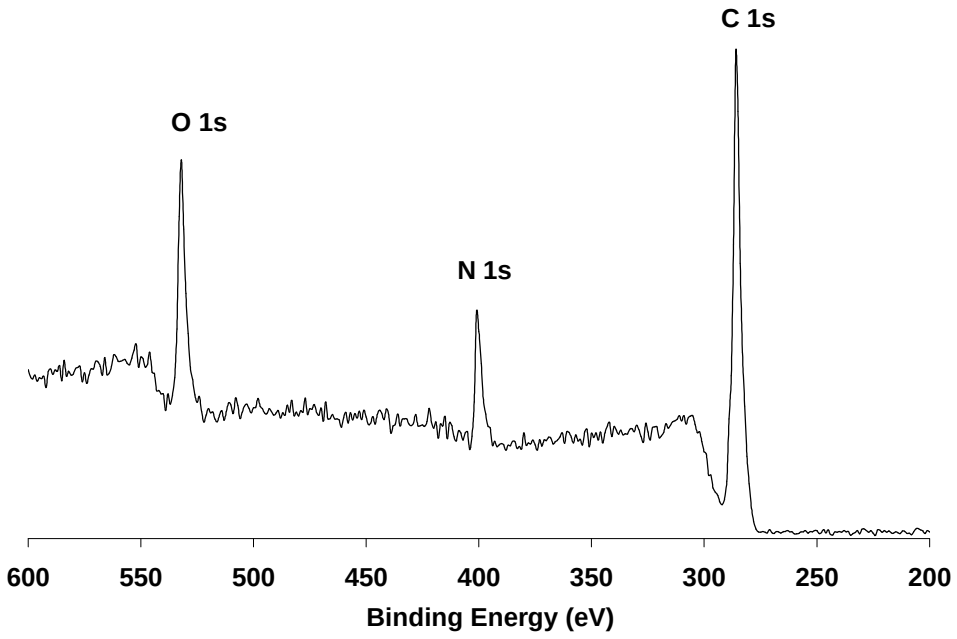

Figure 4.13– XPS spectrum: Nylon 6,6

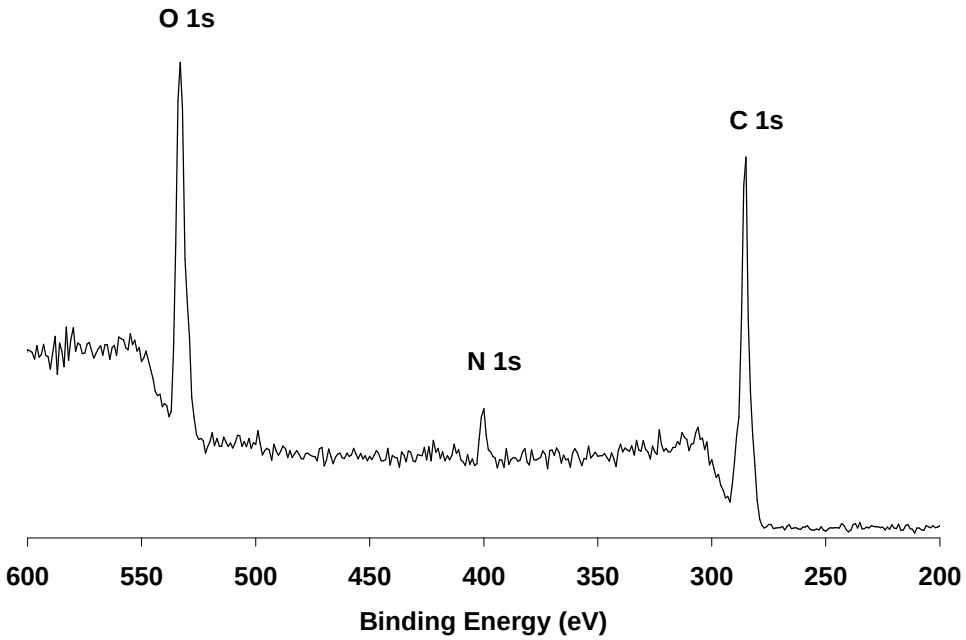

Figure 4.14– XPS Spectrum: AG/D Nylon (100 mM DMTMM)

Solution-Grafted (SG) Nylon

Solution-Grafting was performed with 1/1 DMTMM/CO_2H at 1 g/L and 11 g/L PAA. Before PAA desorption, equal amounts of PAA were detected at 1 g/L and 11 g/L PAA, as shown by increased O/C ratios and decreased N/C ratios (Figure 4.15), as well increased PAA surface fractions (Table 4.3). After PAA desorption, the PAA surface fraction decreased at 1 g/L and 11 g/L PAA and the final PAA surface fraction increased with concentration. Solution-Grafting was also performed with 1/4 DMTMM/CO_2H. Figure 4.16 shows XPS atomic ratios for PAA SG/D films at 1 g/L and 11 g/L PAA with 1/4 or 1/1 DMTMM/CO_2H ratios. For each DMTMM/CO_2H ratio, the PAA surface fraction increased with concentration. For each PAA concentration, the PAA surface fraction was equivalent for 1/4 and 1/1 DMTMM/CO_2H ratios.

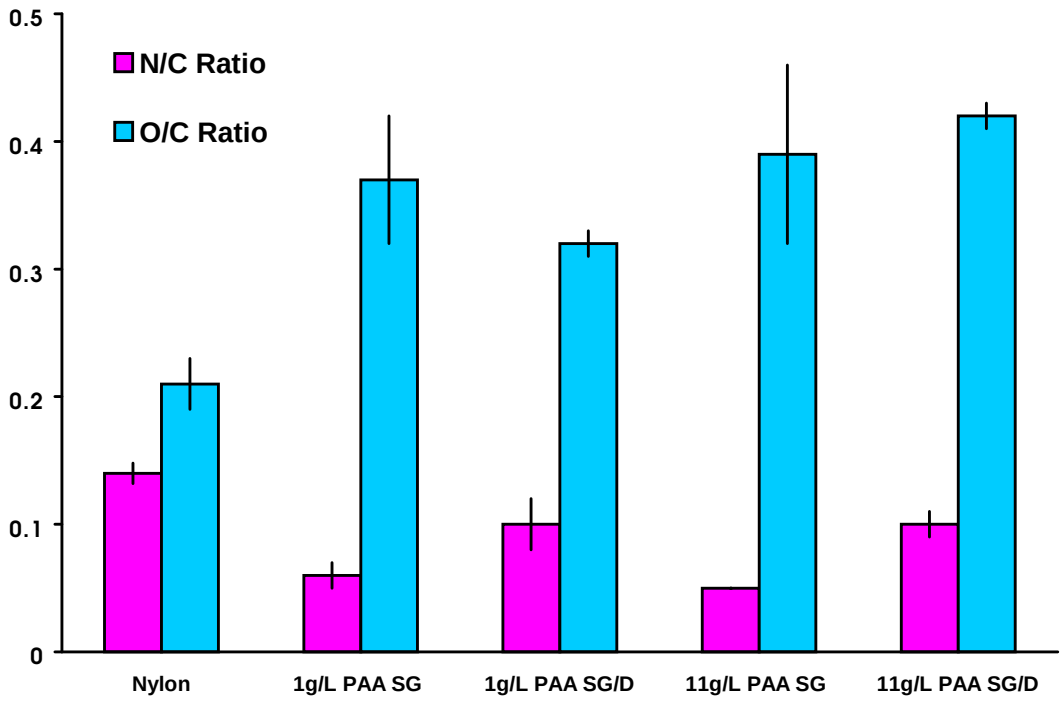

Figure 4.15– XPS Ratios: SG and SG/D Nylon (1/1 DMTMM/CO_2H)

Table 4.3– XPS Surface Fractions: SG and SG/D Nylon (1/1 DMTMM/CO_2H)

Surface Fraction	***1 g/L PAA = 0.015M DMTMM***		***11 g/L PAA = 0.15M DMTMM***	
	SG	**SG/D**	**SG**	**SG/D**
$f_{PAA}^{N(1s)}$	0.62 ± 0.11	0.35 ± 0.10	0.68 ± 0.02	0.40 ± 0.07
$f_{PAA}^{O(1s)}$	0.43 ± 0.10	0.31 ± 0.01	0.47 ± 0.13	0.50 ± 0.02
f_{PAA}^{XPS}	0.53 ± 0.14	0.33 ± 0.07	0.58 ± 0.14	0.45 ± 0.07
f_{PAA}^{XPS} : SG at 1g/L = 11g/L, SG/D at 11g/L > 1g/L				
f_{PAA}^{XPS} : SG/D < SG at 1g/L and 11g/L				

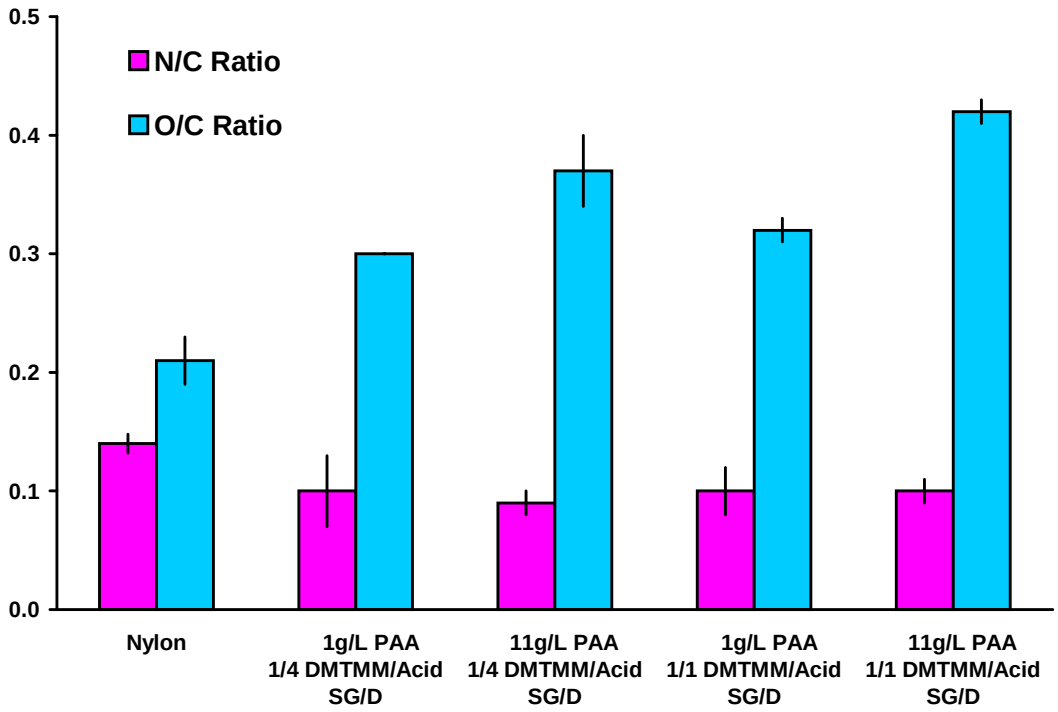

Figure 4.16– XPS Ratios: SG/D Nylon (1/4 or 1/1 DMTMM/CO_2H)

Table 4.4– XPS Surface Fractions: SG/D Nylon (1/4 or 1/1 DMTMM/CO_2H)

Surface Fraction	***1/4 DMTMM/CO_2H***		***1/1 DMTMM/CO_2H***	
	1 g/L PAA	**11 g/L PAA**	**1 g/L PAA**	**11 g/L PAA**
$f_{PAA}^{N(1s)}$	0.31 ± 0.10	0.44 ± 0.02	0.35 ± 0.10	0.40 ± 0.07
$f_{PAA}^{O(1s)}$	0.26 ± 0.02	0.42 ± 0.06	0.31 ± 0.01	0.50 ± 0.02
f_{PAA}^{XPS}	0.28 ± 0.13	0.43 ± 0.04	0.33 ± 0.07	0.45 ± 0.07
f_{PAA}^{XPS} **: For each DMTMM/CO_2H ratio: 11g/L > 1g/L**				
f_{PAA}^{XPS} **: For each PAA level: 1/4 DMTMM/CO_2H= 1/1 DMTMM/CO_2H**				

Adsorption-Grafted Nylon

In the first step of Adsorption-Grafting, PAA was adsorbed on nylon 6,6 films. Significant PAA adsorption occurred at 1 g/L and 11 g/L PAA, as shown by increased O/C and decreased N/C ratios (Figure 4.17). PAA surface fractions increased with PAA concentration (Table 4.5). This agrees with the fact that PAA ionizes to a greater extent in dilute solution, increases the size of the coil in solution and thereby decreases PAA adsorption onto nylon 6,6. Also, greater PAA aggregation may occur at high PAA concentration due less repulsion between chains, resulting in greater PAA adsorption.

In the second step of Adsorption-Grafting, PAA-Adsorbed films were immersed in 100 mM DMTMM. The surface fractions were greater for 11 g/L vs. 1 g/L PAA. For 1g/L PAA, PAA surface coverage increased after grafting and desorption, as shown by increased O/C and decreased N/C (Figure 4.17) and increased $f_{PAA}^{O(1s)}$ and/or $f_{PAA}^{N(1s)}$ values (Table 4.6). For 11 g/L, PAA f_{PAA}^{XPS} was statistically equal after grafting/desorption or grafting/base treatment (pH=12, 70°C, 1 hour). However, after grafting/desorption, $f_{PAA}^{O(1s)}$ was statistically higher. Thus DMTMM activation/grafting is a sufficient method for optimizing PAA surface coverage and PAA-g-nylon is stable to alkaline conditions.

Table 4.5– XPS Surface Fractions: PAA-Adsorbed Nylon.

Surface Fraction	***1 g/L PAA***	***11 g/L PAA***
$f_{PAA}^{N(1s)}$	0.40 ± 0.20	0.47 ± 0.12
$f_{PAA}^{O(1s)}$	0.10 ± 0.04	0.36 ± 0.09
f_{PAA}^{XPS}	0.25 ± 0.21	0.41 ± 0.11
f_{PAA}^{XPS} **: 11g/L > 1g/L**		

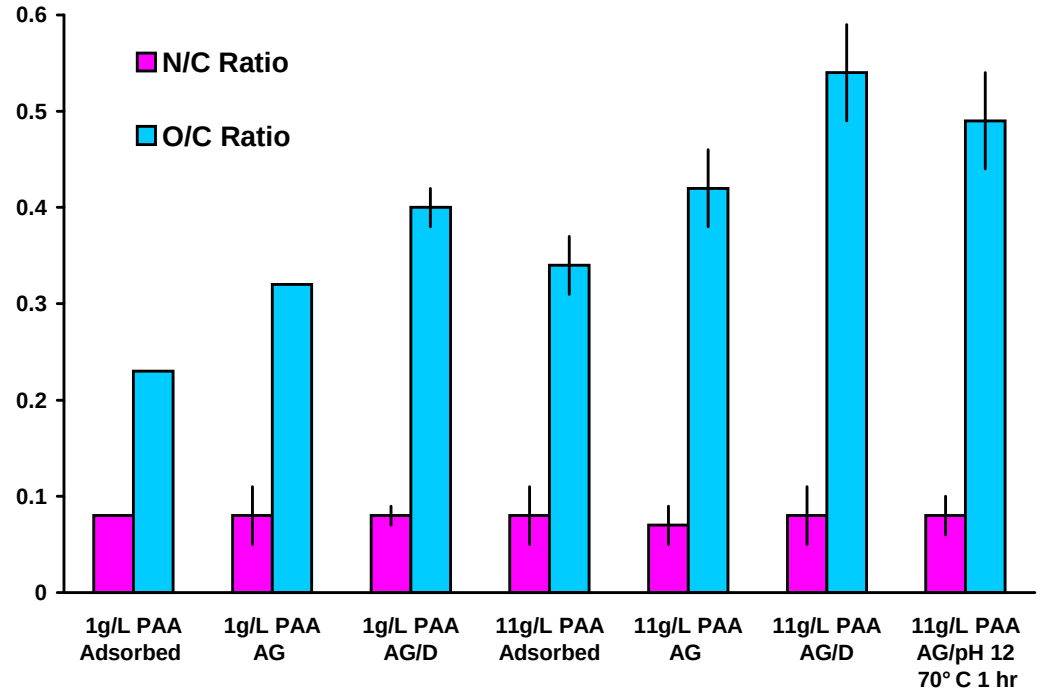

Figure 4.17 – XPS Ratios: Adsorbed, AG and AG/D Nylon (100mM DMTMM)

Table 4.6– XPS Surface Fractions: AG and AG/D Nylon (100mM DMTMM)

Surface Fraction	***1 g/L PAA***		***11 g/L PAA***		
	AG	**AG/D**	**AG**	**AG/D**	**AG/pH 12 70°C, 1 hr**
$f_{PAA}^{N(1s)}$	0.46 ± 0.06	0.50 ± 0.16	0.58 ± 0.14	0.55 ± 0.07	50 ± 0.04
$f_{PAA}^{O(1s)}$	0.31 ± 0.05	0.48 ± 0.07	0.53 ± 0.08	0.73 ± 0.06	64 ± 0.18
f_{PAA}^{XPS}	0.38 ± 0.09	0.49 ± 0.12	0.56 ± 0.12	0.64 ± 0.12	57 ± 0.14
f_{PAA}^{XPS} : For AG & AG/D: 11g/L > 1g/L **f_{PAA}^{XPS} : AG/D > AG at 1g/L** **f_{PAA}^{XPS} : AG/D = AG at 11g/L, while $f_{PAA}^{O(1s)}$: AG/D >AG at 11g/L** **f_{PAA}^{XPS} and $f_{PAA}^{O(1s)}$: AG = AG/(pH=12, 70°C, 1hr) at 11g/L**					

Next, 11 g/L PAA-Adsorbed films were Adsorption-Grafted using 0.5-100 mM DMTMM. N/C and O/C ratios are shown in Figure 4.18 for films prepared at ≤5 mM DMTMM and are shown in Figure 4.19 for films prepared at all DMTMM levels. PAA surface fractions for all DMTMM levels are in Table 4.7. Below 5 mM DMTMM, N/C and f_{PAA}^{XPS} values decreased after PAA desorption. At or above 5 mM DMTMM, N/C and f_{PAA}^{XPS} values were equal before and after PAA desorption. PAA surface coverage increased with DMTMM to $f_{PAA}^{XPS} = 0.74 \pm 0.19$ observed at 5 mM DMTMM and decreased above 5 mM DMTMM. Excess DMTMM may (a) graft certain chains at multiple points, limiting their ability to spread and cover the substrate and/or (b) overactivate adsorbed chains, removing them from the surface before grafting occurs.

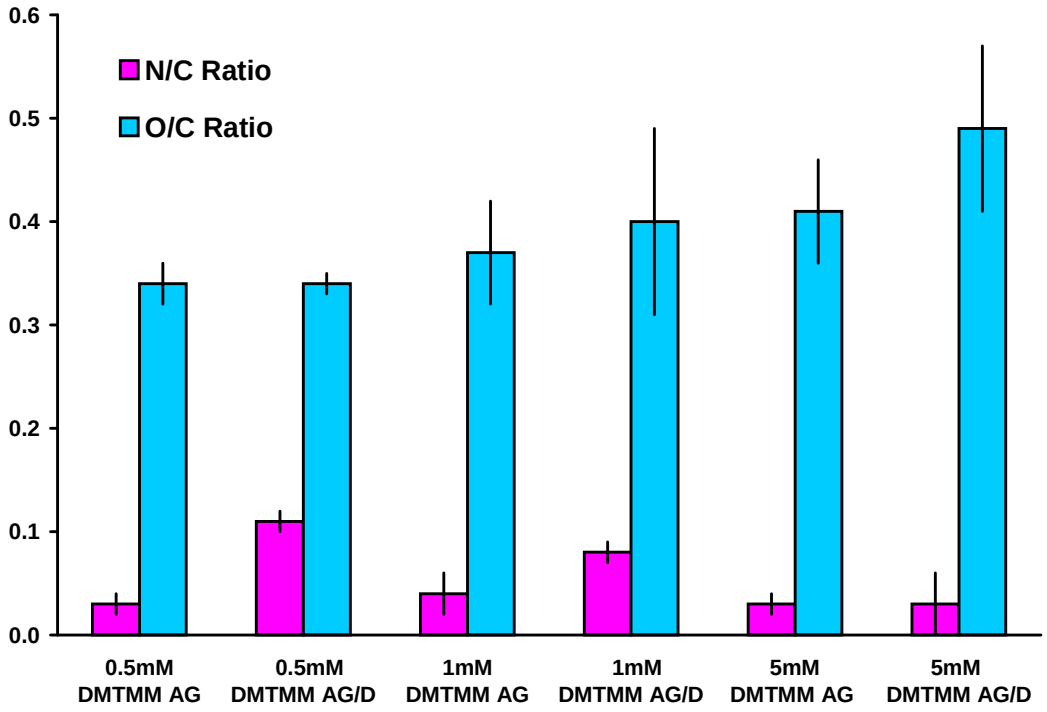

Figure 4.18– XPS Ratios: AG and AG/D Nylon (11g/L PAA, ≤5mM DMTMM)

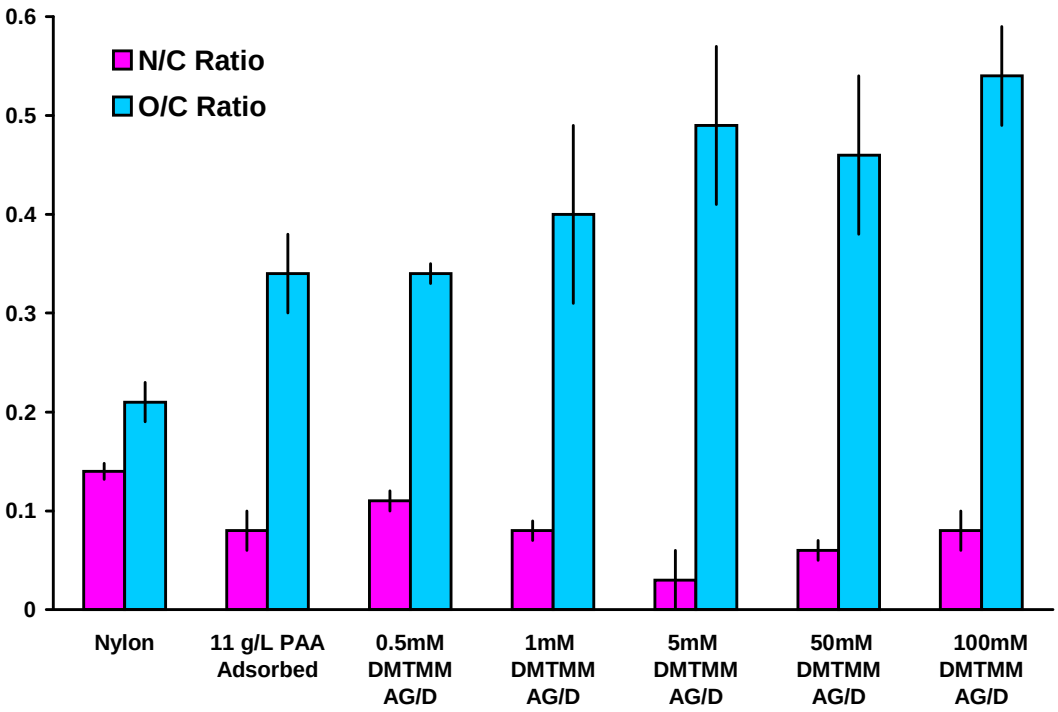

Figure 4.19– XPS Ratios: AG/D Nylon (11g/L PAA, ≤100mM DMTMM)

Table 4.7– XPS Surface Fractions: AG and AG/D Nylon (≤100mM DMTMM)

Surface Fractions		$f_{PAA}^{N(1s)}$	$f_{PAA}^{O(1s)}$	f_{PAA}^{XPS}	f_{PAA}^{XPS} Avg
11 g/L PAA Adsorbed		0.47 ± 0.12	0.36 ± 0.09	**0.41 ± 0.11**	
0.5 mM DMTMM	AG	0.77 ± 0.06	0.39 ± 0.05	0.58 ± 0.21	
	AG/D	0.26 ± 0.03	0.34 ± 0.02	**0.30 ± 0.05**	
1 mM DMTMM	AG	0.76 ± 0.10	0.45 ± 0.10	0.60 ± 0.19	
	AG/D	0.48 ± 0.04	0.48 ± 0.17	**0.48 ± 0.11**	
5 mM DMTMM	AG	0.80 ± 0.06	0.54 ± 0.09	0.67 ± 0.16	**0.72 ± 0.18**
	AG/D	0.80 ± 0.21	0.68 ± 0.16	0.74 ± 0.19	
50 mM DMTMM	AG	0.67 ± 0.01	0.50 ± 0.06	0.58 ± 0.10	**0.60 ± 0.11**
	AG/D	0.61± 0.07	0.61 ± 0.16	0.61 ± 0.12	
100mM DMTMM	AG	0.58 ± 0.14	0.53 ± 0.08	0.56 ± 0.12	**0.60 ± 0.12**
	AG/D	0.55 ± 0.07	0.73 ± 0.06	0.64 ± 0.12	
<5 mM DMTMM: $f_{PAA}^{N(1s)}$ and f_{PAA}^{XPS} AG/D < AG ≥5 mM DMTMM: $f_{PAA}^{O(1s)}$ AG/D > AG ≥5 mM DMTMM: f_{PAA}^{XPS} AG/D = AG : 5 mM > 50 mM = 100 mM					

4.4 CONCLUSIONS

PAA chains were grafted onto nylon 6,6 surfaces using DMTMM. An extremely high correlation between $f_{PAA}(\theta_{Eff})$ and f_{PAA}^{XPS} values was observed, which indicates (a) XPS results are validated despite high standard deviations, (b) PAA layers are ≥ 5 nm, and (c) surface roughness effects are minimal. The best results were observed for 11g/L PAA Adsorption-Grafted nylon using 5 mM DMTMM. Up to this level, PAA surface coverage decreased after desorption, but increased with increasing DMTMM. At this level, the maximum PAA surface coverage was 73% and was shown to resist desorption. Above this level, excess DMTMM slightly reduced the PAA surface coverage.

The PAA surface coverage for 11 g/L PAA Solution-Grafted/Desorbed nylon using 40 mM DMTMM was equal to that for 11 g/L Adsorption-Grafted/ Desorbed nylon at 1 mM DMTMM, both initially and after desorption. This suggests that the same mechanism exists for Solution-Grafting and Adsorption-Grafting. This is reasonable since during Solution-Grafting, PAA can adsorb onto nylon prior to DMTMM addition. The low spreading/grafting efficiency of Solution-Grafting indicates that PAA in solution consume 97.5% of the DMTMM before it reaches the surface.

By using the Adsorption-Grafting method, PAA surface coverage exceeding the RSA "jamming limit" was achieved and the maximum surface coverage closely agrees with θ_∞=0.68 from the PCC-RSA model. If DMTMM promotes the spreading of thick, adsorbed-PAA layers during grafting, the resulting grafted layers should be thinner. In Chapter 6, this hypothesis will be tested by determining PAA layer thicknesses with angle-resolved XPS for various PAA-treated surfaces.

CHAPTER 5

MODIFICATION OF SURFACE-GRAFTED NANOSCAFFOLDS

5.1 INTRODUCTION

Each of the preceding chapters has been leading to the preparation of a fluorinated SGN on nylon 6,6. Up to this point, the DMTMM-activated perfluoralkyl amine modification of PAA and surface-grafting of PAA onto nylon 6,6 have been studied independently. The present chapter will detail the modification of PAA-grafted nylon 6,6 substrates with various amines, including a perfluoroalkyl amine.

Hyperbranched surface-grafted PAA layers have been reported.[63,64] Such layers were prepared by sequentially grafting amine-terminated poly(*t*-butyl acrylate) to CO_2H functional surfaces followed by acrylate side group hydrolysis. Films with 3 PAA layers were >200 nm thick with advancing water contact angles θ_a= 25-30°. Coupling of such hyperbranched PAA layers with 1*H*,1*H*-pentadecafluorooctyl amine (PDFOA) formed very hydrophobic films, θ_a=107-120° for PDFOA modified 3-layer PAA films.[64-66] A similar value (θ_s=110°) was found for poly(1*H*,1*H*-pentadecafluorooctyl acrylamide) (poly(PDFOAm)).[67] The fluorine content for a PDFOA modified 3-layer PAA film from XPS was 46%, corresponding to ~85% of the fluorine content of poly(PDFOAm). Fourier-transform infrared external reflection spectroscopy estimated 30-60% conversion from the ratio of the acid carbonyl peak height (≈1730 cm^{-1}) before and after coupling.

While fluorinated, hyperbranched PAA layers can be synthesized, this is not a suitable commercial treatment of nylon 6,6 in terms of cost, the number of synthetic steps, and the reaction conditions. In the present work, Adsorption-Grafted nylon surfaces (discussed in Chapter 4) were coupled with amines, including a perfluoroalkyl

amine, using DMTMM (Figure 5.1). PAA-g-nylon films were modified with butyl amine in H_2O and with PDFOA in MeOH. In Chapter 3, analogous solution modifications of PAA were performed using the same reaction conditions and 100% and >50% conversions were observed for butyl amine and PDFOA reactions, respectively, when using sufficient DMTMM and amine. However, PAA surface reactions are not expected to be as efficient as solution reactions. Surface-grafted PAA is 2-dimensional while PAA is 3-dimensional in solution. PAA surface-grafted chains are also highly concentrated, which restricts access to PAA groups and reduces their solubility during reaction. Therefore, a method was developed to solubilize PDFOA in H_2O. While PAA is very soluble in H_2O, PAA dissociation will generate an acidic pH at the surface, reducing the overall efficiency of the DMTMM reaction. By adding NaOH to the reaction, the surface can be neutralized while also allowing chains to expand and remain soluble for longer times. Some swelling of nylon 6,6 is also expected under alkaline conditions.

PDFOA was solubilized in H_2O by randomly methylated β-cyclodextrin (RAMEB). Cyclodextrins are naturally occurring cyclic oligoamyloses with 6 (α), 7 (β), 8 (γ), or 9 (δ) α-1,4-linked D-glucose repeat units. Their structure resembles a truncated cone. The interior of the cavity is hydrophobic and the exterior is hydrophilic. Water-soluble cyclodextrins can act as a host, enclosing hydrophobic guest molecules within their cavity, resulting in a water-soluble complex. They can also act as phase-transfer catalysts. Parker and coworkers[68] used cyclodextrins with surfactants during emulsion polymerization of fluorinated monomers, while Storsberg and Ritter[69] and Choi and coworkers[70] performed aqueous free-radical polymerizations of fluorinated monomers using randomly methylated β-cyclodextrin (RAMEB).

X-ray photoelectron spectroscopy (XPS) and contact angle analyses were used to determine the surface fraction of acrylamide groups after modification of PAA-g-nylon.

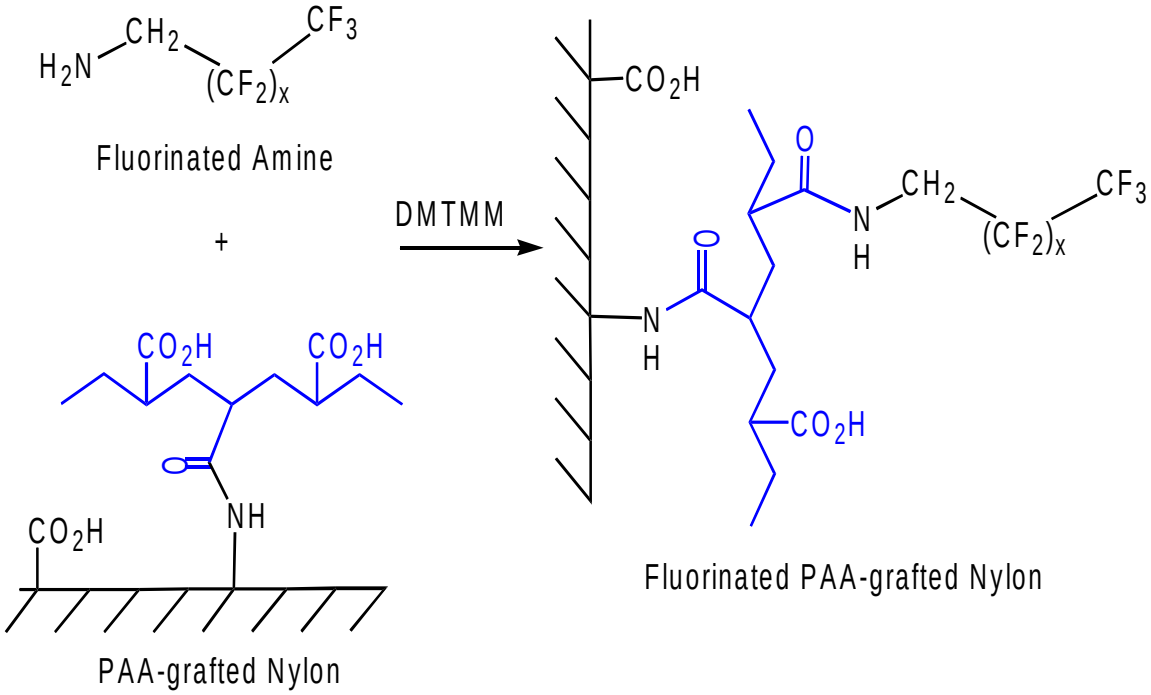

Figure 5.1– Fluorinated Acrylamide-Modification Process for PAA-g-Nylon

5.2 EXPERIMENTAL SECTION

5.2.1 Nomenclature

The sample code for each amine and acrylamide-modified (AmM) PAA group is presented in Table 5.1. The sample code of butyl acrylamide-modified PAA is $BAmM_{98}$-PAA_2, where 'BAmM' stands for butyl acrylamide-modified, the following number '98' is the mol % of acrylamide repeat units, 'PAA' stands for poly(acrylic acid), and the following number '2' is the mol % of acrylic acid repeat units. The sample code of butyl acrylamide-modified PAA-grafted nylon film is BAmM-PAA-g-nylon.

Table 5.1– Amine and Acrylamide Modified PAA (AmM-PAA) Groups

	Acrylamide-Modified (AmM) PAA	
Selected Amines = R–NH_2	**Abbreviation**	**R Group**
Butyl Amine (BA)	BAmM-PAA	$(CH_2)_3CH_3$
1H,1H-Pentadecafluorooctyl Amine (PDFOA)	PDFOAmM-PAA	$CH_2C_7F_{15}$

5.2.2 *Materials*

Nylon 6,6 film (M_n = 12 kg/mol, DuPont Canada), poly(acrylic acid) powder (PAA, M_w = 450 kg/mol, Aldrich), randomly methylated-β-cyclodextrin (RAMEB, M_n = 1.31 kg/mol, Aldrich), butyl amine (Aldrich), methanol (MeOH, Aldrich), sodium hydroxide (NaOH, Fisher), sodium thiocyanate (NaSCN, Fisher), 4-(4,6-dimethoxy-1,3,5-triazin-2-yl)-4-methylmorpholinium chloride (DMTMM, Acros Organics), trifluoroacetic acid (TFAA, SynQuest Laboratories) and 1*H*,1*H*-pentadecafluorooctylamine (PDFOA, SynQuest Labs) were used as received.

5.2.3 *Typical Procedures*

Modification of PAA-Grafted (or PAA-Adsorbed) Nylon

Amine (4.5 mmol) was dissolved in reaction solvent (35 ml) with vigorous mixing at 25°C. Butyl amine was dissolved in distilled H_2O while PDFOA solutions were prepared in either MeOH or distilled H_2O (3/1 RAMEB/PDFOA). The pH of aqueous PDFOA solution was adjusted to pH=7 or pH=12 with NaOH. PAA AG/D nylon films (11g/L PAA and 5 mM DMTMM, Chapter 4, Section 4.2.2) were immersed in amine solution for 15 min. DMTMM (960 mg, 4.5 mmol) was dissolved in the reaction solvent (10 ml) and added to each amine solution (0.1M DMTMM, 0.1M amine) to initiate surface modification of the CO_2H groups. The reactions proceeded for 24 hr.

Purification of Acrylamide-Modified PAA-Grafted Nylon

BAmM-PAA-g-nylon films were (1) rinsed overnight in distilled H_2O, (2) immersed in HCl solution (pH=3) for 15 min., (3) rinsed in distilled H_2O overnight, (4) immersed in aqueous NaOH (pH=12) solution for 15 minutes, (5) rinsed overnight in distilled H_2O, (6) wiped with a Kimwipe™ cloth wet with distilled H_2O, (7) wiped with a Kimwipe™ cloth wet with acetone, and (8) air dried.

PDFOAmM-PAA-g-nylon films were (1) rinsed overnight in MeOH, (2) immersed in a TFAA solution in MeOH (pH=3) for 15 min., (3) rinsed in MeOH overnight, (4) immersed in aqueous NaOH (pH=12) solution for 15 minutes, (5) rinsed overnight in distilled H_2O, (6) wiped with a Kimwipe™ cloth wet with distilled H_2O, (7) wiped with a Kimwipe™ cloth wet with acetone, and (8) air dried.

5.2.4 Data Analysis

Contact Angle Analysis for Acrylamide-Modified PAA-g-Nylon

Instrumentation and technique were presented in Chapter 4, Section 4.2.3. Acrylamide surface fractions were determined from the Cassie equation, expressed for PDFOAmM-PAA-g-nylon groups by the parameter, $f_{PDFOAmM-PAA}(\theta_{Eff})$:

$$f_{PDFOAmM\text{-}PAA}(\theta_{Eff}) = \frac{cos\theta_{Eff} - cos\theta_{PAA-g-Nylon}}{cos\theta_{poly(PDFOAm)} - cos\theta_{PAA-g-Nylon}} \qquad (5.1)$$

where θ_{Eff} is the effective contact angle for a PDFOAmM-PAA-g-nylon film and $\theta_{PAA-g-Nylon}$ and $\theta_{poly(PDFOAm)}$ are the observed contact angles for PAA-g-nylon and

poly(PDFOAm) references, respectively ($\theta_{poly(PDFOAm)}$=110° and $\theta_{PAA-g-Nylon}$=35°). For BAmM-PAA-g-nylon films, $\theta_{poly(BAm)}$ was measured for a cast $BAmM_{98}$-PAA_2 film (prepared in Chapter 3, Section 3.2.5).

XPS Analysis for Acrylamide-Modified PAA-g-Nylon

XPS instrumentation was described in Chapter 4, Section 4.2.3. Acrylamide surface fractions were determined by comparing the acrylamide-modified PAA-g-nylon surface composition with that for Adsorbed-Grafted nylon (11g/L PAA, 5 mM DMTMM) (C=66%, O=32%, N=2%) and the molecular formula of the acrylamide-modified repeat unit. PDFOA (F=63%, C=33%, N=4%), for example, forms a PDFOAm repeat unit (F=54%, C=39%, N=3.5%, O=3.5%). To determine the surface fraction of PDFOAmM-PAA groups, the largest XPS peaks specific to PDFOA and PAA-g-nylon were used: F(1s) and O(1s), respectively. The surface fraction of PDFOAmM-PAA groups determined from the XPS F(1s) peak is expressed by the parameter $f^{F(1s)}_{PDFOAmM-PAA}$:

$$f^{F(1s)}_{PDFOAmM\text{-}PAA} = \%F_{PDFOAmM\text{-}PAA} \Big/ \%F_{poly(PDFOAm)} \qquad (5.2)$$

where $\%F_{PDFOAmM-PAA}$ and $\%F_{poly(PDFOAm)}$ are the atomic percentages of fluorine obtained from the F(1s) photoelectron signal (~690 eV) of PDFOAmM-PAA-g-nylon film and poly(PDFOAm) reference, respectively. The theoretical value of 54% fluorine from the PDFOAm molecular formula (excluding hydrogen which is not detected) was used for the PDFOAm reference.

The surface fraction of PDFOAmM-PAA groups determined from the XPS O(1s) peak is expressed by the parameter $f^{O(1s)}_{PDFOAmM-PAA}$:

$$f^{O(1s)}_{PDFOAmM-PAA} = \frac{\left(\%O_{PDFOAmM-PAA} - \%O_{PAA-g-Nylon}\right)}{\left(\%O_{poly(PDFOAm)} - \%O_{PAA-g-Nylon}\right)} \qquad (5.3)$$

where $\%O_{PAA-g-Nylon}$ and $\%O_{PDFOAmM-PAA}$ are the atomic percentages of oxygen observed from the $O(1s)$ photoelectron signal (~532 eV) on a PAA-g-nylon film before and after reaction with PDFOA, and $\%O_{poly(PDFOAm)}$ is the atomic percentage of oxygen observed from the $O(1s)$ photoelectron signal (~532 eV) for a poly(PDFOAm) reference. The theoretical value of 4% oxygen from the PDFOAm molecular formula (excluding hydrogen which is not detected) was used for the PDFOAm reference.

An average PDFOAm-PAA surface fraction $f^{XPS}_{PDFOAmM-PAA}$ is defined below:

$$f^{XPS}_{PDFOAmM-PAA} = \left(f^{F(1s)} + f^{O(1s)}\right)/2 \qquad (5.4)$$

There are no XPS peaks specific to butyl amine or PAA-g-nylon. Surface fractions were determined from the N(1s), O(1s), and C(1s) photoelectron signals using the theoretical composition for poly(BAm) (C=78%, O=11%, N=11%) and then an average surface fraction of BAmM-PAA groups was obtained from these three values.

5.3 RESULTS AND DISCUSSION

5.3.1 Contact Angle Analysis

Table 5.2 presents contact angles for PAA-Grafted nylon prior to reaction, as well as for each reference polymer. For poly(butyl acrylamide), $\theta_{poly(BAm)}$ = 82±2° was observed and for poly(PDFOAm), $\theta_{poly(PDFOAm)}$ = 110° was used.[67] The θ_{H_2O} values and acrylamide surface fractions for modified PAA-g-nylon films are also shown. For all reactions, PAA-g-nylon was transformed from a hydrophilic to a hydrophobic surface. For BAmM-PAA-g-nylon film, θ_{Eff}=83±4° corresponds to $f_{BAmM-PAA}(\theta_{Eff})$=1.01±0.10. For PDFOAmM-PAA-g-nylon reactions in MeOH and H_2O (pH=7), θ_{Eff}=107±2° and 108±2°, respectively, while for reaction in H_2O at pH=12, θ_{Eff}=116±3°. The $f_{PDFOAmM-PAA}(\theta_{Eff})$ values were ≥0.96 for all PDFOAmM-PAA-g-nylon films.

Table 5.2– Contact Angles and Surface Fractions: AmM-PAA-g-Nylon

Surfaces	θ_{Eff} **(°)**	$f(\theta_{Eff})$
PAA-Grafted Nylon	35 ± 6	
$BAmM_{98}$-PAA_2 (Chapter 3, 3.2.5)	82 ± 2	
poly(PDFOAm)[67]	110	
BAmM-PAA-g-Nylon	83 ± 4	1.01 ± 0.10
PDFOAmM-PAA-g-Nylon		
MeOH	107 ± 2	0.96 ± 0.03
H_2O 3/1 RAMEB/NH_2 pH = 7	108 ± 2	0.97 ± 0.03
H_2O 3/1 RAMEB/NH_2 pH = 12	116 ± 3	1.08 ± 0.04

5.3.2 *XPS Analysis*

1H, 1H-Pentadecafluorooctyl amine (PDFOA) Modified PAA-grafted-Nylon 6,6

Figure 5.2 shows an XPS spectrum for PDFOAmM-PAA-graft-nylon 6,6 film.

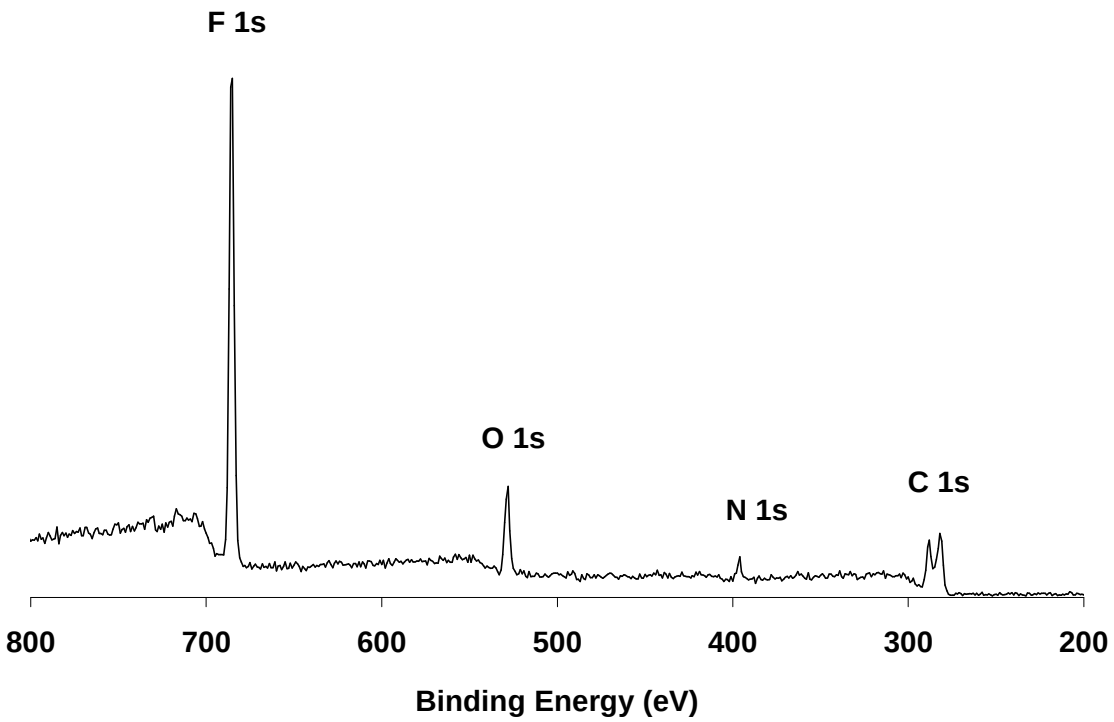

Figure 5.2– XPS spectrum: PDFOAmM-PAA-g-Nylon

Table 5.3 presents atomic % and surface fractions for PDFOAmM-PAA films. Without DMTMM, %F was • 2, verifying covalent PDFOA reaction with PAA-g-nylon using DMTMM. For MeOH and H_2O pH=7 reactions, 48% and 53% acrylamide surface fractions were observed, respectively, which agree with the 52% acrylamide content which initiated precipitation of PDFOAmM-PAA chains from MeOH (Chapter 3). Each $f^{XPS}_{PDFOAmM-PAA}$ value was lower than the corresponding $f(\theta_{Eff})$ value. This is reasonable, since DMTMM and PDFOA should still have access to exterior PAA groups after

PDFOAmM-PAA graft chains precipitate. For the H_2O pH=12 reaction, 89% acrylamide surface fraction was observed. At this pH, PAA chains are neutralized and expanded, which may have increased both the efficiency of reaction as well as the access to interior PAA groups. All $f^{F(1s)}_{PDFOAmM-PAA}$ values are greater than $f^{O(1s)}_{PDFOAmM-PAA}$ values, which may indicate segregation of fluorine groups to the air interface.

Table 5.3– XPS Atomic % and Surface Fractions: PDFOAmM-PAA-g-Nylon

Atomic %	***PDFOAm Repeat Unit***	***PDFOAmM-PAA-g-Nylon 6,6***		
		MeOH	**H_2O pH=7**	**H_2O pH=12**
N	4	4 ± 0	4 ± 0	3 ± 0
O	4	20 ± 2	18 ± 0	9 ± 1
C	39	46 ± 2	48 ± 2	38 ± 2
F	54	29 ± 1	30 ± 2	51 ± 3
Surface Fraction				
$f^{F(1s)}_{PDFOAmM-PAA}$		0.54 ± 0.01	0.56 ± 0.03	0.94 ± 0.06
$f^{O(1s)}_{PDFOAmM-PAA}$		0.42 ± 0.06	0.50 ± 0.01	0.84 ± 0.05
$f^{XPS}_{PDFOAmM-PAA}$		0.48 ± 0.08	0.53 ± 0.04	0.89 ± 0.08

Butyl Amine Modified PAA-grafted-Nylon 6,6

Figure 5.3 shows an XPS spectrum of BAmM-PAA-g-nylon 6,6 film. Table 5.4 presents atomic % and BAmM-PAA surface fractions. PAA modification was >70%. This was less than expected from the analogous solution modification from Chapter 3, which was driven to 100% conversion by using excess DMTMM and butyl amine. However, all BAmM-PAA reaction products with ≥77% Bam content eventually precipitated from solution. It seems that PAA graft chains are more sensitive to changes in solubility than PAA chains in solution. At the precipitation point, interior PAA groups are no longer accessible.

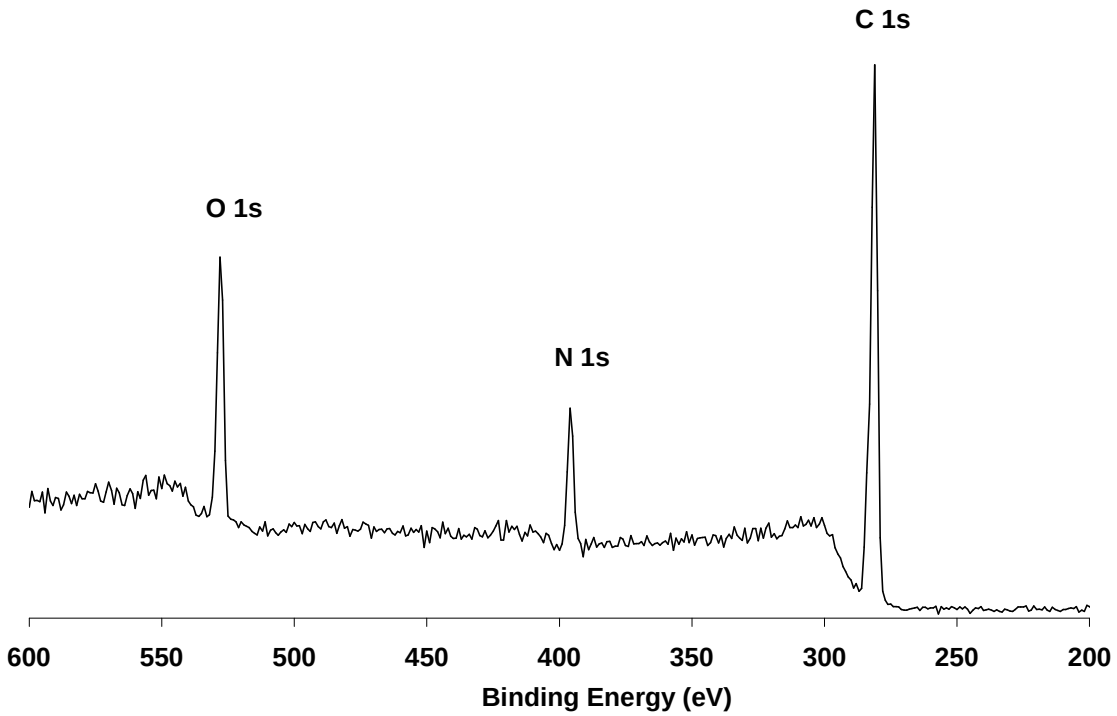

Figure 5.3– XPS spectrum: BAmM-PAA-g-Nylon

Table 5.4– XPS Atomic % and Surface Fractions: BAmM-PAA-g-Nylon

Atomic %	*BAm Repeat Unit*	*BAmM-PAA-g-Nylon 6,6 Film*
N	11	10 ± 2
O	11	17 ± 2
C	78	73 ± 1
Surface Fraction		
$f^{N(1s)}_{BAmM-PAA}$		0.87 ± 0.18
$f^{O(1s)}_{BAmM-PAA}$		0.73 ± 0.11
$f^{C(1s)}_{BAmM-PAA}$		0.56 ± 0.07
$f^{XPS}_{BAmM-PAA}$		0.72 ± 0.17

5.4 CONCLUSIONS

PAA-g-nylon films were successfully modified with 1H, 1H-pentadecafluorooctyl or butyl amine. For butyl amine, acrylamide surface fractions from contact angle and XPS were ~100% and ~72%, respectively. For 1H, 1H-pentadecafluorooctyl amine, acrylamide surface fractions from contact angle and XPS were ~48% and 53%, respectively, for MeOH or H_2O/RAMEB reactions. Higher results from contact angle reveal an excess of acrylamide groups in the top 1-2 nm. XPS acrylamide surface fractions corresponded to the acrylamide content at which analogous solution-modified chains precipitated. Thus PAA graft chain precipitation appears to limit the reaction. A more uniform PDFOA reaction exceeding the solubility limit was observed at pH=12 possibly due to a combination of (a) greater reaction efficiency, (b) greater graft chain solubility, and (c) greater access below the surface. Acrylamide surface fractions from contact angle and XPS were ~100% and ~89%, respectively. Since all $f^{F(1s)}_{PDFOAmM-PAA}$ values are greater than corresponding $f^{O(1s)}_{PDFOAmM-PAA}$ values, fluorine groups may be segregating to the air interface. This is expected for fluorinated surfaces. Further investigation using angle-resolved XPS (ARXPS) analysis was performed for these films and is presented in Chapter 6.

CHAPTER 6

ANGLE-RESOLVED XPS ANALYSIS OF POLYMERS

6.1 INTRODUCTION

XPS and contact angle analyses suggest that PAA adsorption, grafting, and desorption processes follow the Post-Adsorption Conformational Change RSA (PCC-RSA) model. In this model, polymers undergo reversible adsorption followed by irreversible post-adsorption spreading. Surface coverage exceeding the RSA "jamming limit" was observed for large spreading magnitude Σ and low rates of spreading K_s and desorption K_d. The spreading magnitude Σ and the rates of spreading K_s and desorption K_d should be small for PAA adsorption, resulting in thick PAA layers with relatively low surface coverage. However, during DMTMM activation and grafting, PAA chains can spread and reversibly adsorb/desorb to equilibrium surface coverage. The final PAA layers should be thinner and have greater surface coverage. ARXPS analysis was used to provide further experimental data to compare to the PCC-RSA model. The chemical composition of PAA-treated surfaces was measured as a function of depth and models were used to characterize PAA thicknesses and surface fractions.

XPS and contact angle analyses also suggest that modification of PAA-g-nylon surfaces depends upon the solubility of PAA graft chains during the reaction. Fluorochemical reactions proceeded farther under ionizing conditions. Additionally, the extent of modification decreased with depth. ARXPS analysis was used to provide further experimental data to compare with these results. The chemical composition of PDFOAmM-PAA-g-nylon surfaces was measured as a function of depth and models were used to determine the distribution of PDFOAmM-PAA groups.

6.2 EXPERIMENTAL SECTION

6.2.1 ARXPS Measurement

XPS instrumentation was described in Chapter 4, Section 4.2.3. A sample stage with a 6° slit geometry was tilted at variable angles: θ = 0, 30, 45, 60 and 75° (escape depths: $d = \lambda\cos\theta \sim 1\lambda$, $6\lambda/7$, $5\lambda/7$, $\lambda/2$ and $\lambda/4$). Spectra of individual peaks were taken at 25 eV analyzer pass energy and 800 μm X-ray spot size. Raw peak intensities $I_i(\theta)$ were corrected for atomic sensitivity factors S_i and normalized to 100%.

6.2.2 ARXPS Depth Profile Reconstruction

Inelastic Mean Free Path λ

Table 6.1 shows $\lambda_i^{1\ keV}$ values for nylon, PAA and poly(PDFOAm) with λ_i values (Equation 2.10) for electrons traveling in the polymers. For Al K_α x-rays, the K.E. values were: C1s=1.2, N1s=1.1, O1s=0.95 and F1s=0.79 keV. Nylon and PAA λ_i values were used for PAA-treated nylon and poly(PDFOAmM) λ_i values were used for PDFOAmM-PAA-g-nylon profiles.

Table 6.1 – Values of Inelastic Mean Free Path λ

Polymer Matrix	$\lambda_i^{1\ keV}$ ***(nm)***[10]	λ_i ***(nm)***			
		C 1s	**N 1s**	**O 1s**	**F 1s**
Nylon	3.0	3.5	3.2	2.9	---
PAA	2.8	3.2	3.0	2.7	---
poly(PDFOAm)	2.5	2.9	2.7	2.4	2.1

The Microsoft Excel 97 'Solver' Function

The Microsoft Excel 97 'solver' function found parameter values that provided calculated normalized peak intensities $I(\theta)$ for Fractional Overlayer (Equation 2.7), Cumpson and Trapezoid (Equation 2.8) models. The composition depth profile was optimized by a "least-squares" minimization of the sum of squared differences (SSD) between the observed and calculated values for the apparent composition $I_i(\theta)$ as a function of the photoemission angle θ. A close fit between these values indicates that the ARXPS results are reasonable.

Fractional Overlayer Model

The ARXPS.xls[8] spreadsheet was used to fit the Fractional Overlayer model to ARXPS data. This model was applied to PAA-treated surfaces with fixed nylon 6,6 composition. The adjustable parameters were PAA C_C (C_O=100-C_C), surface fraction f and layer thickness t. Since this model assumes a homogeneous substrate partially or completely covered by a homogeneous overlayer of uniform thickness, a depth profile is not generated.

Cumpson Model

The ARXPS version 4.xls[9] spreadsheet was used to calculate the expected apparent compositions $I_i(\theta)$ in a sample with given composition depth profiles $C_i(z)$, as a function of the photoemission angle θ. Three inflection points were positioned at depths which were a function of λ ($z_2=\lambda/3$, $z_3=4\lambda/5$, and $z_4=2\lambda$) for oxygen. The depth profile was defined in terms of adjustable parameters C_2 (=C_1), C_3

and C_4. For PAA-treated surfaces, C_O, C_N, and C_C were evaluated. For PDFOAmM-PAA-g-nylon surfaces, C_O and C_F were evaluated independently, while C_N and C_C were combined.

Trapezoid Model

The ARXPS version 4.xls[9] spreadsheet was used to calculate the expected apparent composition $I(\theta)$ in a sample with a given composition depth profile $C(z)$, as a function of the photoemission angle θ. Two inflection points (z_2 and z_3) were free to move along the depth axis and C_2 (=C_1) was varied. The element concentration was assumed to fall to the fixed C_3 value at some point. For PAA-treated surfaces, C_O was set to fall to the nylon 6,6 bulk value. For PDFOAmM-PAA-g-nylon surfaces, C_F was set to fall to zero.

6.2.3 *ARXPS Data Analysis*

For PAA-treated nylon films, the Fractional overlayer model requires a fixed nylon 6,6 composition in order to calculate the PAA overlayer composition (C_O and C_C), surface fraction and thickness. In section 6.3.1, ARXPS analysis of nylon 6,6 with the Cumpson model will be presented. The nylon 6,6 composition (C_O, C_N, and C_C) was determined by averaging the surface ($z = 0$) and maximum depth ($z = 2\lambda$) composition values from the Cumpson depth profile. For the Cumpson and Trapezoid models, the nylon 6,6 substrate composition was not required. For these models, the PAA reference composition was the theoretical molecular formula (minus hydrogen): C_O=40%, C_N=0%

and C_C= 60%. PAA surface fractions ($f_{PAA}^{C_N}$, $f_{PAA}^{C_O}$ and f_{PAA}^{ARXPS}) were defined based on the overall composition depth profiles using the following equations:

$$f_{PAA}^{C_N} = 1 - \left(C_{N\ \text{Treated Nylon}} / C_{N\ \text{Nylon}}\right) \tag{6. 1}$$

$$f_{PAA}^{C_O} = \frac{\left(C_{O\ \text{Treated Nylon}} - C_{O\ \text{Nylon}}\right)}{\left(C_{O\ \text{PAA}} - C_{O\ \text{Nylon}}\right)} \tag{6. 2}$$

$$f_{PAA}^{ARXPS} = \left(f_{PAA}^{C_N} + f_{PAA}^{C_O}\right) / 2 \tag{6. 3}$$

For PDFOAmM-PAA-g-nylon, the Cumpson and Trapezoid models will be used to determine PDFOAmM-PAA surface fractions ($f_{PDFOAmM-PAA}^{C_F}$, $f_{PDFOAmM-PAA}^{C_O}$ and f_{PAA}^{ARXPS}) as defined by the following equations:

$$f_{PDFOAmM\text{-}PAA}^{C_F} = C_{F\ PDFOAmM\text{-}PAA} / C_{F\ poly(PDFOAm)} \tag{6. 4}$$

$$f_{PDFOAmM-PAA}^{C_O} = \frac{\left(C_{O\ PDFOAmM-PAA} - C_{O\ PAA-g-Nylon}\right)}{\left(C_{O\ poly(PDFOAm)} - C_{O\ PAA-g-Nylon}\right)} \tag{6. 5}$$

$$f_{PDFOAmM-PAA}^{ARXPS} = \left(f_{PDFOAmM-PAA}^{C_N} + f_{PDFOAmM-PAA}^{C_O}\right) / 2 \tag{6. 6}$$

where the poly(PDFOAm) reference composition was the theoretical molecular formula (minus hydrogen): C_F=54% and C_O=4%. The PAA-g-Nylon reference composition was the surface (z = 0) composition determined for Adsorption-Grafted/Desorbed nylon from the Cumpson model (presented in section 6.3.4).

6.3 RESULTS AND DISCUSSION

6.3.1 Nylon 6,6

Normalized peak intensities $I_i(\theta)$ are shown in Table 6.2. At 0°, bulk values were observed: $I_N(\theta)$=12%, $I_O(\theta)$=13% and $I_C(\theta)$=75%. Toward the surface (75°), $I_O(\theta)$ values increased while $I_C(\theta)$ decreased.

Table 6.2 – Normalized Intensities: Nylon 6,6

Angle θ	$I_i(\theta)$		
	%N	%O	%C
75°	11	19	70
60°	11	17	72
45°	12	15	73
30°	12	14	74
0°	12	13	75

Cumpson Model

From the Cumpson depth profile, the surface composition (0 nm) was C_O=23%, C_N=11% and C_C=66% (Figure 6.1, arrows show the axis for each element). A transition was observed from 2 nm to 5.4 nm with C_O decreasing, C_N and C_C increasing to a composition slightly different from expected bulk values: C_O=10%, C_N=14% and C_C=76%. Figure 6.2 shows a good fit between observed and calculated $I_i(\theta)$ values (arrows show the axis for each element). **NOTE**: Nylon 6,6 substrate composition will be defined as the average of the Cumpson model compositions at the surface (0 nm) and bulk (5.4 nm): **C_O=17%, C_N=12% and C_C= 71%.**

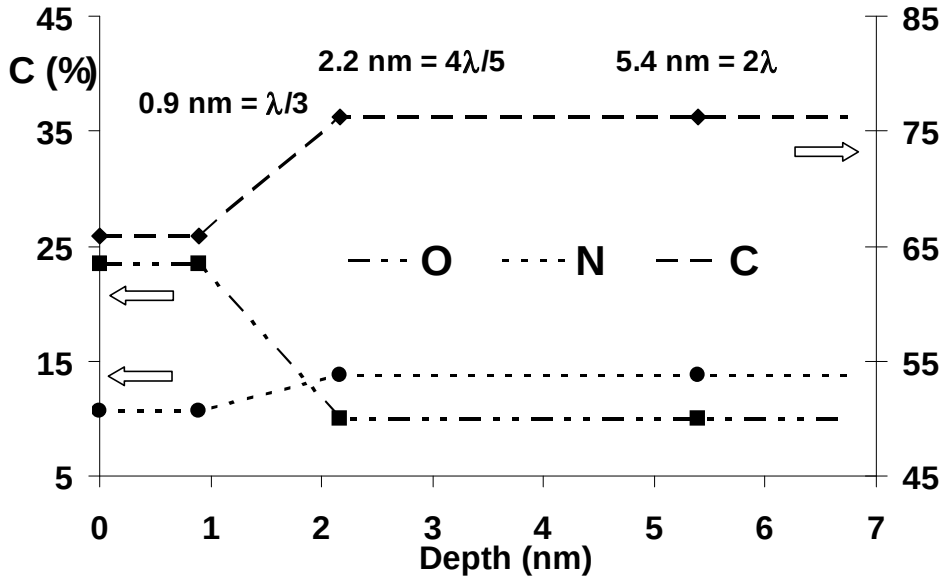

Figure 6.1– Nylon 6,6: Cumpson Depth Profile

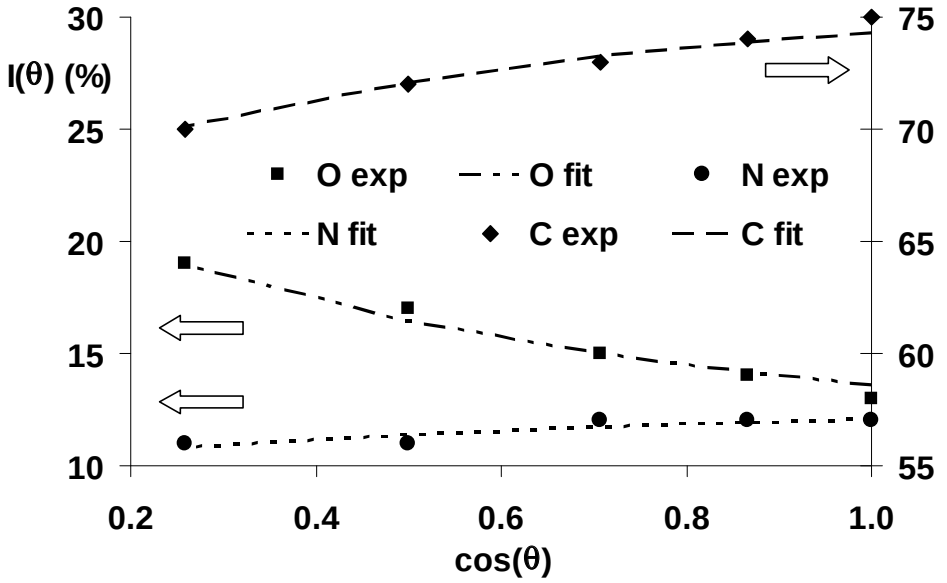

Figure 6.2– Nylon 6,6: Cumpson Fit

6.3.2 PAA-Adsorbed Nylon

Normalized peak intensities $I_i(\theta)$ for 11 g/L PAA-Adsorbed nylon are shown in Table 6.3. No significant changes with depth were observed for $I_i(\theta)$ values.

Table 6.3 – Normalized Intensities: PAA-Adsorbed Nylon

Angle θ	$I_i(\theta)$ %N	%O	%C
75°	7	23	70
60°	7	23	70
45°	7	22	71
30°	7	23	70
0°	7	22	71

Fractional Overlayer Model

Parameters f, t, and C_i are shown in Figure 6.3. PAA composition agreed with theory and PAA layer fraction agreed with $f_{PAA}(\theta_{Eff})=0.34\pm0.04$ and $f_{PAA}^{N(1s)}=0.47\pm0.12$, $f_{PAA}^{O(1s)}=0.36\pm0.09$, and $f_{PAA}^{XPS}=0.41\pm0.11$ from Chapter 4. As expected, the PAA layer thickness was ≤10 nm.[1] Figure 6.4 shows a good fit between observed and calculated $I_i(\theta)$ values.

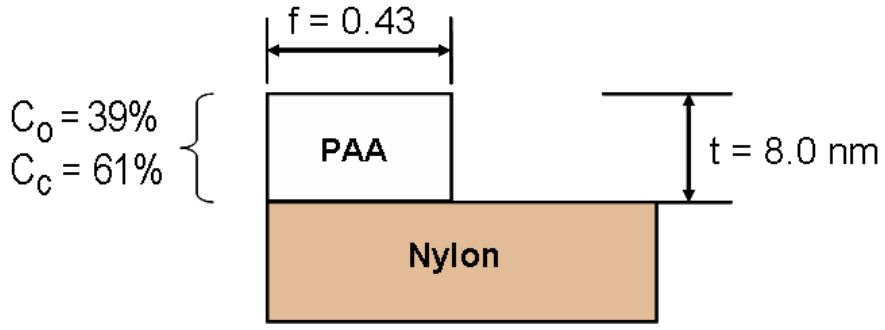

Figure 6.3– PAA-Adsorbed Nylon: Fractional Overlayer Parameters

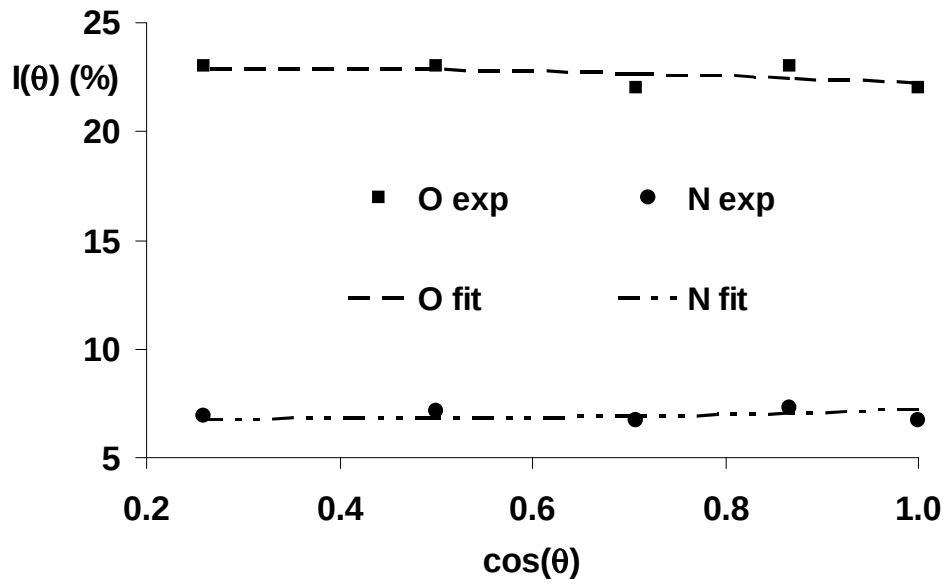

Figure 6.4– PAA-Adsorbed Nylon: Fractional Overlayer Fit

Cumpson Model

From the Cumpson depth profile (Figure 6.5), the surface composition was C_O=26%, C_N=7.2% and C_C=67%. A C_O transition was observed from 2.2 to 5.6 nm while C_N was constant. The composition at 5.6 nm was C_O=23%, C_N=7.0% and C_C=70%. This agrees with the Fractional Overlayer Model. Figure 6.6 shows a good fit between observed and calculated $I_i(\theta)$ values. PAA surface fractions at 0 nm were determined (Equations 6.1–6.3): $f_{PAA}^{C_N} = f_{PAA}^{C_O} = f_{PAA}^{ARXPS} = 0.40$, which agree with $f_{PAA}(\theta_{Eff})$, f_{PAA}^{XPS} (Chapter 4), and Fractional Overlayer model values. The PAA surface fraction decreased gradually with depth (Figure 6.7), indicating a distribution of PAA layer thicknesses rather than the single PAA layer thickness assumed by the Fractional Overlayer model. However, the distribution of PAA thickness appears to be narrow.

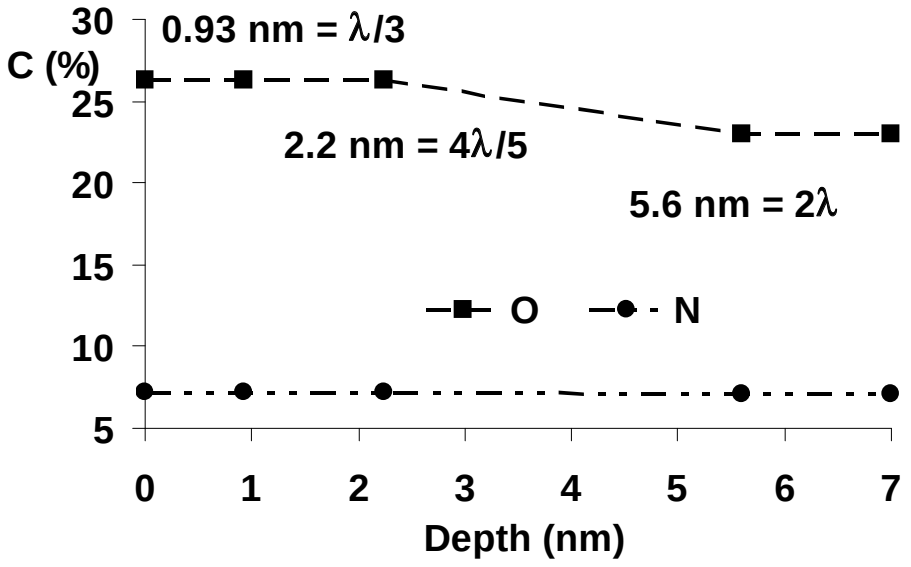

Figure 6.5– PAA-Adsorbed Nylon: Cumpson Depth Profile

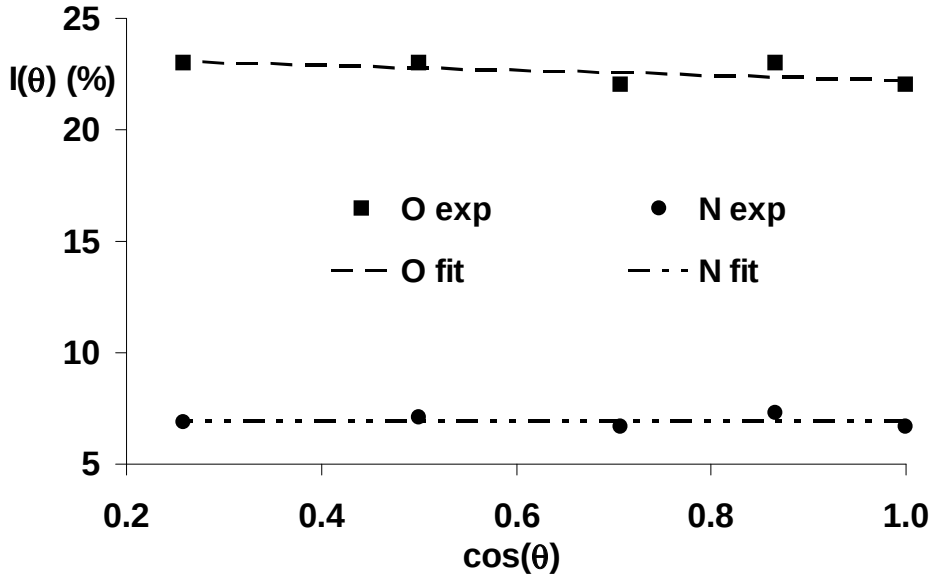

Figure 6.6– PAA-Adsorbed Nylon: Cumpson Fit

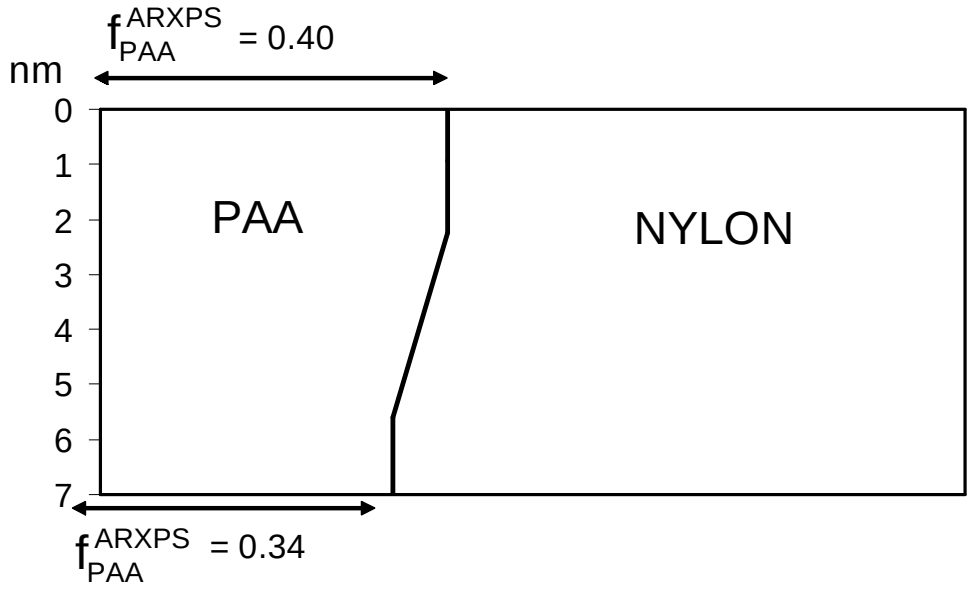

Figure 6.7– PAA-Adsorbed Nylon: Cumpson Parameters

Trapezoid Model

The C_O depth profile is shown in Figure 6.8. The C_3=17% value was fixed at the nylon 6,6 average Cumpson composition (Section 6.3.1) and C_2, z_2, and z_3 were variable parameters. The surface value of C_2=26% corresponds to $f_{PAA}^{C_O}$ =0.39 (Equation 6.2). This agrees with $f_{PAA}(\theta_{Eff})$ and f_{PAA}^{XPS} (Chapter 4) and Fractional Overlayer and Cumpson model values. Figure 6.9 shows a good fit between observed and calculated $I_i(\theta)$ values. PAA surface fraction undergoes a fairly sharp decrease with depth (Figure 6.10), indicating a narrow PAA layer thickness distribution from ~5-7 nm, which correlates well with the Fractional Overlayer model, but not as well with the Cumpson model.

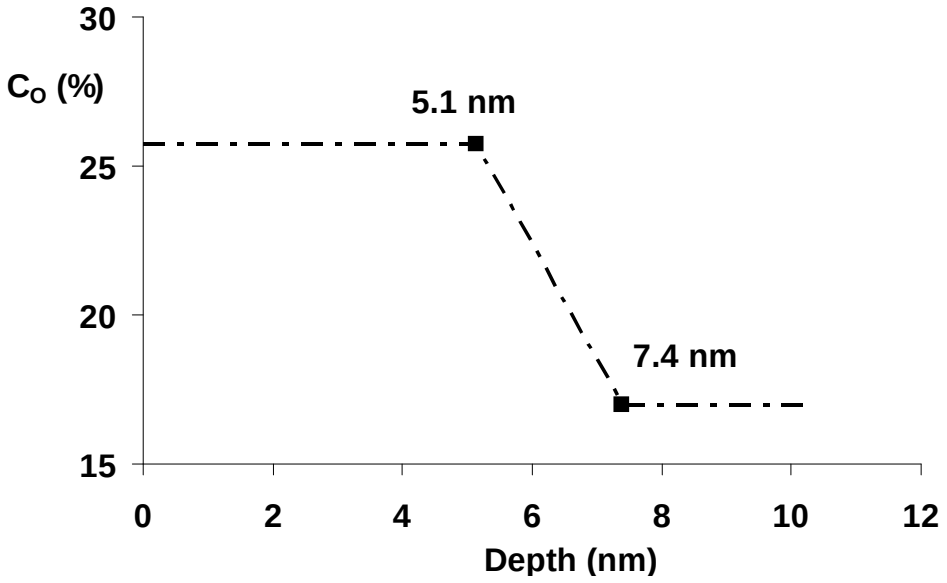

Figure 6.8– PAA-Adsorbed Nylon: Trapezoid Depth Profile

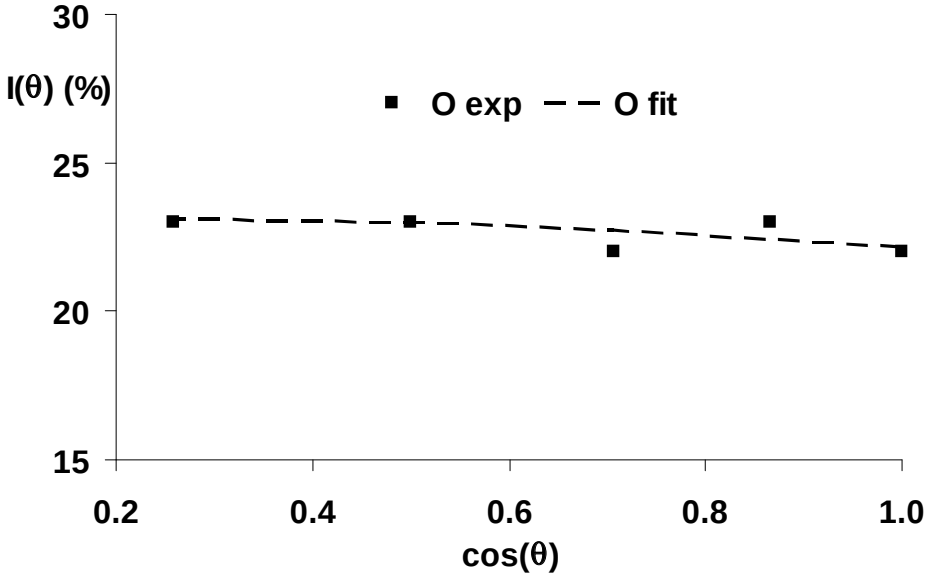

Figure 6.9– PAA-Adsorbed Nylon: Trapezoid Fit

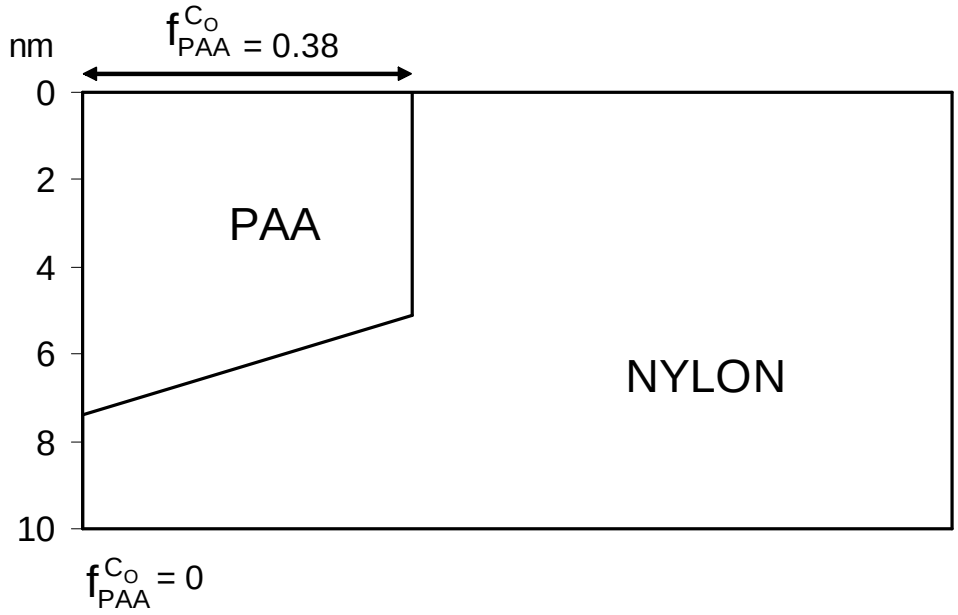

Figure 6.10– PAA-Adsorbed Nylon: Trapezoid Parameters

Solution-Grafted/Desorbed (SG/D) Nylon 6,6 Film

Normalized peak intensities $I_i(\theta)$ for SG/D (11g/L PAA, 40 mM DMTMM) are shown in Table 6.4. Toward the surface (75°), $I_N(\theta)$decreased, while $I_O(\theta)$ increased.

Table 6.4 – Normalized Intensities: SG/D Nylon

Angle	**$I_i(\theta)$**		
θ	**%N**	**%O**	**%C**
75°	7	22	72
60°	8	21	71
45°	8	20	72
30°	7	20	73
0°	9	20	72

Fractional Overlayer Model

Parameters f, t, and C_i for are shown in Figure 6.11. PAA composition agreed with theory and PAA layer fraction agreed with $f_{PAA}(\theta_{Eff})$=0.45±0.03, $f_{PAA}^{N(1s)}$ = 0.40±0.07, $f_{PAA}^{O(1s)}$ = 0.50±0.02, and f_{PAA}^{XPS} = 0.45±0.07 (Chapter 4). Figure 6.12 shows a good fit between observed and calculated $I_i(\theta)$ values. The SG/D PAA layer thickness was less than the adsorbed PAA layer thickness.

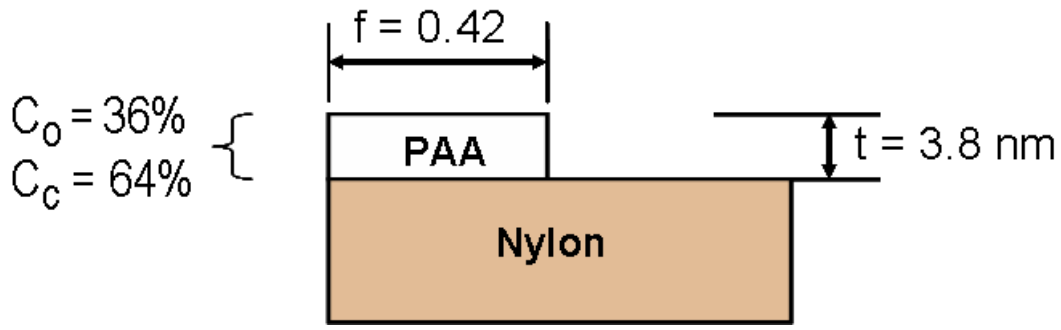

Figure 6.11– SG/D Nylon: Fractional Overlayer Parameters

Cumpson Model

From the Cumpson depth profile (Figure 6.13), the surface composition was C_O=25%, C_N=6.5% and C_C=69%. A C_O transition (0.93-5.6 nm) and a C_N transition (0.93-2.2 nm) were observed. The composition at 5.6 nm was C_O=19%, C_N =9.7% and C_C=72%. Figure 6.14 shows a good fit between observed and calculated $I_i(\theta)$ values. PAA surface fractions at 0 nm were determined (Equations 6.1–6.3): $f_{PAA}^{C_N}$=0.46, $f_{PAA}^{C_O}$=0.34 and f_{PAA}^{ARXPS}=0.40, which agree with $f_{PAA}(\theta_{Eff})$, f_{PAA}^{XPS} (Chapter 4) and Fractional Overlayer model values. PAA surface fraction significantly decreased with depth (Figure 6.15), indicating a wide PAA layer thickness distribution.

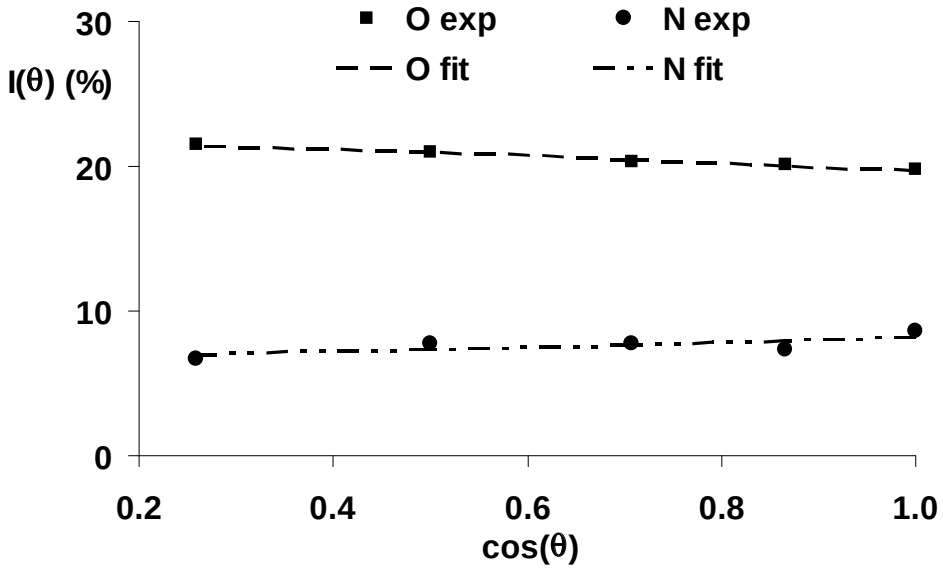

Figure 6.12– SG/D Nylon: Fractional Overlayer Fit

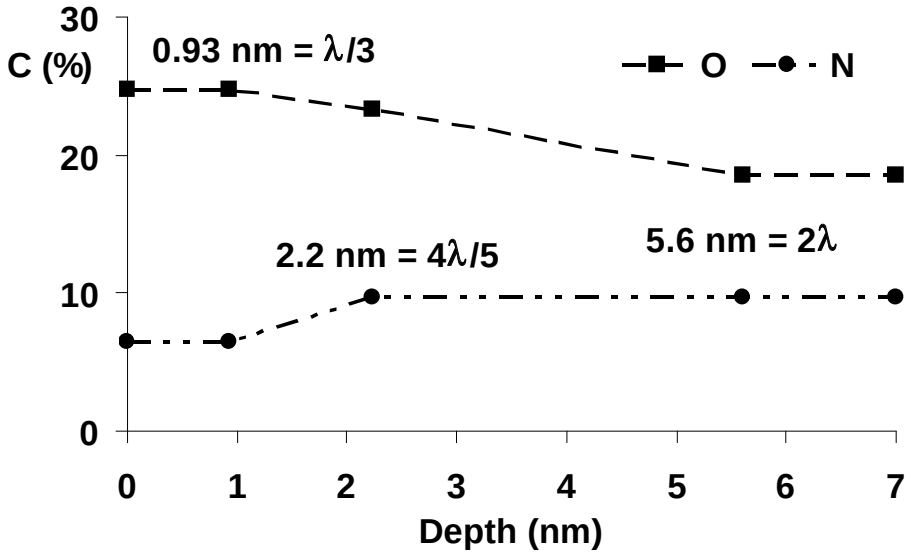

Figure 6.13– SG/D Nylon: Cumpson Depth Profile

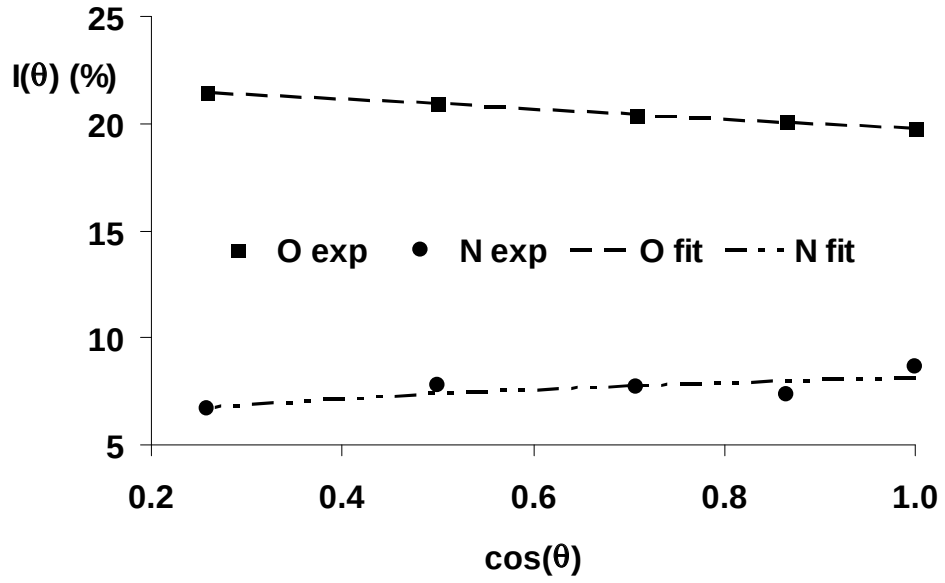

Figure 6.14– SG/D Nylon: Cumpson Fit

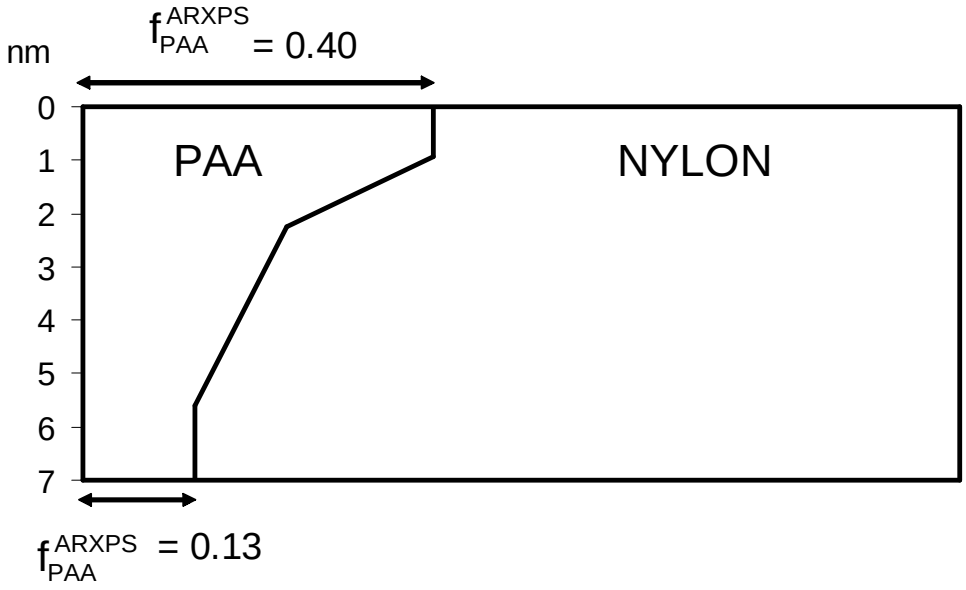

Figure 6.15– SG/D Nylon: Cumpson Parameters

Trapezoid Model

The C_O depth profile is shown in Figure 6.16. The C_3=17% value was fixed at the nylon 6,6 substrate composition (Section 6.3.1) and C_2, z_2, and z_3 were variable parameters. A surface value of C_2=24% corresponds to $f_{PAA}^{C_O}$=0.32 (Equation 6.2). This is slightly lower than $f_{PAA}(\theta_{Eff})$ and f_{PAA}^{XPS} (Chapter 4) and Fractional Overlayer and Cumpson model values. Figure 6.17 shows a good fit between observed and calculated $I_i(\theta)$ values. The large PAA surface fraction transition with depth (Figure 6.18) indicates a broad PAA layer thickness distribution from ~1-8 nm, which correlates reasonably well with the Cumpson model, but not as well with the Fractional Overlayer model.

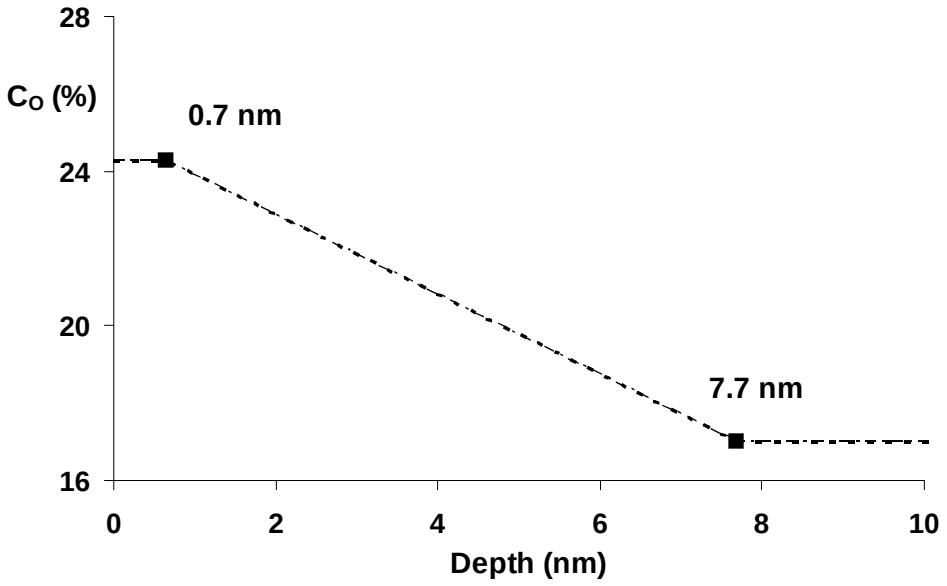

Figure 6.16– SG/D Nylon: Trapezoid Depth Profile

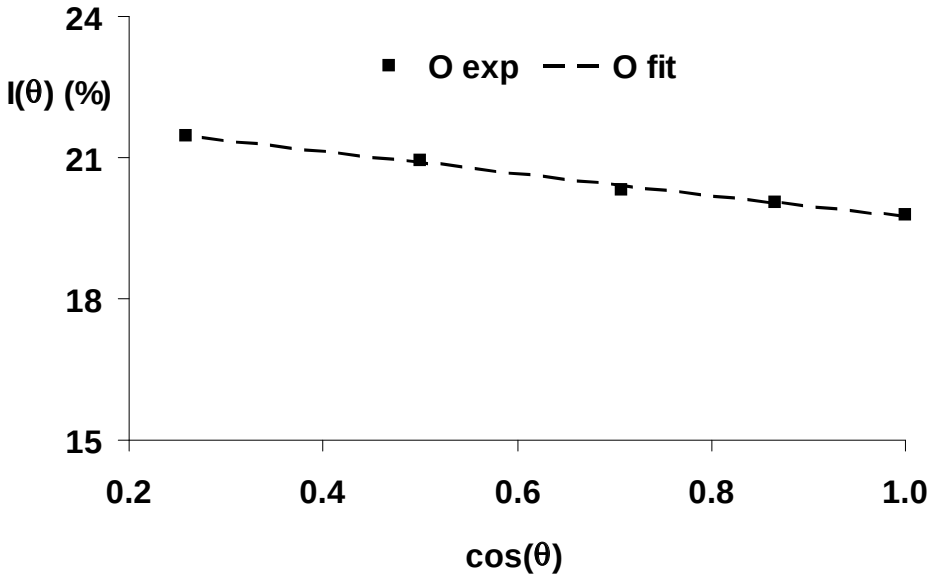

Figure 6.17– SG/D Nylon: Trapezoid Fit

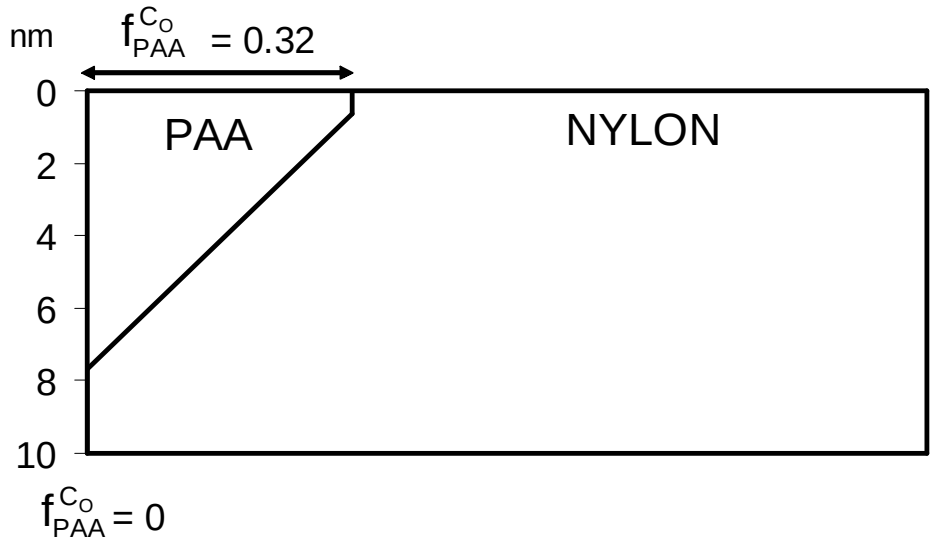

Figure 6.18– SG/D Nylon: Trapezoid Parameters

6.3.3 Adsorption-Grafted/Desorbed (AG/D) Nylon

Normalized peak intensities $I_i(\theta)$ for AG/D nylon (11 g/L, 5 mM DMTMM) are shown in Table 6.5. Toward the surface (75°), $I_N(\theta)$ decreased while $I_O(\theta)$ increased.

Table 6.5 – Normalized Intensities: AG/D Nylon

Angle	$I_i(\theta)$		
θ	%N	%O	%C
75°	2	30	68
60°	4	28	68
45°	4	28	68
30°	6	28	67
0°	6	26	67

Fractional Overlayer Model

Parameters f, t, and C are shown in Figure 6.19. PAA layer composition agreed with theory. PAA layer fraction agreed with $f_{PAA}(\theta_{Eff})=0.78\pm0.07$, $f_{PAA}^{N(1s)}=0.80\pm0.21$, $f_{PAA}^{O(1s)} = 0.68 \pm 0.16$, and $f_{PAA}^{XPS} = 0.74 \pm 0.19$ from Chapter 4. The AG/D layer thickness was lower while the surface fraction was higher compared to Adsorbed PAA. This suggests thick adsorbed PAA layers spreading during grafting. The "least squares" match in Figure 6.20 shows a good fit between observed and calculated $I_i(\theta)$ values.

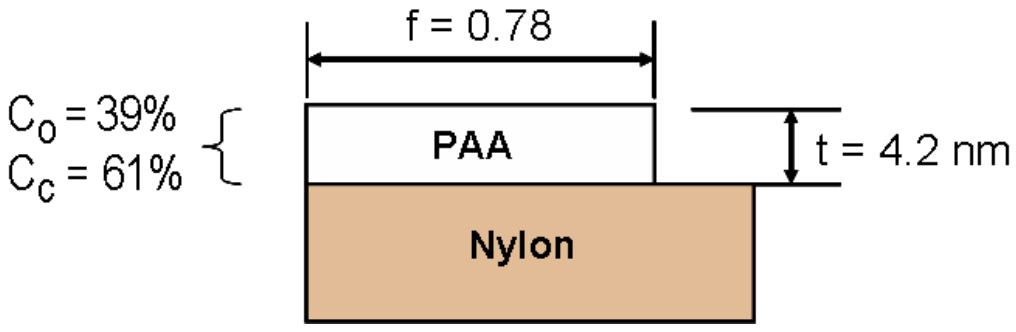

Figure 6.19– AG/D Nylon: Fractional Overlayer Parameters

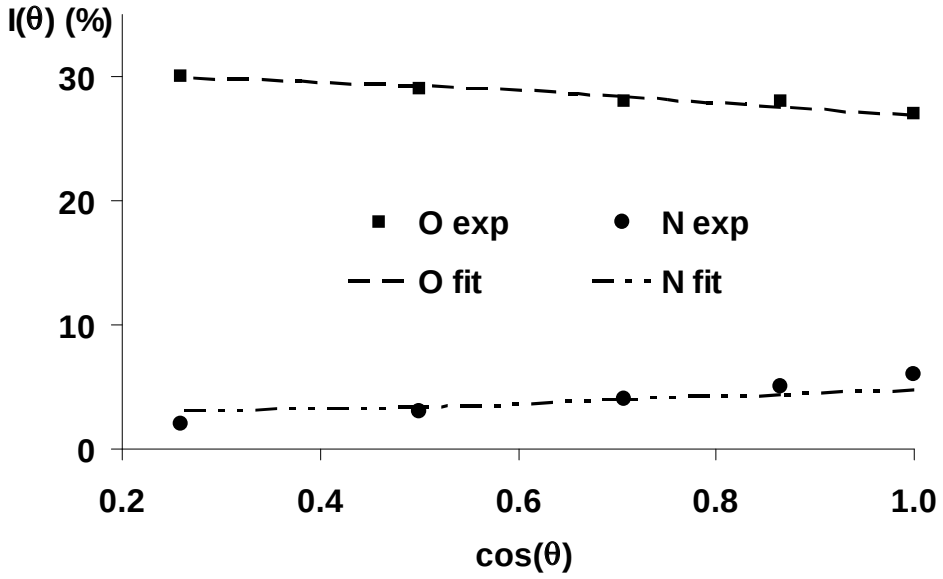

Figure 6.20– AG/D Nylon: Fractional Overlayer Fit

Cumpson Model

From the Cumpson depth profile (Figure 6.21), the surface composition was C_O=34%, C_N =2.0% and C_C = 64%. Transitions from 0.93 to 5.6 nm for C_O and 2.2 to 5.6 nm for C_N were observed. The composition at 5.6 nm was C_O=25%, C_N =12% and C_C=63%. Figure 6.22 shows a good fit between observed and calculated I(θ) values. PAA surface fractions at the surface (0 nm) were determined (Equations 6.1-6.3): $f_{PAA}^{C_N}$=0.83, $f_{PAA}^{C_O}$=0.76, and f_{PAA}^{ARXPS}=0.80, which are slightly higher than $f_{PAA}(\theta_{Eff})$, f_{PAA}^{XPS} (Chapter 4) and Fractional Overlayer model values. PAA surface fraction significantly decreased with depth (Figure 6.23), indicating a wide PAA layer thickness distribution greater than that of SG/D or Adsorbed PAA.

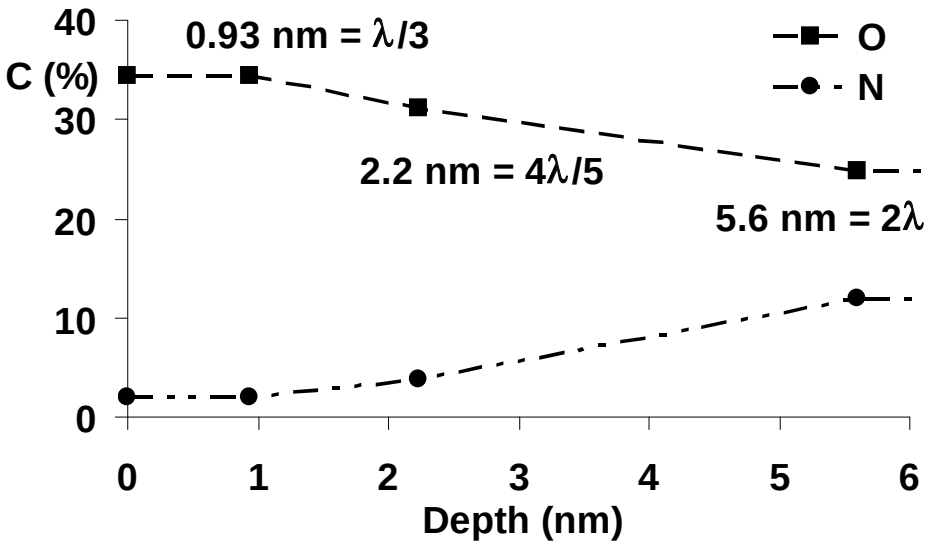

Figure 6.21– AG/D Nylon: Cumpson Depth Profile

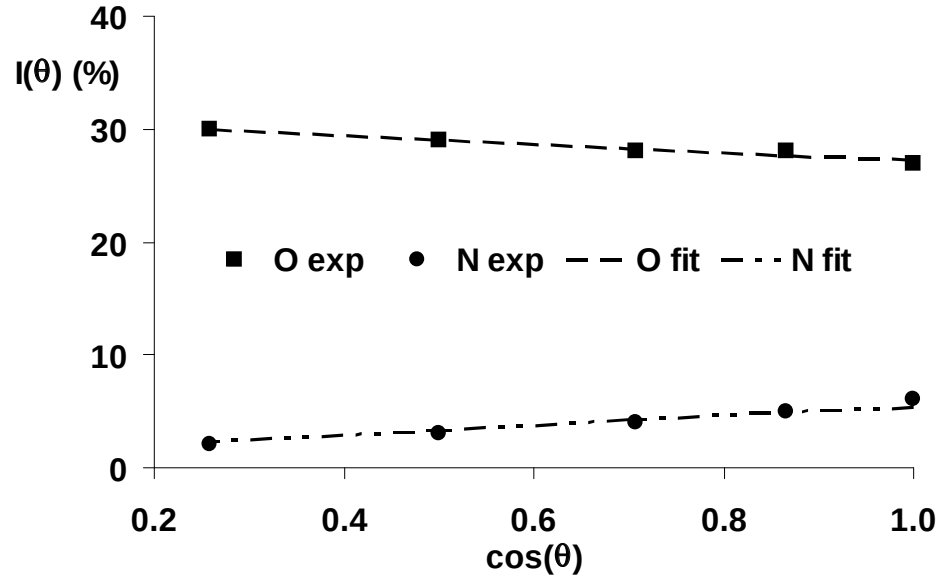

Figure 6.22– AG/D Nylon: Cumpson Fit

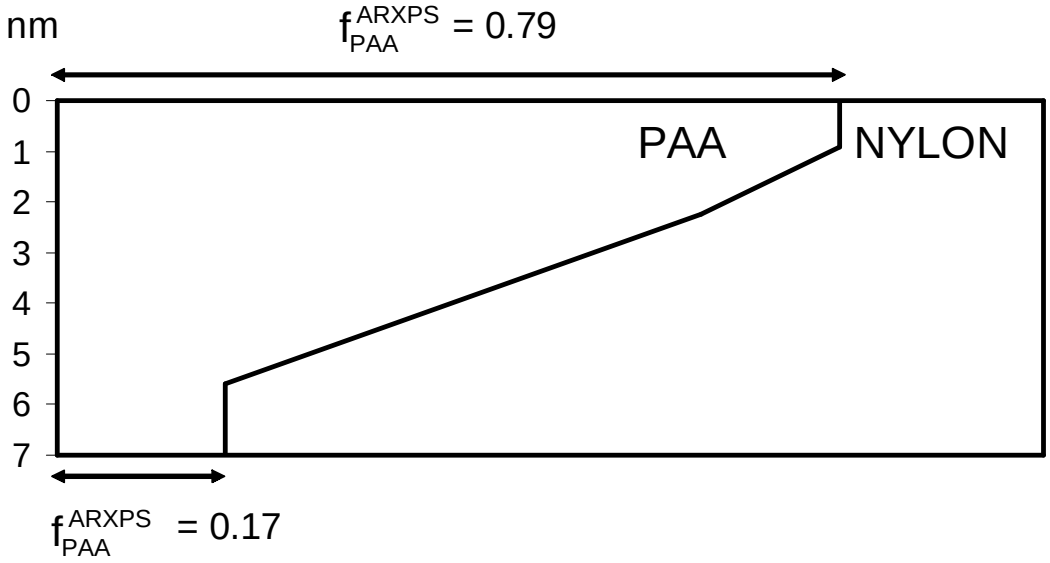

Figure 6.23– AG/D Nylon: Cumpson Parameters

Trapezoid Model

The C_O depth profile is shown in Figure 6.24. The C_3=17% value was fixed at the nylon 6,6 substrate composition (Section 6.3.1) and C_2, z_2, and z_3 were variable parameters. A surface value of C_2=34% corresponds to $f_{PAA}^{C_O}$ =0.73 (Equation 6.2). This agrees with $f_{PAA}(\theta_{Eff})$ and f_{PAA}^{XPS} (Chapter 4) and Fractional Overlayer and Cumpson model values. Figure 6.25 shows a good fit between observed and calculated $I_i(\theta)$ values. PAA surface fraction decreases significantly with depth (Figure 6.26), indicating a broad PAA layer thickness distribution ~0.1-12 nm. The transition agrees well with the Cumpson model, but not as well with the Fractional Overlayer model.

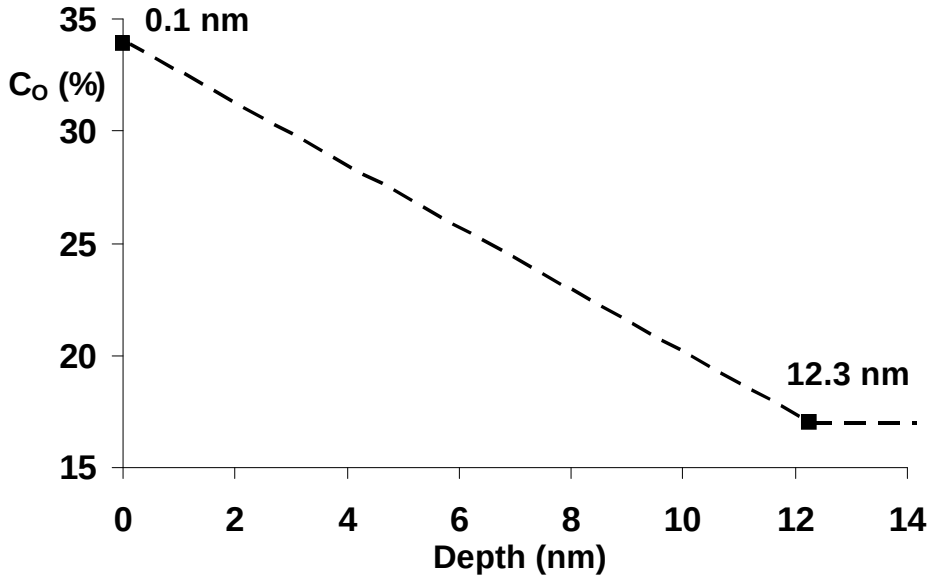

Figure 6.24– AG/D Nylon: Trapezoid Depth Profile

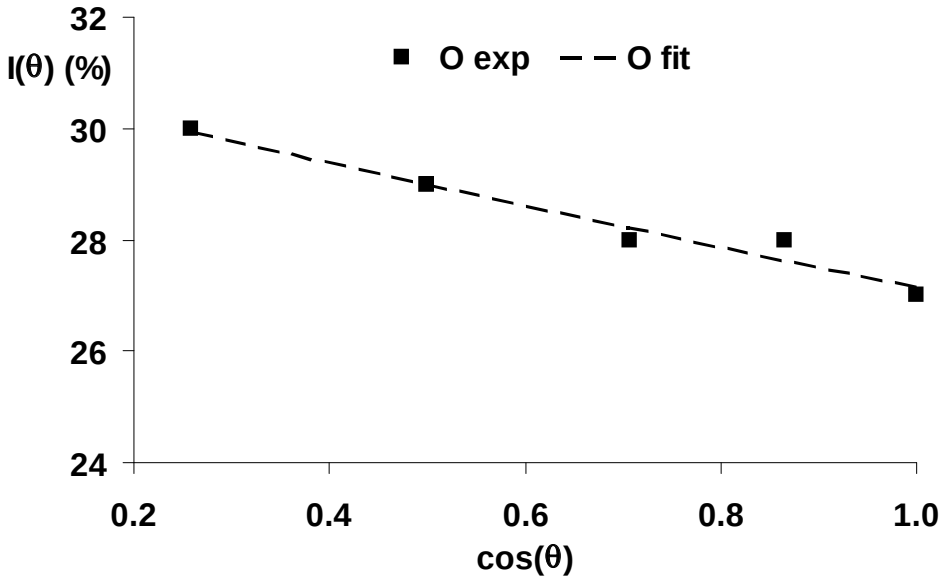

Figure 6.25– AG/D Nylon: Trapezoid Fit

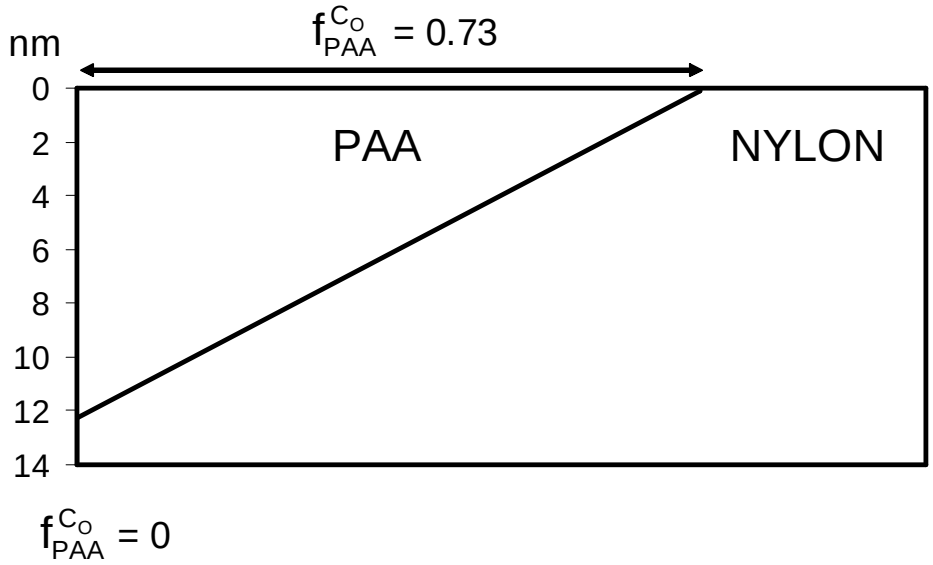

Figure 6.26– AG/D Nylon: Trapezoid Parameters

6.3.5 *Fluorinated PAA-g-Nylon: H_2O, pH=12*

For PDFOAmM-PAA-g-nylon (3/1 RAMEB/NH_2, pH=12), normalized peak intensities $I_i(\theta)$ are shown in Table 6.6. Toward the surface, $I_F(\theta)$ increased, $I_C(\theta)$ decreased and $I_O(\theta)$ and $I_N(\theta)$ were constant. At the surface, $I_F(\theta)$ and $I_N(\theta)$ values were very close to those for poly(PDFOAm), while $I_O(\theta)$ values were higher and $I_C(\theta)$ values were lower than those for poly(PDFOAm).

Table 6.6 – Normalized Intensities: PDFOAmM-PAA-g-Nylon (H_2O pH = 12)

Angle	$I_i(\theta)$			
θ	%N	%O	%C	%F
75°	3	8	35	54
60°	3	8	35	54
45°	3	8	36	52
30°	3	9	37	51
0°	4	9	38	50

Cumpson Model

The Cumpson depth profiles for fluorine and oxygen are shown in Figure 6.27. The surface composition C_F=61% and C_O=8% was constant for 1.9 nm, at which point C_F decreased while C_O increased to a composition at 4.8 nm of C_F=44% and C_O=11%. Figure 6.28 shows a good match between observed and calculated $I_i(\theta)$ values. PDFOAmM-PAA surface fractions were determined from Equations 6.4-6.6 using Cumpson model C_O=34% for PAA AG/Desorbed nylon and theoretical C_F=54% and C_O=4% values for poly(PDFOAm).

At the extreme surface (0 nm): $f^{C_F}_{PDFOAmM-PAA}$=1.13, $f^{C_O}_{PDFOAmM-PAA}$=0.87 and $f^{ARXPS}_{PDFOAmM-PAA}$=1.00, while at 4.8 nm: $f^{C_F}_{PDFOAmM-PAA}$=0.82, $f^{C_O}_{PDFOAmM-PAA}$=0.77 and $f^{ARXPS}_{PDFOAmM-PAA}$=0.79. These agree with contact angle ($f_{PDFOAmM-PAA}(\theta_{Eff})$=1.08±0.04) and the XPS ($f^{XPS}_{PDFOAmM-PAA}$=0.89±0.08) values from Chapter 5. ARXPS indicates uniformly distributed oxygen (Δf^{C_O} = 0.10 for 0 - 4.8 nm) with fluorine surface segregation ($\Delta f^{C_F} \cong 2\Delta f^{ARXPS} \cong 3\Delta f^{C_O}$). From Chapter 5, $\Delta f^{F(1s)-O(1s)}$ = 0.10, which falls between $\Delta f^{C_F-C_O}_{0nm}$=0.26 and $\Delta f^{C_F-C_O}_{4.8nm}$ = 0.05 values.

PDFOAmM-PAA surface fraction vs. depth is shown in Figure 6.29. At 0 nm, $f^{ARXPS}_{PDFOAmM-PAA}$ was 1.00 and f^{ARXPS}_{PAA} was 0.79. At ~5 nm, $f^{ARXPS}_{PDFOAmM-PAA}$ was 0.79 and f^{ARXPS}_{PAA} was 0.17. These results indicate that modification increases both the surface fraction and thickness of the grafted layer. Zhou and coworkers observed that the thickness of hyperbranched PAA layers doubled after similar PDFOA modification.[65]

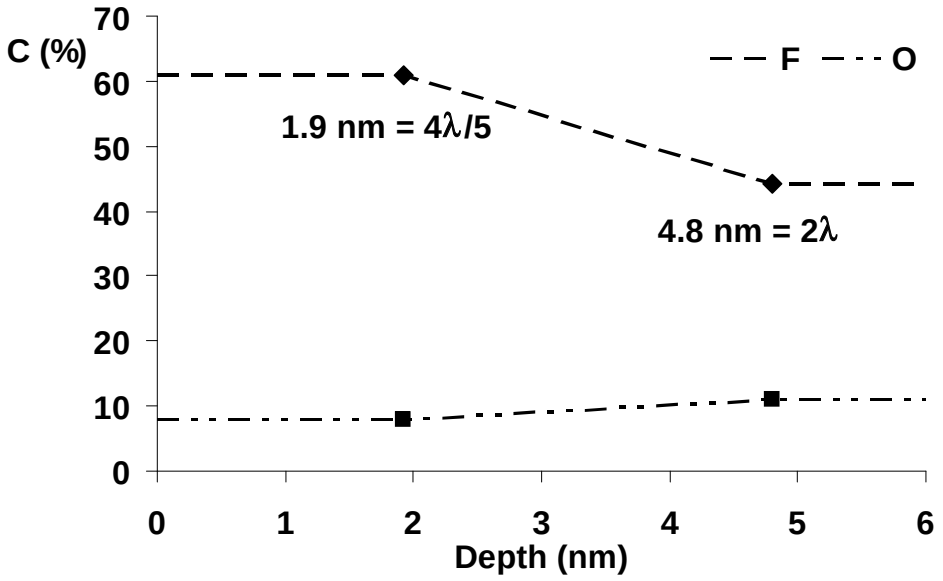

Figure 6.27– PDFOAmM-PAA-g-Nylon (H_2O pH=12): Cumpson Depth Profile

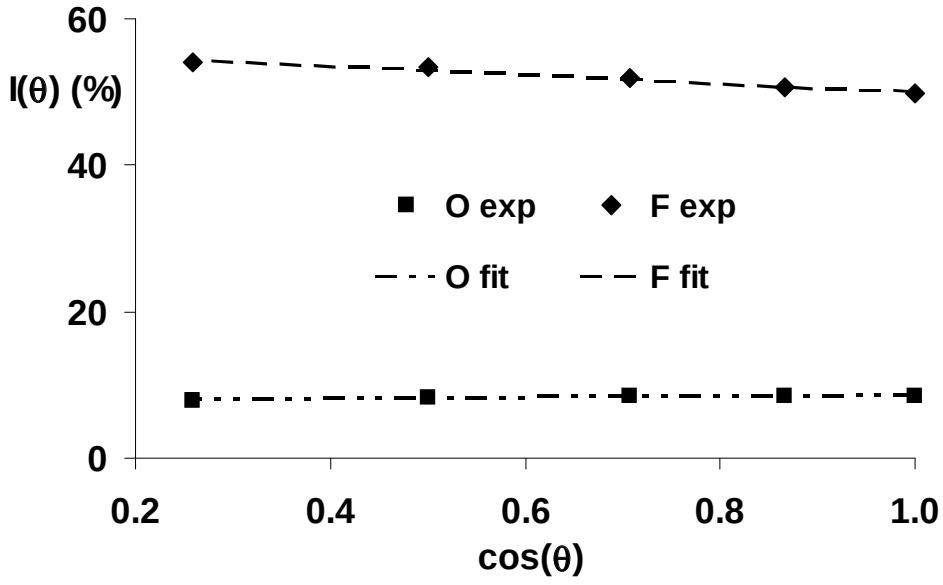

Figure 6.28– PDFOAmM-PAA-g-Nylon (H_2O pH=12): Cumpson Fit

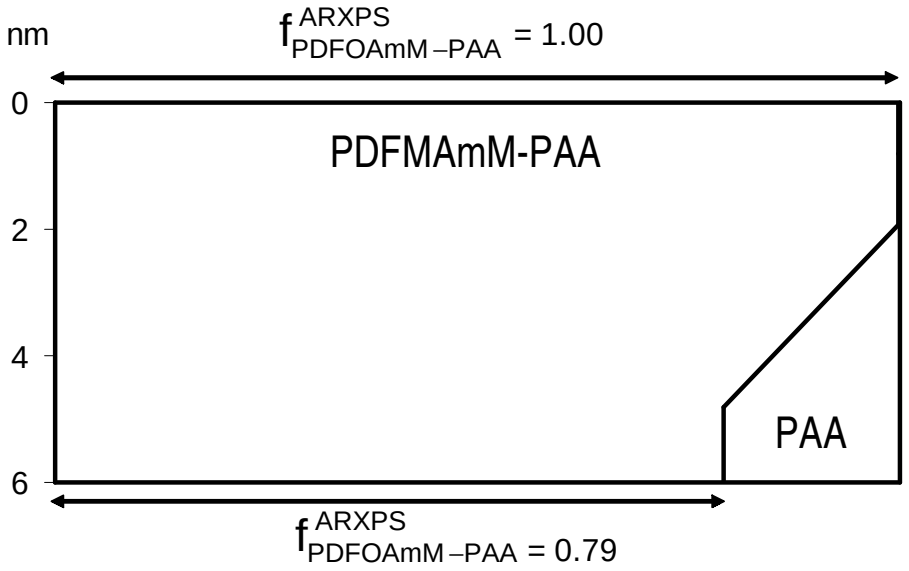

Figure 6.29– PDFOAmM-PAA-g-Nylon (H_2O pH=12): Cumpson Parameters

Trapezoid Model

The C_F depth profile is shown in Figure 6.30, where C_F = 0 at z_3. Figure 6.31 shows a good fit between observed and calculated $I_i(\theta)$ values. The surface composition, C_2=60%, indicates >100% surface coverage ($f^{C_F}_{PDFOAmM-PAA}$ = 1.12, Equation 6.4). This agrees with $f_{PDFOAmM-PAA}(\theta_{Eff})$ and $f^{F(1s)}_{PDFOAmM-PAA}$ from Chapter 5 and the Cumpson model. The PDFOAmM-PAA surface fraction variation with depth (Figure 6.32) points to a thickness distribution of ~3-12 nm.

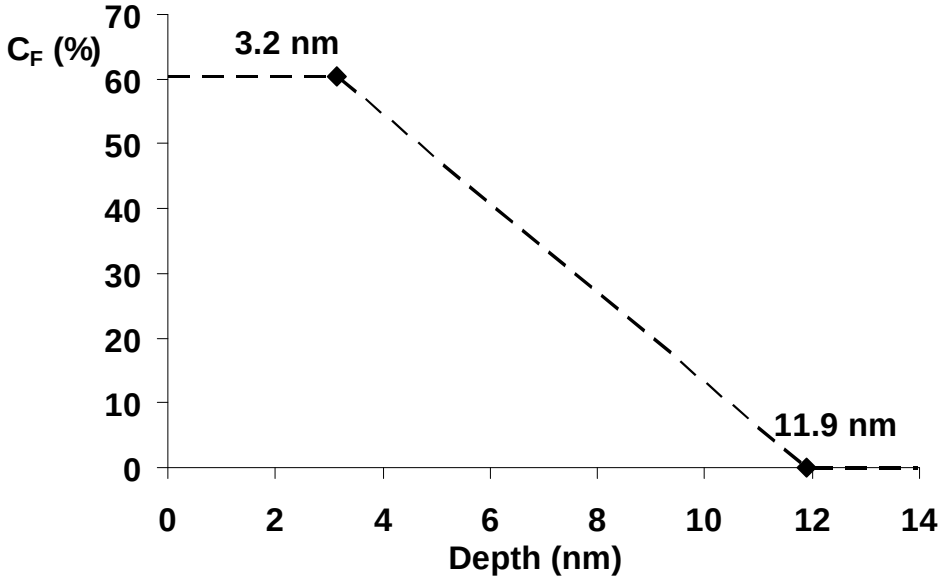

Figure 6.30– PDFOAmM-PAA-g-Nylon (H_2O pH=12): Trapezoid Depth Profile

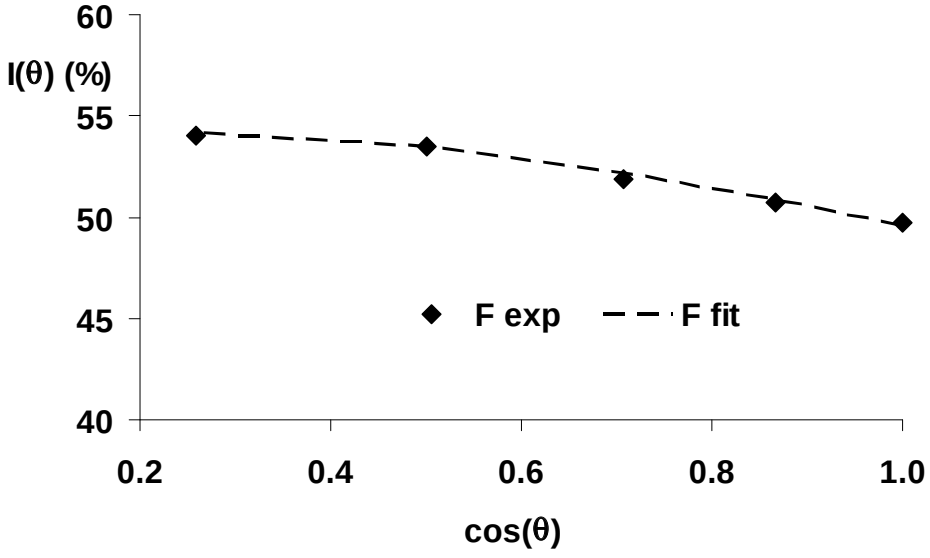

Figure 6.31– PDFOAmM-PAA-g-Nylon (H_2O pH=12): Trapezoid Fit

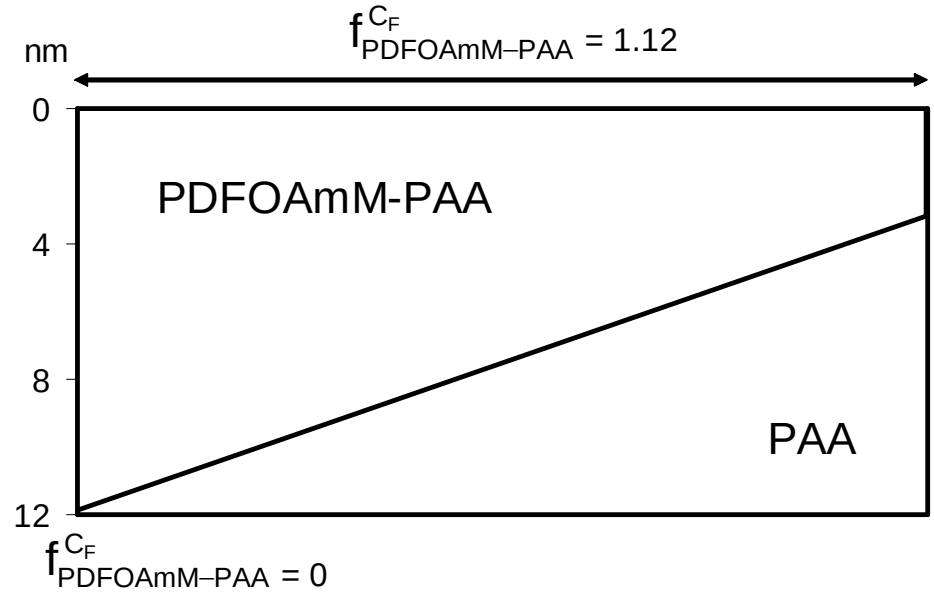

Figure 6.32– PDFOAmM-PAA-g-Nylon (H_2O pH=12): Trapezoid Parameters

6.3.6 *Fluorinated PAA-g-Nylon: MeOH*

For PDFOAmM-PAA-g-nylon (MeOH), normalized peak intensities $I_i(\theta)$ are shown in Table 6.7. Toward the surface, $I_F(\theta)$ increased, $I_C(\theta)$ decreased and $I_O(\theta)$ and $I_N(\theta)$ were constant. At the surface, $I_C(\theta)$ and $I_N(\theta)$ values were very close to those for poly(PDFOAm), while $I_O(\theta)$ values were higher and $I_F(\theta)$ values were lower than those for poly(PDFOAm).

Table 6.7 – Normalized Intensities: PDFOAmM-PAA-g-Nylon (MeOH)

Angle	$I_i(\theta)$			
θ	%N	%O	%C	%F
75°	4	19	41	37
60°	4	19	42	36
45°	4	20	43	33
30°	4	20	44	32
0°	5	22	42	31

Cumpson Model

The Cumpson depth profiles for fluorine and oxygen are shown in Figure 6.33. The surface composition of C_F=43% and C_O=18% was constant for 1.9 nm, after which C_F decreased while C_O increased, with C_O exceeding C_F at 3.6 nm. The composition at 4.8 nm was C_F=16% and C_O=33%. Figure 6.34 shows a good fit between observed and calculated $I_i(\theta)$ values. PDFOAmM-PAA surface fractions were determined from Equations 6.4-6.6 using Cumpson model C_O=34% for PAA AG/Desorbed nylon and theoretical C_F=54% and C_O=4% values for poly(PDFOAm).

At the extreme surface (0 nm): $f^{C_F}_{PDFOAmM-PAA}$=0.79, $f^{C_O}_{PDFOAmM-PAA}$=0.52 and $f^{ARXPS}_{PDFOAmM-PAA}$=0.66. At 4.8 nm: $f^{C_F}_{PDFOAmM-PAA}$=0.29, $f^{C_O}_{PDFOAmM-PAA}$=0.05 and $f^{ARXPS}_{PDFOAmM-PAA}$=0.17. These agree with contact angle ($f_{PDFOAmM-PAA}(\theta_{Eff})$=0.96±0.03) and XPS ($f^{XPS}_{PDFOAmM-PAA}$=0.48±0.09) values from Chapter 5. The PDFOAmM-PAA surface fraction significantly decreased with depth (Figure 6.35): $\Delta f^{C_F} \cong \Delta f^{ARXPS} \cong \Delta f^{C_O} = 0.5$ and $\Delta f^{C_F-C_O}_{0nm} - \Delta f^{C_F-C_O}_{4.8nm} = 0.03$. A transition is observed between a PDFOAmM-PAA rich region at the extreme surface (0 nm) and a PAA rich region (4.8 nm). At 0 nm, $f^{ARXPS}_{PDFOAmM-PAA}$ was 0.66 while f^{ARXPS}_{PAA} was 0.79. However, the C_O value (33%) at 4.8 nm is nearly equal to the value for the AG/D surface at 0 nm before reaction (34%). Therefore, the modification reaction appears to increase the thickness but NOT the surface fraction of the grafted layer.

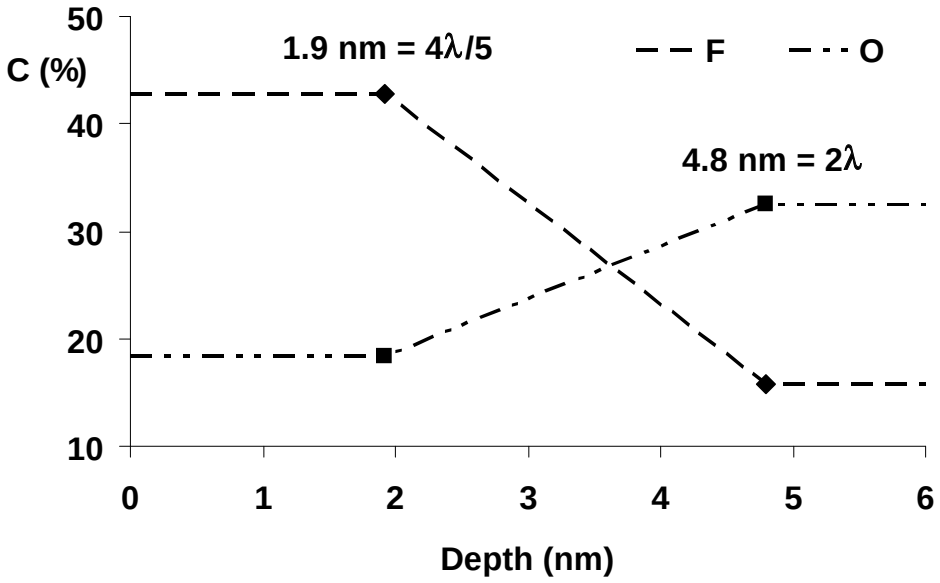

Figure 6.33– PDFOAmM-PAA-g-Nylon (MeOH): Cumpson Depth Profile

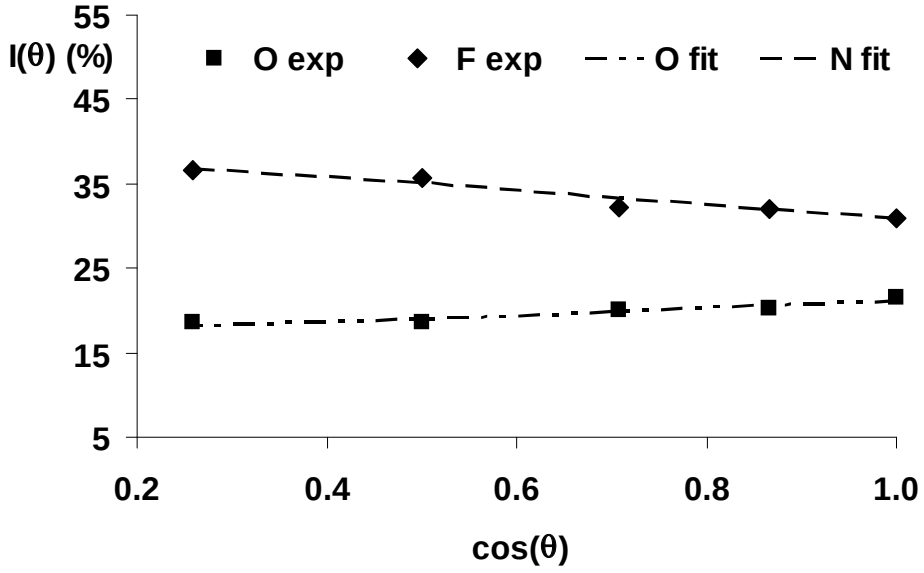

Figure 6.34– PDFOAmM-PAA-g-Nylon (MeOH): Cumpson Fit

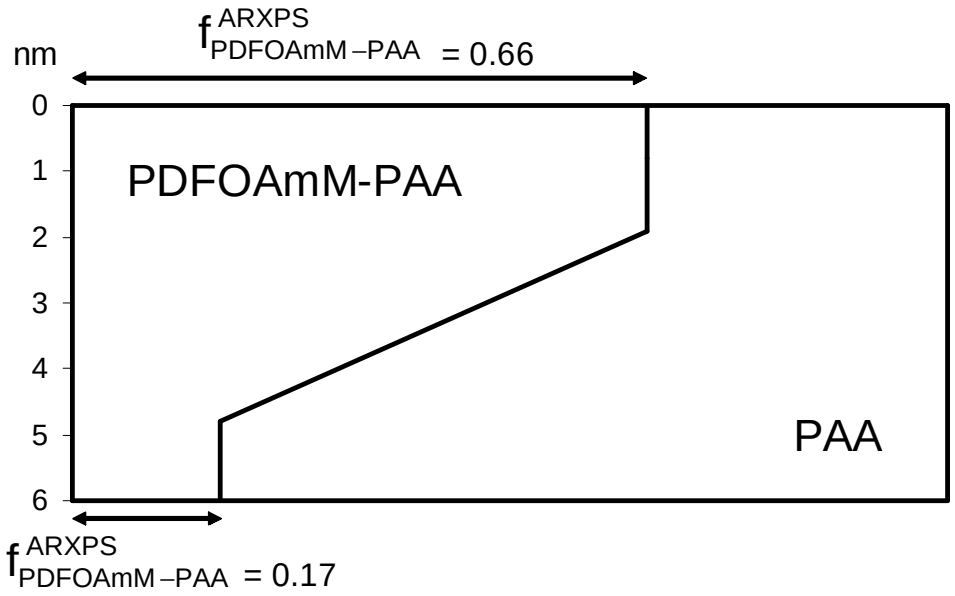

Figure 6.35– PDFOAmM-PAA-g-Nylon (MeOH): Cumpson Parameters

Trapezoid Model

The C_F depth profile is shown in Figure 6.36, where $C_F = 0$ at z_3. At the surface C_2=43%, which corresponds to $f^{C_F}_{PDFOAmM-PAA} = 0.79$ (Equation 6.4). These values are lower than contact angle values but agree with XPS and Cumpson model values. Figure 6.37 shows a good fit between observed and calculated $I_i(\theta)$ values. Figure 6.38 reveals a PDFOAmM-PAA thickness distribution of ~2-8 nm, which are thinner layers compared to the layers prepared in H_2O/RAMEB at pH=12.

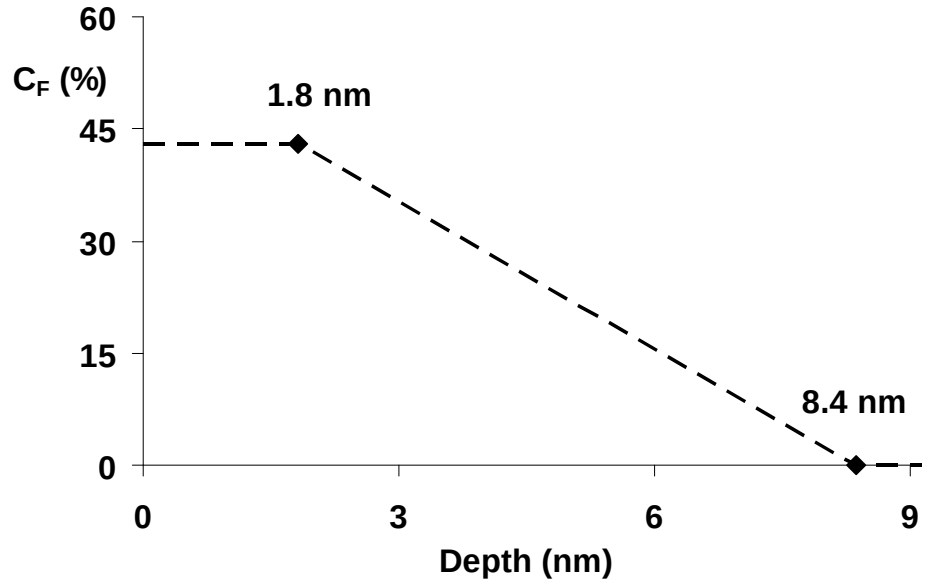

Figure 6.36– PDFOAmM-PAA-g-Nylon (MeOH): Trapezoid Depth Profile

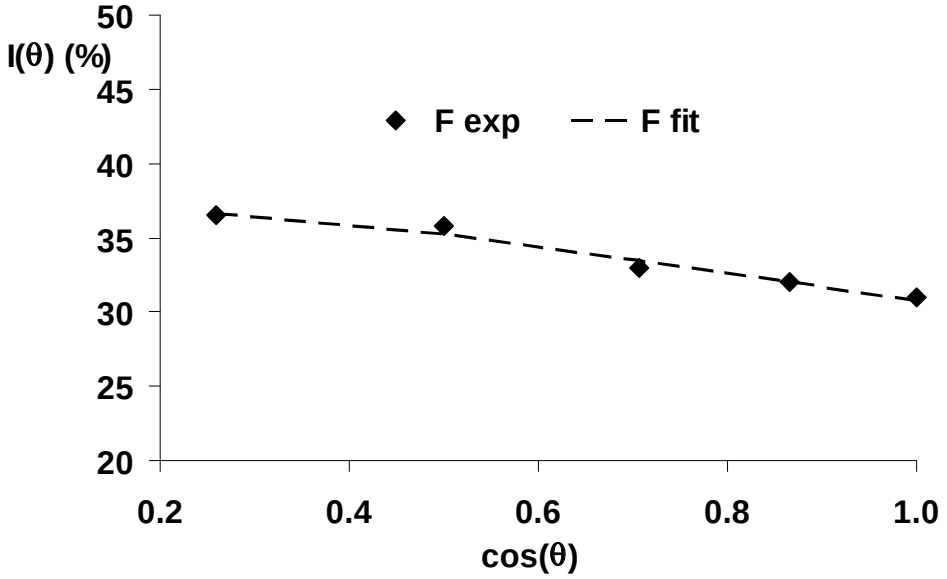

Figure 6.37– PDFOAmM-PAA-g-Nylon (MeOH): Trapezoid Fit

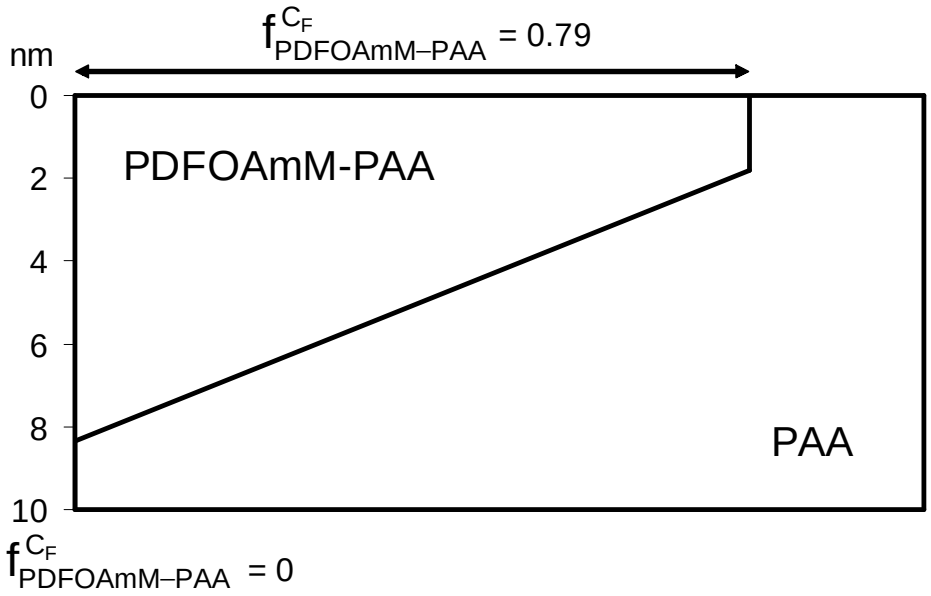

Figure 6.38– PDFOAmM-PAA-g-Nylon (MeOH): Trapezoid Parameters

6.3.7 *Comparison of ARXPS models*

Turning now to a comparison of the three depth profile models employed in this study, a "goodness of fit" estimate is given in Table 6.8 for each model profile, expressed as the sum of the squared differences (SSD) between (a) observed and calculated %O, %N, and %O+%N I(θ) values for untreated and PAA-treated nylon or (b) observed and calculated %O, %F, and %O+%F I(θ) values for PDFOAmM-PAA-g-nylon. Since the Cumpson model employs no special knowledge about the profile shape, this model performs more favorably than the trapezoid model which forces the %O of PAA-g-nylon and %F of PDFOAmM-PAA-g-nylon to set values at some depth beneath the surface. The Fractional Overlayer model, which makes assumptions about both composition and structure, is less consistent than the Cumpson and Trapezoid models.

Table 6.8- SSD for Calculated and Experimental $I_i(\theta)$ Values: Fitting of Data with ARXPS Models

Sample	i	Cumpson	Trapezoid	Fractional Overlayer
Nylon 6,6	O	0.716		
	N	0.267		
	O+N	0.984		
Adsorbed PAA	O	0.795	0.882	0.871
	N	0.270		0.386
	O+N	1.065		1.257
SG/D 40 mM DMTMM	O	0.008	0.010	0.038
	N	0.804		0.887
	O+N	0.812		0.925
AG/D 5 mM DMTMM	O	0.219	0.213	1.031
	N	0.736		1.989
	O+N	0.955		3.021
PDFOAmM-PAA-g-nylon: H_2O pH=12	O	0.090	0.508	
	F	0.327		
	O+F	0.417		
PDFOAmM-PAA-g-nylon: MeOH	O	0.514	0.182	
	F	0.469		
	O+F	0.984		

6.4 CONCLUSIONS

Nylon 6,6 ARXPS analysis was performed with the Cumpson model. At the surface, higher than expected C_O and lower than expected C_C and C_N values were observed. Close to expected values for a nylon 6,6 repeat unit were observed within 2 nm of the surface. Thus it is clear that the nylon 6,6 substrate is not uniform.

Adsorbed, Solution-Grafted/Desorbed, and Adsorbed-Grafted/Desorbed nylon 6,6 ARXPS analysis was performed with the Fractional Overlayer, Cumpson, and Trapezoid models. PAA surface coverage was >70% for Adsorption-Grafted/Desorbed nylon. Overall, the Cumpson model displayed the lowest sum of squared difference (SSD) values, followed by the Trapezoid and then the Fractional Overlayer models. The

Fractional Overlayer model, which assumes uniform overlayer and uniform substrate compositions, provided PAA surface fractions consistent with Cumpson and Trapezoid models as well as with XPS (f_{PAA}^{XPS}) and contact angle ($f_{PAA}(\theta_{Eff})$) values. However, the Fractional Overlayer model calculated a single PAA layer thickness value while the Cumpson and Trapezoid models revealed PAA layer thickness distributions.

The PAA layer thickness of PAA-Adsorbed nylon was greater than that of Adsorbed-Grafted nylon, which was greater than that of Solution-Grafted nylon. Thus the Adsorption-Grafting mechanism follows the Post-Adsorption Conformational Change RSA (PCC-RSA) Model. First PAA adsorbs onto nylon 6,6 in thick islands. Next, DMTMM activates PAA for spreading and grafting across the surface into thinner layers. A proposed structure for an Adsorbed-Grafted nylon surface is shown in Figure 6.39.

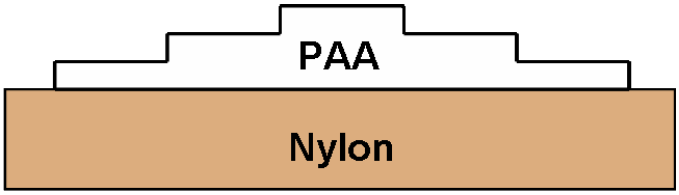

Figure 6.39– Proposed Structure for an Adsorbed-Grafted Nylon Surface

For the PDFOAmM-PAA-g-nylon reaction in H_2O pH=12, the Cumpson and the Trapezoid models revealed >100% PDFOAmM-PAA surface fraction at the exterior. This exceeds the >70% Adsorption-Grafted/Desorbed PAA surface fraction, indicating that modification spreads the grafted layer even further across the surface. The fluorine concentration decreased slightly with depth, while the oxygen concentration did not, indicating a highly fluorinated region with fluorine surface segregation. The thickness of

the grafted layer was also found to be greater after fluorination. The Trapezoid model revealed a PDFOAmM-PAA rich region ~3-12 nm. For the MeOH reaction, the Cumpson model revealed a less fluorinated surface (>60% PDFOAmM-PAA surface fraction) ~ 2 nm thick covering a PAA-rich region. While the overall grafted layer was also found to be thicker after MeOH modification, the Trapezoid model found a thin PDFOAmM-PAA region ~2-8 nm. Proposed structures for PDFOAmM-PAA-g-nylon surfaces prepared in MeOH or H_2O pH=12 are shown in Figure 6.40.

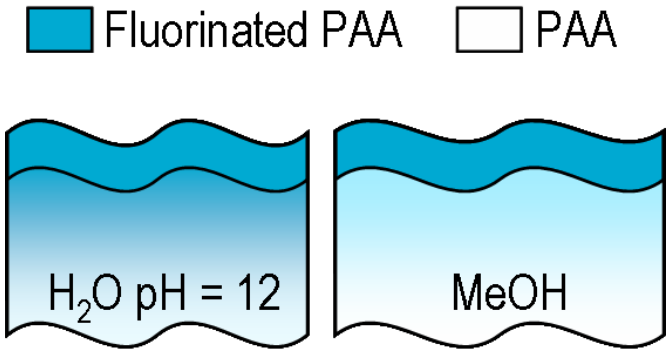

Figure 6.40– Proposed Structure for PDFOAmM-PAA-g-Nylon Surfaces

CHAPTER 7

SURFACE MODIFICATION OF TEXTILES

7.1 INTRODUCTION

Fluorinated PAA surface-grafted nanoscaffolds (SGNs) have been successfully prepared on nylon 6,6 films. The next step is to prepare and evaluate fluorinated SGNs on nylon 6,6 fabrics and carpet. The treatments will be evaluated in several categories: water and oil repellency, stain resistance, and stability to alkaline conditions.

7.2 EXPERIMENTAL SECTION

7.2.1 Materials

Nylon fabric (filament nylon 6,6 taffeta, semi-dull, scoured, heat-set, 59 g/m^2, TestFabrics Inc.), nylon carpet (nylon 6,6 single level loop-pile, 814 g/m^2 fiber, J&J Industries), poly(acrylic acid) powder (PAA, M_w=450 kg/mol, Aldrich), sodium hydroxide (NaOH, Fisher), methanol (MeOH, Aldrich), randomly methylated-β-cyclodextrin (RAMEB, M_n=1.31 kD, Aldrich), 4-(4,6-dimethoxy-1,3,5-triazin-2-yl)-4-methylmorpholinium chloride (DMTMM, Acros Organics), 1*H*,1*H*-pentadecafluorooctylamine (PDFOA, SynQuest Labs), hexadecane (Aldrich), and Kool-Aid® (cherry) were used as received.

7.2.2 Typical Procedures

Synthesis of PAA Surface-Grafted Nylon Fabric

PAA (3.30 g, 45.8 mmol) was dissolved in distilled H_2O (300 ml) with vigorous mixing at 25°C. A 20×20 cm^2 nylon fabric held on a 15-cm diameter embroidery hoop

was immersed in the PAA solution. The fabric and solution were placed on a rotary stirrer overnight to adsorb PAA onto the fabric surface. After adsorption was complete, the fabric was immersed in distilled H_2O and rinsed with vigorous mixing for 24 hr. This step was repeated twice with fresh distilled H_2O. For surface grafting, the PAA-Adsorbed fabric was immersed in 0.10 M DMTMM solution prepared by dissolving DMTMM (8.30 g, 30.0 mmol) in distilled H_2O (300 ml) with vigorous mixing at 25°C. The reaction proceeded for 24 hr. At this point, the PAA Adsorption-Grafted fabric was rinsed with distilled H_2O for 1 hr and air dried.

PDFOA Modification of PAA Surface-Grafted Nylon Fabric

MeOH reaction

At 25°C, PDFOA (12.0 g, 30 mmol) was dissolved in MeOH (280 ml). The PAA Adsorption-Grafted fabric was immersed in the solution for 15 min. DMTMM (8.30 g, 30 mmol) was dissolved in MeOH (20 ml) and added to the PDFOA solution to initiate the modification of CO_2H groups. The reaction proceeded for 24 hr.

H_2O, pH=12 reaction

At 40°C, RAMEB (121 g, 90 mmol), NaOH (0.120 g, 3 mmol), and PDFOA (12.0 g, 30 mmol) were mixed in distilled H_2O (280 ml) until a clear solution formed. The solution was cooled to 25°C and the PAA Adsorption-Grafted fabric was immersed in the solution for 15 min. DMTMM (8.30 g, 30 mmol) was dissolved in distilled H_2O (20 ml) and added to the RAMEB/NaOH/PDFOA solution to initiate the modification of CO_2H groups. The reaction proceeded for 24 hr.

Post-treatment of PDFOAmM-PAA-g-Nylon Fabric

PDFOAmM-PAA-g-nylon fabric was (1) rinsed overnight in distilled H_2O, (2) rinsed in an aqueous 0.01M RAMEB solution at 40°C for 15 min., (3) rinsed in distilled H_2O at 40°C for 15 minutes, (4) rinsed overnight in distilled H_2O, and (6) air dried.

Synthesis of PAA Surface-Grafted Nylon Carpet

PAA (3.85 g, 53.5 mmol) was dissolved in distilled H_2O (350 ml) with vigorous mixing at 25°C. A 14×14 cm^2 nylon carpet square was immersed in the PAA solution. The carpet and solution were placed on a rotary stirrer overnight to adsorb PAA onto the fiber surface. After adsorption was complete, the carpet was immersed in distilled H_2O and rinsed with rotary mixing for 24 hr. This step was repeated twice with fresh distilled H_2O. For surface grafting, the PAA-Adsorbed carpet was immersed in 0.10 M DMTMM solution prepared by dissolving DMTMM (9.89 g, 35.0 mmol) in distilled H_2O (350 ml) with vigorous mixing at 25°C. The reaction proceeded for 24 hr. At this point, the PAA Adsorption-Grafted carpet was rinsed with distilled H_2O for 1 hr and air dried.

PDFOA Modification of PAA Surface-Grafted Nylon Carpet

MeOH reaction

PDFOA (6.0 g, 15 mmol) was dissolved in MeOH (120 ml) at 25°. A 7×7 cm^2 PAA Adsorption-Grafted carpet square was immersed in the solution for 15 min. DMTMM (4.15 g, 15 mmol) was dissolved in MeOH (30 ml) and added to the PDFOA solution to initiate modification of CO_2H groups. The reaction proceeded for 24 hr.

H_2O, pH=12 reaction

At 40°C, RAMEB (59.0 g, 45 mmol), NaOH (0.060 g, 1.5 mmol), and PDFOA (6.0 g, 15 mmol) were mixed in distilled H_2O (120 ml) until a clear solution formed. The solution was cooled to 25°C and a 7×7 cm^2 section of PAA Adsorption-Grafted carpet was immersed in the solution for 15 min. DMTMM (4.15 g, 15 mmol) was dissolved in distilled H_2O (30 ml) and added to the RAMEB/NaOH/PDFOA solution to initiate modification of CO_2H groups. The reaction proceeded for 24 hr.

Post-treatment of PDFOAmM-PAA-g-Nylon Carpet

PDFOAmM-PAA-g-nylon carpet was (1) rinsed overnight in distilled H_2O, (2) rinsed in an aqueous 0.01M RAMEB solution at 40°C for 15 min., (3) rinsed in distilled H_2O at 40°C for 15 minutes, (4) rinsed overnight in distilled H_2O, and (6) air dried.

Alkaline Treatment of PAA-g-Nylon and PDFOAmM-PAA-g-Nylon Carpets

PAA-g-Nylon and PDFOAmM-PAA-g-nylon were (1) immersed in 1M NaOH (pH=14) for 2 hr and (2) rinsed in MeOH. This treatment was used to convert PAA CO_2H groups into their sodium salts to enhance stain repellency and to evaluate the stability of these surface-grafted layers to the highly alkaline conditions used in commercial steam-cleaning processes.

7.2.3 Evaluation of Textile Substrates

Water Repellency of Fabrics and Carpets

The textile specimens were placed flat on a smooth, horizontal surface. Small drops (approximately 0.5 cm) of distilled water were placed on the specimen surface from a dropper from a height of approximately 0.5 cm above the surface. The drops were observed for 30 s. The specimens were evaluated for drop wetting and/or wicking around the drops. The test was repeated with double strength cherry-flavored Kool-Aid® at 25°C for photographs.

Oil Repellency of Fabrics

The textile specimens were placed flat on a smooth, horizontal surface. Small drops of hexadecane (approximately 0.5 cm) were placed on the specimen surface from a dropper from a height of approximately 0.5 cm above the surface. The drops were observed for 30 s. The specimens were evaluated for drop wetting and/or wicking around the drops.

Stain Resistance of Carpets

The textile specimens were immersed 3-4 cm in double strength cherry-flavored Kool-Aid® at 60°C for 60 s, rinsed in cold water for 30 s, and dried at 60°C. Specimens were observed for wetting and/or wicking and residual stain was assessed after drying.

7.3 RESULTS AND DISCUSSION

7.3.1 Water Repellency

Both nylon 6,6 and PAA-g-nylon fabrics and carpets were highly water wetting and water drops were immediately absorbed by the fibers and spread by wicking. However, all PDFOAmM-PAA-g-nylon fabrics and carpets were extremely water repellant. Water drops were not absorbed into the fibers and were readily removed by overturning the substrate or by wicking up into a Kim-wipe™ tissue. A comparison is shown between untreated and PDFOAmM-PAA-g-nylon fabrics using a drop of double strength cherry-flavored Kool-Aid® in Figure 7.1.

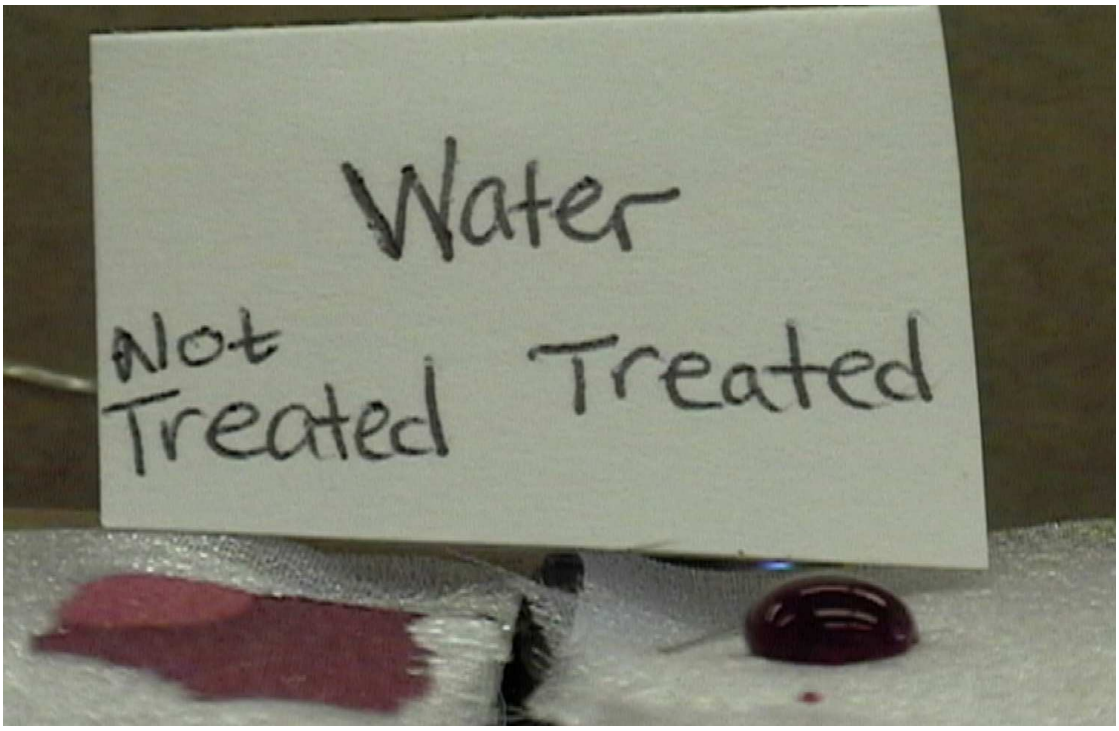

Figure 7.1– Water repellency of untreated and PDFOAmM-PAA-g-nylon fabrics

7.3.2 Oil Repellency

Both nylon 6,6 and PAA-g-nylon fabrics and carpets were highly oil wetting and oil drops were immediately absorbed by the fibers and spread by wicking. However, all PDFOAmM-PAA-g-nylon fabrics and carpets were extremely water repellant. Oil drops were not absorbed into the fibers and were readily removed by overturning the substrate or by wicking up into a Kim-wipe™ tissue. A comparison is shown between untreated and PDFOAmM-PAA-g-nylon fabrics using an oil drop in Figure 7.2.

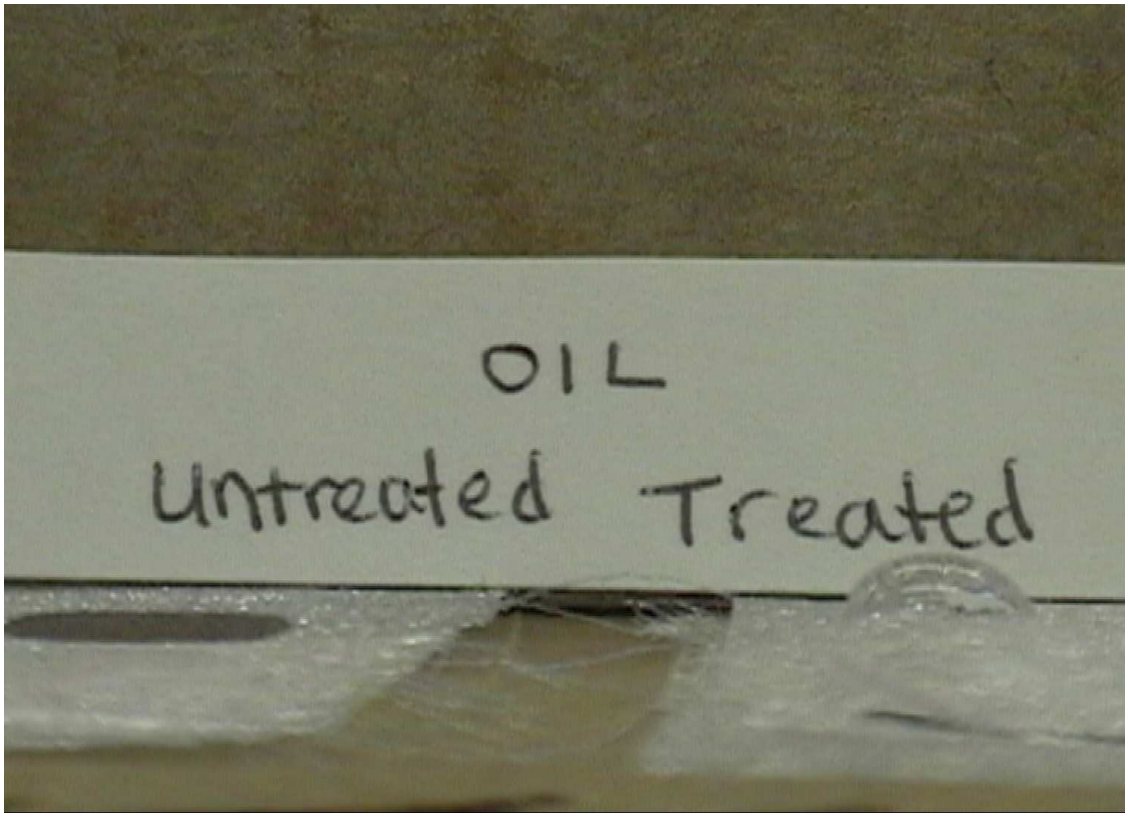

Figure 7.2– Oil repellency of untreated and PDFOAmM-PAA-g-nylon fabrics

7.3.3 *Stain Resistance*

Both nylon 6,6 and PAA-g-nylon carpets were highly wetting and double strength cherry-flavored Kool-Aid® immediately absorbed into the fibers and spread upward by wicking. After rinsing, significant fiber staining was observed from the tip of the tufts down to the backing. All PDFOAmM-PAA-g-nylon carpets were extremely water repellant and double strength cherry-flavored Kool-Aid® did not spread above the immersion line. After rinsing, there was light staining at the tip of the tufts only. Staining for the H_2O, pH=12 treatment was significantly less than for MeOH treatment. A comparison between nylon, PAA-g-nylon and PDFOAmM-PAA-g-nylon (H_2O, pH=12) carpets is shown in Figure 7.3.

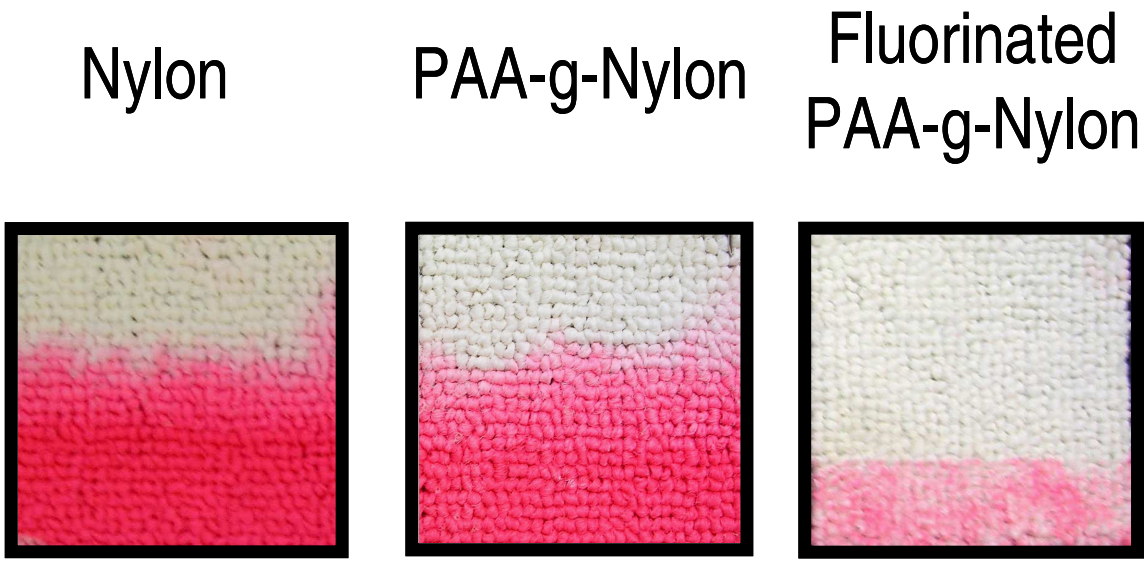

Figure 7.3– Stain Resistance of Nylon 6,6 Carpets After SGN Modification

After treating PAA-g-nylon carpet with NaOH, stain resistance was significantly improved. The exterior tuft fibers, but not the interior fibers, were stained. The most reasonable explanation is that NaOH treatment converts PAA acid groups to their carboxylate anions. However, if NaOH had hydrolyzed nylon 6,6 chains, additional carboxylate anions may have been generated. Since NaOH treatment on nylon 6,6 film does not result in surface damage (Chapter 4), it is unlikely to occur on the fibers. After NaOH treatment, no significant change was observed for the H_2O, pH=12 or MeOH reaction samples. Since stain resistance for ionized PAA-g-nylon was less than the stain resistance for PDFOAmM-PAA-g-nylon samples, such results are understandable. A front and cross-sectional comparison between PAA-g-nylon, NaOH-treated PAA-g-nylon and PDFOAmM-PAA-g-nylon (H_2O, pH=12) carpets is shown in Figure 7.4.

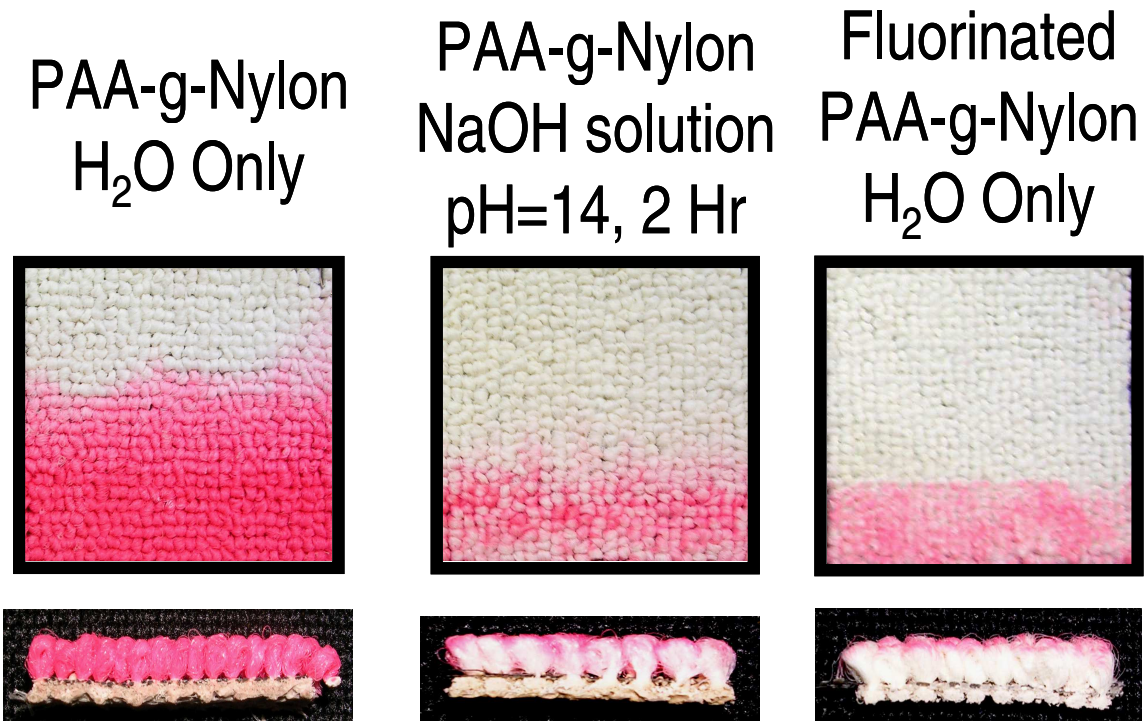

Figure 7.4– Stain Resistance of H_2O and NaOH Treated SGN-Modified Carpets

7.4 CONCLUSIONS

Nylon 6,6 fabrics and carpets were also Adsorption-Grafted and modified with 1H, 1H-pentadecafluorooctyl amine in RAMEB/H_2O at pH=12. The fluorochemical treatment was shown to be stable to alkaline conditions. Significant water and oil repellency was observed after fluorochemical modification, such that both wetting and wicking were prevented. After ionizing PAA-g-nylon, the stain resistance was slightly improved. However, fluorochemically modified PAA-g-nylon with or without ionization was more stain resistant. More improvements are still necessary, since staining still occurs at the tips of the carpet tufts. Such improvements may involve applying traditional stain resisting polymers with PAA prior to grafting and fluorochemical modification.

CHAPTER 8

CONCLUSIONS AND FUTURE RECOMMENDATIONS

8.1 CONCLUSIONS

8.1.1 Solution Modification of PAA

- Various acrylamide derivatives of PAA were prepared using DMTMM condensing reagent. With taurine, ethanolamine, and butyl amine in H_2O, PAA modification was ~100% (40-50% NH_2/DMTMM efficiency, 0.5–11g/L PAA). Taurine and ethanolamine derivatives were soluble in H_2O, while butyl amine derivative with ≥77% acrylamide content precipitated from H_2O.
- With perfluorinated alkyl amines in MeOH, 100% modification was not achieved. Higher levels of modification were achieved with dilution. At 0.5 g/L PAA, ~80% modification with 1*H*,1*H*-pentadecafluorooctylamine (PDFOA) was observed at 40% NH_2/DMTMM efficiency. PDFOA derivatives with ≥52% acrylamide content precipitated from MeOH.
- Significant goals of this research were achieved:
  - Optimal conditions were established for various acrylamide modification reactions of PAA chains in solution using DMTMM condensing reagent.
  - Solubility limitations of the acrylamide derivatives were identified for future comparison with acrylamide modification reactions of surface-grafted PAA chains in solution using DMTMM condensing reagent.

8.1.2 Synthesis of Surface-Grafted Nanoscaffolds

- PAA grafting onto nylon 6,6 films with DMTMM coupling reagent successfully transformed the nylon surface from water repellant to water wetting.
- PAA surface fractions were determined from XPS and contact angle measurements: f_{PAA}^{XPS} and $f_{PAA}(\theta_{Eff})$ values were statistically equal.
- All PAA surface fractions increased with PAA concentration.
- The best results were achieved for Adsorption-Grafted/Desorbed nylon. PAA surface fractions increased with DMTMM to a maximum of 72% (11 g/L PAA, 5mM DMTMM) and then decreased beyond 5mM DMTMM.
- The PAA surface fraction for Solution-Grafted/Desorbed film at 11 g/L PAA and 40 mM DMTMM was equivalent to that for Adsorption-Grafted/Desorbed film at 11 g/L PAA and 1 mM DMTMM. This suggests that Solution-Grafting is actually an Adsorption-Grafting process, which is reasonable since films are immersed in PAA solution prior to the addition to DMTMM. The low efficiency of grafting indicates that PAA chains from solution consume 97.5% of the DMTMM before it reaches the surface.
- Significant goals of this research were achieved:
  - The fact that equivalent PAA surface fractions were observed by XPS and contact angle measurement confirmed that PAA layers were ≥ 5 nm thick.
  - The Adsorption-Grafting technique was developed, which successfully grafted PAA onto nylon 6,6 using an minimal amount of DMTMM condensing reagent. The maximum surface coverage obtained by the Adsorption-Grafting process closely agrees with the PCC-RSA model, which predicts $\theta_\infty = 0.68$.

8.1.3 Modification of Surface-Grafted Nanoscaffolds

- Acrylamide modification of PAA-g-nylon 6,6 substrates was successful: butyl amine (BA) and 1H, 1H-pentadecafluorooctyl amine (PDFOA) transformed the surfaces from water wetting to water repellant.
- The contact angles for BAmM-PAA-g-nylon (82°) and PDFOAmM-PAA-g-nylon films (>100°) indicated ~100% acrylamide surface fractions in the top 0.1-1 nm.
- The surface fraction from XPS for BAmM was ~72% and for PDFOAm was 48% and 53% in MeOH and H_2O/RAMEB pH=7, respectively. The PDFOAm surface fraction was 89% in H_2O/RAMEB pH=12, indicating a more uniform reaction. All surface fractions indicate fewer acrylamide groups in the top 5 vs. 0.1-1 nm.
- Significant goals of this research were achieved:
  - Randomly methylated β-cyclodextrin (RAMEB) successfully solubilized PDFOA in H_2O. The similarity between MeOH and H_2O/RAMEB pH=7 reactions indicates similar PAA graft chain dimensions in these solvents.
  - The BAm and PDFOAm (MeOH or H_2O pH=7) surface fractions agree with the acrylamide contents of the analogous solution-modified PAA chains at their insolubility point, which suggests that PAA graft-chain precipitation prevents DMTMM and amines from accessing interior PAA groups.
  - At pH=12, a more uniform distribution of PDFOAmM-PAA groups was achieved and the PDFOAmM-PAA group surface fraction surpassed the solubility limit. Possible explanations include (a) greater reaction efficiency, (b) greater graft chain solubility, and (c) greater surface access.

8.1.4 Angle-Resolved XPS Analysis of Polymers

- ARXPS analysis of Nylon 6,6 using the Cumpson model revealed higher C_O and lower C_C and C_N values than expected within the top 2 nm.
- ARXPS analysis of PAA-treated nylon using the Cumpson, Trapezoid and Fractional Overlayer models found the best "goodness of fit" for the Cumpson model, followed by the Trapezoid and then the Fractional Overlayer models.
- The PAA surface coverage for Adsorption-Grafted/Desorbed nylon (>70%) was higher than for Adsorbed and Solution-Grafted nylon. Close agreement was observed between the Cumpson, Trapezoid and Fractional Overlayer models and these values agreed with previous XPS f_{PAA}^{XPS} and contact angle $f_{PAA}(\theta_{Eff})$ values.
- The thickness of Adsorbed PAA was fairly uniform, while Adsorption-Grafted and Solution-Grafted PAA layers displayed a distribution of thickness values.
- ARXPS analysis of PDFOAmM-PAA-g-nylon using Cumpson and Trapezoid models was performed. Over 100% PDFOAmM-PAA surface coverage was achieved by modifying an Adsorption-Grafted PAA layer in H_2O at pH=12. Thus fluorination further spread the grafted layer across the surface. Also, the total grafted layer was thicker after fluorination and the PDFOAmM-PAA region had a wide thickness distribution (3-12 nm).
- In MeOH, over 60% PDFOAmM-PAA surface coverage was achieved and both a PDFOAmM-PAA rich exterior and a PAA rich interior were observed. While the total grafted layer was still thicker after fluorination, the grafted layer was not spread further across the surface and the PDFOAmM-PAA region was slightly thinner (2-8 nm) than observed for H_2O at pH=12.

- Significant goals of this research were achieved:
  - ARXPS was used to determine PAA surface fractions and layer thicknesses for various PAA-treated nylon films.
    - Surface fractions from XPS and contact angle analysis were confirmed.
    - The Adsorption-Grafting mechanism conformed to the Post-Adsorption Conformational Change RSA (PCC-RSA) model.
  - ARXPS was used to determine PDFOAmM-PAA surface fractions and layer thicknesses for MeOH and H_2O pH=12 reactions.
    - Fluorochemical modification of Adsorption-Grafted nylon was restricted by PAA graft chain solubility for MeOH reaction solvent. However, a much higher level of modification was observed the H_2O, pH=12 reaction. Over 100% fluorochemical surface coverage was achieved even though the PAA surface coverage of nylon was ~70-80%.

8.1.5 Surface Modification of Textiles

- Nylon 6,6 fabrics and carpets were PAA-grafted and fluorochemically modified
- PAA-g-nylon carpet displayed poor stain resistance.
- NaOH-treated PAA-g-nylon carpet displayed significant stain resistance.
- Fluorochemical modification produced the highest stain resistance.
  - Fluorochemical modification in H_2O, pH=12 was better than in MeOH.
  - NaOH treatment had no effect on Fluorochemically modified carpet.
- Fluorochemical modification significantly improved water and oil repellency.
  - Both wicking and wetting were prevented

- The fluorochemical treatment was stable to alkaline conditions, which is a primary factor in the removal of traditional fluorochemical treatments.
- Significant goals of this research were achieved:
  - Fluorochemical modification of nylon 6,6 substrates was successful.
  - Fluorinated substrates displayed significant water and oil repellency.
  - Fluorinated substrates displayed improved stain repellency.
  - Fluorinated treatments were stable to alkaline conditions.
  - Limitations of fluorinated treatments were identified.

8.2 RECOMMENDATIONS

8.2.1 Evaluation of pH Dependence of DMTMM Amidation

In the present work, addition of NaOH greatly enhanced the extent of reaction of PAA-g-nylon 6,6 with PDFOA. One explanation is that PAA may increase the pH at the surface, limiting the efficiency of the DMTMM amidation reaction. NaOH neutralization of PAA groups would thus enhance the reaction. To study the effect of pH on the efficiency of DMTMM, model compounds (for example, acrylic acid and butyl amine) should be amidated with DMTMM in H_2O at various pH values.

8.2.2 SGNs with Superior Surface Coverage and Thickness

In the present work, the Adsorption-Grafting process achieved a 72% PAA surface fraction on nylon 6,6 using PAA at M_w = 450,000 g/mol. This M_w was selected on the basis of prior work by Michielsen and coworkers.[57-59] Larger PAA chain should have an advantage in the Adsorption-Process, however, since PAA surface coverage

increased as islands of adsorbed PAA spread across the surface during DMTMM grafting. Larger PAA chains should be able to spread across greater distances, possibly to 100% surface coverage. Further, these larger PAA chains should create thicker layers. These two factors together should provide better protection of the substrate.

8.2.3 SGNs with Reduced Surface Reorganization

For long term protection, greater PAA surface coverage and thicker PAA layers may not be sufficient. Hydrophilic PAA groups can bury themselves below more hydrophobic nylon 6,6 polymer segments to reduce surface energy. Surface restructuring depends on PAA chain mobility, which in turn, depends on the glass transition temperature (T_g) of the substrate. By increasing the T_g of PAA chains, a greater number of PAA groups will remain at the surface. This can been achieved by converting PAA CO_2H groups (T_g=379 K) into their $Na^+CO_2^-$ salts (T_g=503 K). Polyvalent metal ions increase T_g to a greater extent due to the formation of metal complexes with multiple CO_2H groups, ex. $Zn^{+2}(CO_2)_2^{-2}$ (T_g = 694 K).[43] A carboxylic acid–Cu^{2+} ion complex was used to expand and fix poly(methacrylic acid) (PMAA) chains grafted on the surface of PET. Such complexes were stable in alkaline conditions but PMAA CO_2H groups were regenerated at pH=3.[72]

8.2.4 Surface Chemical Imaging with NanoSIMS

In the present work, surface heterogeneity has been evaluated by contact angle and x-ray photoelectron spectroscopy. However, these techniques deliver information which is an average over large areas. A better understanding of the behavior of these

surfaces would be gained from studying surface heterogeneities on the nanometer scale. The CAMECA NanoSIMS 50 is a new ion microprobe which has the ability to extend the SIMS analysis to extremely small areas or volumes (50 nm size in cesium, 150 nm in oxygen) while maintaining extremely high sensitivity at High Mass Resolution. One of these instruments is in operation at the Department of Materials at Oxford. The CAMECA NanoSIMS 50 could be used to reveal the horizontal nanoscale chemical heterogeneity of the top 1 nm of nylon, PAA-g-nylon, and PDFOAmM-PAA-nylon films.

8.2.5 Nylon 6,6 Carpets with Superior Stain Resistance

Nylon 6,6 has a limited number of CO_2H groups on the surface which can be ionized to improve stain resistance. While this should be evaluated, the effect is not expected to be as significant as achieved by the fluorochemical surface treatments of nylon 6,6 carpets presented in this work. Future work should focus on incorporating traditional nylon 6,6 stainblockers to achieve complete stain resistance. Such materials include condensates of formaldehyde with phenolsulfonic acid, naphtholsulfonic acids, or sulfonates of dihydroxydiphenylsulfone, or their mixtures. In addition, nonaromatic sulfonic acid compounds have been claimed as stainblockers. In this way, the CO_2H groups of PAA can be used for grafting and fluorochemical modification, while the OH and SO_3Na groups of the stain resist polymer can occupy the nylon dye sites. The fluorochemical portion would still be permanently attached to the surface, while the stainblockers could be bound by ionic interactions alone or could be crosslinked through their phenolic groups, for example, to improve fastness.

8.2.6 Evaluation of Carpet Soiling

While oil repellencies of fluorochemically modified nylon fabrics and carpets were evaluated, further testing is recommended to evaluate their soil resistance. The AATCC Test Method 123-2000 for Carpet Soiling: Accelerated Soiling and AATCC Test Method 122-2000 Carpet Soiling: Service Soiling Methods were developed by the American Association of Textile Chemists and Colorists (AATCC). In the first method, carpet is tumbled together with prepared synthetic soil in a laboratory mill for a predetermined time and the soiling propensity of the carpet is measured. In the second method, carpets are exposed to normal foot traffic in a controlled test area. The samples are evaluated at predetermined intervals to evaluate the soiling propensity of the carpet.

8.3 NEXT GENERATION RESEARCH

8.3.1 Dense Brush Polymers

The current research has focused on a "grafting-to" approach for polymer surface modification. PAA reactive groups were bound to the surface of nylon 6,6 by chemical coupling via DMTMM. However, in any "grafting-to" approach, the surface-attached chains build up a diffusion barrier at the surface which slows down the attachment of additional polymer chains at the surface. In addition, a diffusion barrier has been shown to form during the coupling of reactive PAA groups with fluorinated amines due to the low solubility of highly fluorinated polymers.

To circumvent such limitations, polymers can be grown at surfaces by immobilization of an initiator or vinyl group at the surface followed by radical-chain polymerization in-situ (a "grafting-from" method). If reactive sites are not present on the

surface for immobilization, the only choice is to create them. Typically chemical treatments or ionizing radiation are applied to create radicals on the surface. However, such techniques are not very surface specific and side reactions occur when using ionizing radiations, such as cross-linking and chain scission of the substrate polymer.

An alternate approach would combine "grafting-to" and "grafting-from" techniques. Once PAA has been grafted onto nylon, PAA CO_2H groups can be modified with amine-functional monomers: N-(2-aminoethyl) methacrylate and N-(2-aminopropyl) methacrylamide are commercially available, while N-(2-aminoethyl) acrylamide can readily be synthesized from acrylic acid monomer and ethylene diamine using DMTMM. Free radical polymerization can be performed at these vinyl groups in the presence of fluorinated vinyl monomer and an initiator. By using PAA to amplify the number of polymerization sites, the resulting polymers should have a dense brush structure.

8.3.2 Smart Surfaces

In some applications, plasma induced crosslinking during graft polymerization is a desirable side reaction. Badyal and coworkers[73,74] observed that complexation of cationic fluorosurfactants to CO_2H functional plasma polymer surfaces resulted in markedly different behavior (hydrophilic/oleophobic) compared to traditional CO_2H functional polymer complexes with cationic fluorosurfactants (hydrophobic/oleophobic). High contact angles were observed toward both oil and water for a maleic anhydride copolymer first complexed with cationic fluorosurfactant in solution and then spin-coated, as well as for a spin-coated copolymer film complexed with surfactant. However, a maleic anhydride plasma polymer-surfactant complex repelled oil but spread water.

Similar results were found using acrylic acid polymers. One explanation was that crosslinking of the plasma polymer surface restricts accessibility for the fluorosurfactant below the surface; in turn this may suppress interdigitation, cooperative binding, and layering of the perfluoroalkyl tails. Thus the surfactant-polyelectrolyte monolayer may reorganize to allow water molecules to interact with the hydrophilic subsurface.

In this example, it has been shown that small changes can result in complete changes in surface properties. There are many possible smart surfaces that might be designed, each with the ability to switch from a spreading surface to a repellant surface under various conditions. In the present research, PAA was grafted from solution onto nylon 6,6 surfaces to produce a stain resistant surface of high anionic charge. After PAA grafting, the surface is highly hydrophilic and displays a low contact angle. However, after fluorochemical modification, the nylon 6,6 surface is hydrophobic and oleophobic. This is designed to prevent spills, dirt or oils from penetrating the surface.

It may be desirable to create a nylon 6,6 surface that is hydrophilic, anionic and oleophobic. The surface would remain soil and stain repellant, but water would wet the surface to improve the release of adhered soil. Such oleophobic/hydrophilic behavior is also potentially attractive for antifogging applications, where spreading of water droplets and oil repellency are both desired. To accomplish this, a step could be inserted after PAA is grafted onto nylon and prior to the fluorochemical modification of PAA-g-nylon. In this step, the PAA chains would be crosslinked by a diamine, such as ethylene diamine, by DMTMM. This would restrict fluorochemical modification to the outermost region in the same way plasma crosslinked PAA restricts cationic fluorosurfactant.

REFERENCES

(1) Vermette, P.; Meagher, L. *Langmuir* **2002**, *18*, 10137.

(2) Young, T. *Philosophical Transactions of the Royal Society of London* **1805**, *95*, 65.

(3) Cassie, A. B. D. *Discussions of the Faraday Society* **1952**, *75*, 5041.

(4) Wenzel, R. N. *Journal of Industrial and Engineering Chemistry* **1936**, *28*, 988.

(5) Garbassi, F.; Morra, M.; Occhiello, E. *Polymer surfaces:from physics to technology*; Revised and updated ed.; John Wiley & Sons: West Sussex, 1998.

(6) Scofield, J. H. *Journal of Electron Spectroscopy and Related Phenomena* **1976**, *8*, 129.

(7) Cumpson, P. J. *Journal of Electron Spectroscopy and Related Phenomena* **1995**, *73*, 25.

(8) Paynter, R. W. *Surface and Interface Analysis* **1999**, *27*, 103.

(9) Paynter, R. W. *Surface and Interface Analysis* **1981**, *3*, 186.

(10) Cumpson, P. J. *Surface and Interface Analysis* **2001**, *31*, 23.

(11) Tanuma, S.; Powell, C. J.; Penn, D. R. *Surface and Interface Analysis* **1991**, *17*, 911.

(12) Kier, L. B.; Murray, W. J.; Hall, L. H. *Journal of pharmaceutical sciences* **1976**, *65*, 1226.

(13) Bicerano, J. *Prediction of Polymer Properties*; 1st. ed.; Marcel Dekker, Inc., New York, N.Y., 1993.

(14) *Modern Techniques Of Surface Science*; Second ed.; Cambridge University Press: Cambridge, UK, 1994.

(15) van de Grampel, R. D.; Ming, W.; Gildenpfennig, A.; van Gennip, W. J. H.; Krupers, M. J.; Laven, J.; Niemantsverdriet, J. W.; Brongersma, H. H.; van der Linde, R. *Progress in Organic Coatings* **2002**, *45*, 273.

(16) Khorana, H. G. *Chemical Reviews* **1953**, *53*, 145.

(17) DeTar, D. F.; Silverstein, R. *Journal of the American Chemical Society* **1966**, *88*, 1013.

(18) DeTar, D. F.; Silverstein, R. *Journal of the American Chemical Society* **1966**, *88*, 1020.

(19) Wang, K. T.; Iliopoulos, I.; Audebert, R. *Polymer Bulletin* **1988**, *20*, 577.

(20) Wang, T. K.; Iliopoulos, I.; Audebert, R. *Polymer Preprints (American Chemical Society, Division of Polymer Chemistry)* **1989**, *30*, 377.

(21) Magny, B.; Lafuma, F.; Iliopoulos, I. *Polymer* **1992**, *33*, 3151.

(22) Anghel, D. F.; Alderson, V.; Winnik, F. M.; Mizusaki, M.; Morishima, Y. *Polymer* **1998**, *39*, 3035.

(23) Petit, F.; Iliopoulos, I.; Audebert, R. *Journal de Chimie Physique et de Physico-Chimie Bioligique* **1996**, *93*, 887.

(24) Petit, F.; Iliopoulos, I.; Audebert, R.; Szoenyi, S. *Langmuir* **1997**, *13*, 4229.

(25) Staros, J. V.; Wright, R. W.; Swingle, D. M. *Analytical Biochemistry* **1986**, *156*, 220.

(26) Sehgal, D.; Vijay, I. K. *Analytical Biochemistry* **1994**, *218*, 87.

(27) Matsusaki, M.; Serizawa, T.; Kishida, A.; Endo, T.; Akashi, M. *Bioconjugate Chemistry* **2002**, *13*, 23.

(28) Kunishima, M.; Kawachi, C.; Morita, J.; Terao, K.; Iwasaki, F.; Tani, S. *Tetrahedron* **1999**, *55*, 13159.

(29) Kunishima, M.; Kawachi, C.; Iwasaki, F.; Terao, K.; Tani, S. *Tetrahedron Letters* **1999**, *40*, 5327.

(30) Kunishima, M.; Kawachi, C.; Hioki, K.; Terao, K.; Tani, S. *Tetrahedron* **2001**, *57*, 1551.

(31) Govindaraju, V.; Young, K.; Maudsley, A. *NMR in Biomedicine* **2000**, *13*, 129.

(32) Pouchert, C. J.; Behnke, J., Eds. *The Aldrich Library of ^{13}C and ^{1}H FT NMR Spectra*; 1st ed.; Aldrich Chemical Company, 1993; Vol. 1.

(33) Feder, J. *Journal of Theoretical Biology* **1980**, *87*, 237.

(34) Adamczyk, Z.; Siwek, B.; Zembala, M.; Weronski, P. *Journal of Colloid and Interface Science* **1997**, *185*, 236.

(35) Adamczyk, Z.; Zembala, M.; Siwek, B.; Warszynski, P. *Journal of Colloid and Interface Science* **1990**, *140*, 123.

(36) Adamczyk, Z.; Siwek, B.; Zembala, M.; Belouschek, P. *Advances in Colloid and Interface Science* **1994**, *48*, 151.

(37) Adamczyk, Z.; Warszynski, P. *Advances in Colloid and Interface Science* **1996**, *63*, 41.

(38) Jin, X.; Wang, N. H. L.; Tarjus, G.; Talbot, J. *Journal of Physical Chemistry* **1993**, *97*, 4256.

(39) Douglas, J. F.; Scheider, H. M.; Frantz, P.; Lipman, R.; Granick, S. *Journal of Physics: Condensed Matter* **1997**, *9*, 7699.

(40) van Tassel, P. R.; Viot, P.; Tarjus, G.; Talbot, J. *Journal of Chemical Physics* **1994**, *101*, 7064.

(41) van Tassel, P. R.; Viot, P.; Tarjus, G. *Journal of Chemical Physics* **1997**, *106*, 761.

(42) Flory, P. J. *Principles of Polymer Chemistry*; Cornell University Press: Ithaca, New York, 1953.

(43) Lechner, M. D.; Nordmeier, E.; Steinmeier, D. G.; Brandrup, J.; Immergut, E. H.; Grulke, E. A. In *Polymer Handbook*; Wiley: New York, 1989.

(44) Aseyev, V. O.; Tenhu, H.; Klenin, S. I. *Macromolecules* **1998**, *31*, 7717.

(45) Böhme, U.; Scheler, U. *Macromolecular Symposia* **2002**, *184*, 349.

(46) Wilkins, D. K.; Grimshaw, S. B.; Receveur, V.; Dobson, C. M.; Jones, J. A.; Smith, L. J. *Biochemistry* **1999**, *38*, 16424.

(47) *CRC Handbook of Chemistry and Physics*; 65th ed.; CRC Press, Inc.: Boca Raton, Florida.

(48) Newman, S.; Krigbaum, W. R.; Laugier, C.; Flory, P. J. *Journal of Polymer Science* **1954**, *14*, 451.

(49) Okubo, T. *Journal of Physical Chemistry* **1989**, *93*, 6860.

(50) Okubo, T. *Macromolecules* **1989**, *22*, 1818.

(51) Hoffman, H.; Liveri, M. L. T.; Cavasino, F. P. *Journal of the Chemical Society, Faraday Transactions* **1997**, *93*, 3161.

(52) Schweins, R.; Hollmann, J.; Huber, K. *Polymer* **2003**, *44*, 7131.

(53) Reith, D.; Müller, B.; Müller-Plathe, F.; Wiegand, S. *Journal of Chemical Physics* **2002**, *116*, 9100.

(54) Taylor, T. J.; Stivala, S. S. *Polymer* **1996**, *37*, 715.

(55) Taylor, T. J.; Stivala, S. S. *Journal of Polymer Science: Part B: Polymer Physics* **2003**, *41*, 1263.

(56) Tate, M. L.; Kamath, Y.; Wesson, S. P.; Ruetsch, S. B. *Journal of Colloid and Interface Science* **1996**, *177*, 579.

(57) Michielsen, S. *Journal of Applied Polymer Science* **1999**, *73*, 129.

(58) Tobiesen, F. A.; Michielsen, S. *Journal of Polymer Science: Part A: Polymer Chemistry* **2002**, *40*, 719.

(59) Sherrill, J.; Michielsen, S.; Stojiljkovic, I. *Journal of Polymer Science: Part A: Polymer Chemistry* **2003**, *41*, 41.

(60) Cole, D.; Howard, G. J. *Journal of Polymer Science: Part A-2* **1972**, *10*, 993.

(61) Cole, D.; Howard, G. J. *Journal of Polymer Science: Part A-2* **1972**, *10*, 1013.

(62) Vermette, P.; Gengenbach, T.; Divisekera, U.; Kambouris, P. A.; Griesser, H. J.; Meagher, L. *Journal of Colloid and Interface Science* **2003**, *259*, 13.

(63) Zhou, Y.; Bruening, M.; Bergbreiter, D.; Crooks, R.; Wells, M. *Journal of the American Chemical Society* **1996**, *118*, 3773.

(64) Peez, R. F.; Dermody, D. L.; Franchina, J. G.; Jones, S. J.; Bruening, M. L.; Bergbreiter, D. E.; Crooks, R. M. *Langmuir* **1998**, *14*, 4232.

(65) Zhou, Y.; Bruening, M.; Liu, Y.; Crooks, R.; Bergbreiter, D. *Langmuir* **1996**, *12*, 5519.

(66) Bruening, M.; Zhou, Y.; Aguilar, G.; Agee, R.; Bergbreiter, D.; Crooks, R. *Langmuir* **1997**, *13*, 770.

(67) Li, X.-D.; Aoki, A.; Miyashita, T. *Langmuir* **1996**, *12*, 5444.

(68) Parker, H.-Y. In *US Patent #5,969,063*; Rohm and Haas Company: United States, 1999.

(69) Storsberg, J.; Ritter, H. *Macromolecular Chemistry and Physics* **2002**, *203*, 812.

(70) Choi, S. W.; Kretschmann, O.; Ritter, H.; Ragnoli, M.; Giancarlo, G. *Macromolecular Chemistry and Physics* **2003**, *204*, 1475.

(71) Jin, Y.; Huang, R. Y. M. *Journal of Applied Polymer Science* **1988**, *36*, 1799.

(72) Uchida, E.; Iwata, H.; Ikada, Y. *Polymer* **2000**, *41*, 3609.

(73) Hutton, S. J.; Crowther, J. M.; Badyal, J. P. S. *Chemistry of Materials* **2000**, *12*, 2282.

(74) Lampitt, R. A.; Crowther, J. M.; Badyal, J. P. S. *Journal of Physical Chemistry B* **2000**, *104*, 10329.

VITA

Kimberlee Fay Thompson was born on March 18, 1971, in Tampa, Florida. At the age of 4, she moved to Conyers, Georgia. While she no longer had a tangerine tree in her backyard, she grew to appreciate the beauty of dogwood blossoms. In 1989 she graduated from Heritage High School and attended Georgia Institute of Technology in Atlanta, Georgia. Selecting chemistry as a major, she enrolled in polymer electives and spent her summers working for Dr. Arthur Ragauskas at the Institute of Paper Science and Technology and Dr. Fred Cook in the Textile Engineering Department. In 1994 she graduated with a Bachelor of Science. She continued at Georgia Institute of Technology, earning a Master of Science in Textile Chemistry under Dr. Wayne Tincher. Her thesis was titled "The Role of Singlet Oxygen in the Bleaching of Cotton". After graduating in 1996, she worked briefly at Amoco Polymers Carbon Fiber Division in Alpharetta, Georgia before being hired as senior R&D chemist with Sawgrass Technologies in Charleston, South Carolina in 1997. In this position, she developed numerous inks and coatings for digital heat-transfer printing of textiles. She is the author/coauthor of several patents and one of her inventions is currently in the market - the Natura® Digital Apparel System (laser toner) for cotton apparel.

In 2001, she returned to Georgia Institute of Technology and began a Ph.D. program in Polymer Science under thesis advisor Dr. Stephen Michielsen. In May 2005, she successfully defended her dissertation titled "Modification of Polymeric Substrates via Surface-Grafted Nanoscaffolds". After graduation she plans to continue her path of research and innovation.